



UNIVERSITAT DE LES
ILLES BALEARS

Tesi Doctoral

Divide and conquer

Resonance induced by competitive interactions

Author:
Teresa Vaz Martins



Instituto de Física Interdisciplinar y Sistemas Complejos

2010

Raúl Toral Garcés, Catedràtic de la Universitat de les Illes Balears, certifica que aquesta tesi doctoral ha estat realitzada sota la seva direcció pel Sra. Teresa Maria Vaz Martins, i perquè quedi constància escrita firma

a Palma 2 de Novembre de 2010.

Raúl Toral Garcés

Divide and conquer
**Resonance induced by competitive
interactions**

by

Teresa Vaz Martins

Graduate (Universidade do Porto) 2004
M.Sc. (Universitat de les Illes Balears) 2010

TESI

presentada a la

Universitat de les Illes Balears

per optar al grau de

DOCTORA EN FÍSICA

Desembre 2010

Divide and conquer
**Resonance induced by competitive
interactions**

Copyright 2010

by

Teresa Vaz Martins

Acknowledgements

I am very grateful to Raúl Toral for the way he directed this PhD. I was lucky to find a person full of good ideas and insight, that allows for the right amount of independence, with whom we can discuss freely with the confidence that if we propose something strange he will stop us at the right time when it gets silly, but not too soon before ideas can be explored. Additionally, and very importantly, he was reliable, generous and uncomplicated throughout the entire PhD.

During these years, I was very fortunate to have been surrounded by a very stimulating group at IFISC, whose support enabled me to complete this thesis successfully, and whose mixture of enthusiasm and rigour is inspiring. It would be too long to enumerate all the people at IFISC that somehow contributed to the thesis, by making IFISC as it is. Fortunately, its director Maxi San Miguel shares and contributes to the the overall spirit, so I thank him in representation of the entire institute.

I would also like to acknowledge Valeria Livina, Ana Majtey, Miguel Pineda and Claudio Tessone, who contributed in one way or another to the results of the thesis; Maria Augusta Santos that gave me the idea of coming to IFISC; and Rubén Tolosa and Eduardo Herráiz whose expertise with computers was indispensable. My thanks extend to Jaume Pons and Jaume Carot, and also Marga Prohens and Marga Moranta: I can never remember which last name corresponds to which person, but I do remember each one and that they helped very generously with all the bureaucratic aspects of

the thesis.

Although I don't like to get personal, the success of a PhD done abroad is very much dependent on the friends we find on the way. With Ana, Maria Sabeva and Maria Victoria V. Ojosnegros I explored Mallorca, India and Barcelona, I considered crazy alternative projects in case Physics didn't pay well, we shared many experiences... Most importantly, I found friends for life - a very rare thing. And here I must also mention Ari, Aaron, Titi, Damian, Simon, Hector, Frank and Julio.

Another good result of this was a random meeting Valeria that turned into a real friendship. I am also grateful to her mother Tamara Livina for all the bureaucratic trouble she went through to invite me to Russia and for the wonderful way she welcomed in her house. Also, thank you Laska from Siberia.

From Portugal, I have to acknowledge my friends Lucy, Tatiana and Yu o Grande, and especially my family. Thanks to my parents, Maria Beatriz Vaz and Mário Décio Martins, my aunt Teresa B. Vaz and my sisters Lena and Raquel for their love and support throughout all the years, and to my little nephew Pedro in the last 2 and a half years - indeed his entire life - for considering me an awesome godmother that appears from the sky once in a while.

Contents

ACKNOWLEDGEMENTS	i
Resumen	ix
Resumo	xi
Summary	xiii
I Introduction	1
1 Systems with thresholds	3
1.1 Bistable systems	3
1.1.1 Thresholds: tipping points	5
1.2 Nonlinear oscillators	6
1.2.1 <i>Spatial</i> and <i>temporal</i> thresholds	10
1.3 Excitable systems	12
1.3.1 Active rotator	14
1.3.2 The FitzHugh-Nagumo model	15

1.3.3	<i>Hard and soft thresholds</i>	16
1.4	Sociophysics models	19
1.4.1	A discrete model	22
1.4.2	A continuous model	23
2	Ordering role of disorder	29
2.1	Stochastic resonance	30
2.1.1	Stochastic resonance in a bistable system	32
2.1.2	Excitable systems	34
2.2	Measures	36
2.3	Diversity induced resonance	39
2.4	Is diversity required at all?	43
II	Original Research	47
3	The ϕ^4 model	51
3.1	The bistable model	52
3.2	Signal amplification	53
3.3	Spectral analysis	60
3.4	Conclusions	65
4	A discrete bistable model	67
4.1	Noise and diversity	67
4.2	Model	69
4.3	Simulation results	71
4.4	Mean-field approach	73
4.5	Mechanism	77

4.5.1	Microscopic point of view	77
4.5.2	Macroscopic point of view	81
4.6	Conclusions	87
5	Mass media reception in a continuous opinion model	89
5.1	Introduction	89
5.2	Model	90
5.3	Results	91
5.4	Summary and Conclusions	96
6	Synchronisation induced by repulsive interactions in the van der Pol oscillator	101
6.1	Introduction	101
6.2	Model	103
6.3	Desynchronisation among the unforced oscillators, $A = 0$. .	104
6.4	Synchronisation with the external signal, $A \neq 0$	111
6.4.1	Strong fast signals benefit from intermediate p	113
6.4.2	Weak slow signals benefit from very high p	117
6.5	Further applications: FitzHugh-Nagumo	118
6.6	Conclusions	121
III	Conclusions	125
7	Conclusions and Outlook	127
7.1	Future work	130

IV	Appendices	133
A	Spectral Analysis	135
B	A method to detect potential wells	139
C	The rewiring algorithm mentioned in the Divide and Conquer chapter 4	143
D	Master Equation for the Deffuant model with repulsive links	145
	D.1 Model	145
	D.2 The Master equation	146
	D.2.1 Attractive part	146
	D.2.2 Repulsive part	148
	D.2.3 The Master Equation	151
	D.2.4 Integration limits at the boundaries	154
	D.2.5 The normalization condition	156
	D.2.6 Numerical integration of the Master Equation - practical issues	159
	D.2.7 Strange Master Equation results	159
E	Some calculus concerning The Van der Pol system	161
	E.0.8 The system	162
	E.0.9 The anti-phase solution	162
	E.0.10 How repulsive links modify the amplitude of oscillations	164
	E.0.11 The measure G	164
	Bibliography	166

CONTENTS

vii

Index

176

Curriculum vitae

179

Resumen

El objetivo de esta tesis es responder a la siguiente pregunta:

Puede la presencia de interacciones competitivas mejorar la respuesta a un forzamiento externo?

Esta es una pregunta muy general, y nuestro enfoque es encontrar varios sistemas-prototipo, para verificar el dominio de aplicación del fenómeno y explorar diferentes mecanismos.

Vamos a comenzar por abordar el efecto de las interacciones competitivas en la respuesta a señales débiles, en el caso de sistemas constituidos por unidades biestables para las cuales la señal es subumbral. Veremos que la respuesta es óptima para una proporción intermedia de enlaces repulsivos, y por lo tanto vamos a utilizar la expresión "resonancia inducida por interacciones competitivas", en analogía con los conocidos efectos de resonancia estocástica y resonancia inducida por diversidad.

A continuación vamos a estudiar cómo las interacciones competitivas afectan a la respuesta a las señales externas - *publicidad* - en el modelo de formación de opinión de Deffuant *et al.* . Se trata de un tipo intrínsecamente diferente de sistema y, como tal, tanto el mecanismo de respuesta, así como los resultados, son bastante diferentes. La presencia de interacciones competitivas puede impedir la formación de grupos de agentes, cuya opinión se

encuentra fuera de la cuenca de influencia de la señal externa. Vamos a comprobar que una sociedad de mentalidad estrecha sólo puede formar un consenso en respuesta a la influencia de la publicidad si los agentes interactúan a través de una combinación de vínculos positivos y repulsivos.

Por último, vemos las condiciones para la sincronización con una señal externa en un sistema de osciladores van der Pol, haciendo hincapié en el hecho de que la probabilidad de enlaces repulsivos que desincroniza los osciladores entre ellos, es la misma que es capaz de sincronizar todo el sistema con un forzamiento externo.

Resumo

O objectivo desta tese é responder à seguinte pergunta:

Será que a presença de interacções competitivas pode melhorar a resposta dum sistema a um forçamento externo?

Sendo esta uma pergunta muito geral, optámos por verificar o domínio de aplicação do fenómeno e explorar diferentes mecanismos em vários sistemas-protótipo.

Começamos por abordar o efeito de interacções competitivas na resposta a sinais débil, no caso de sistemas constituídos por unidades biestáveis para as quais o sinal é sublimar. Veremos que a resposta é óptima para uma proporção intermédia de interacções repulsivas, e portanto utilizarei a expressão "resonância induzida por interacções competitivas", em analogia com os conhecidos efeitos de resonância estocástica y resonância induzida por diversidade.

Em seguida estudaremos o modo como as interacções competitivas afectam a resposta a sinais externos - *publicidade* - no modelo de formação de opinião de Deffuant *et al.*. Tratando-se de um tipo intrínsecamente diferente de sistema, tanto o mecanismo de resposta, como os resultados, são distintos. A presença de interacções competitivas pode impedir a formação

de grupos de agentes cuja opinião se encontre fora da zona de influência do sinal externo. Comprovaremos que uma sociedade de mentalidade estreita só pode atingir um consenso na resposta à influência da publicidade se os agentes interagem através de uma combinação de ligações positivas e repulsivas.

Por último, analisaremos as condições para uma sincronização com um sinal externo num sistema de osciladores van der Pol, acentuando o facto de que a probabilidade de interacções repulsivas que desincroniza os osciladores entre si, é a mesma que é capaz de sincronizar todo o sistema com um forçamento externo.

Summary

Since few systems exist in isolation, a key question is how a system responds to an environmental forcing. Whether we think about how the brain can encode information, a fish detect food in muddy waters, or an advertiser influence the market, this very general challenge spans different disciplines and is dealt with by the adoption of different strategies. Nevertheless, those strategies basically fall into one of two categories: either to increase the strength of the external forcing, or to optimise the capability of the system to respond to the signal. This last strategy is the object of this thesis: specifically, we will show that extended systems that interact via a combination of attractive and repulsive links are able to optimise their response to an external forcing, for some fraction of repulsive links. Thus, the title *Divide and Conquer* in analogy with the ancient Roman strategy of controlling populations with a not so big army by dividing the subjects one against another.

The thesis is divided in two parts, where the first part sets the background to understand and contextualise the original results that will be presented in the second part. We start, in Chapter 1 by reviewing the basic characteristics of the systems that will be the object of the thesis, and whose common characteristic is the possession of some form of threshold that cannot be surpassed by weak signals.

The second chapter places the thesis in a broader context of the effects of disorder in the response properties of nonlinear systems subjected to weak forcing. Indeed, this work is closely related to a very active research area that emerged in the 80's following the discovery of *stochastic resonance*, a phenomenon by which noise cooperates with a weak forcing to raise it above the threshold for detection, and two decades later, in 2006, of *diversity induced resonance*, that firmly identified disorder as the key factor leading to an enhancement of the response.

There isn't an *a priori* reason to anticipate that there will be a single mechanism of response enhancement through competitive interactions. We chose to orient our research towards the exploration of the mechanism in several systems with different characteristics. We wanted to find how broad the area of application is, and whether there is a single general mechanism or if, on the contrary, different systems exploit different routes to achieve the same goal.

We begin by studying the effect of competitive interactions on the response to external forcing, in the case of systems composed by bistable units for which the signal is subthreshold. We will verify that the response is optimal for an intermediate proportion of repulsive links, and thus the expression "Resonance induced by competitive interactions", that is the subtitle of the thesis. In Chapter 3 we will establish the phenomenon in the prototypical bistable continuous model where the phenomenon of stochastic resonance was first discovered; and in Chapter 4 we study a discrete model of opinion formation. We will then continue with two non-bistable models. The first, in Chapter 5, is a modification of the Deffuant *et al.* model of opinion formation to include repulsive interactions, and the second, in Chapter 6, is a system of van der Pol oscillators.

Finally, the last chapter summarises the principal conclusions of our results, and describes possible future research lines.

Part I

Introduction

Systems with thresholds

This first chapter introduces the systems that will appear throughout the rest of the thesis, and some of the approaches to deal with them. The common feature of these systems is the possession of some form of threshold: either clear-cut or soft, temporal or spatial, thresholds separate two qualitatively different behaviours. Talking about thresholds makes most sense with respect to external forcing.

This property is characteristic for a large class of systems coming from vastly different areas. We will begin by addressing three types of dynamical systems - bistable, nonlinear oscillator and excitable -, and then we will present two sociophysics opinion models.

1.1 Bistable systems

While linear systems can only have one - or none - stable states, nonlinear systems are characterised by the possible existence of multiple equilibrium states, periodic oscillations and even chaotic behaviour, which necessarily leads to thresholds that separate different states. The simplest example of a system with a threshold has two stable states, separated by a barrier that can only be overcome by an external driving force. Bistability underlies many

natural phenomena, such as chemical reactions [1], bacterial infections [2,3], synthetic gene-regulatory network [4], some climate processes [5], among others.

A typical Z-shaped curve (Fig. 1.1), illustrates the response of a bistable system to an external signal S . Bistability is commonly associated with hysteresis, implying that the dependency of the response on the signal intensity depends on the direction of change (arrows in the picture 1.1). When the stimulus grows beyond a threshold $S = B$, the system switches from the state 1 to state 2; and when the stimulus decreases the system remains in the same state, until the saddle-node bifurcation point is reached when $S = A$, leading to a jump to the upper steady state. In case the signal can not reach the value $S = A$ the first switch is irreversible. The region between $S = A$ and $S = B$ is characterised by the coexistence of two stable steady states, plus an unstable state. In that region, the state of the system depends on initial conditions and on the history of the system.

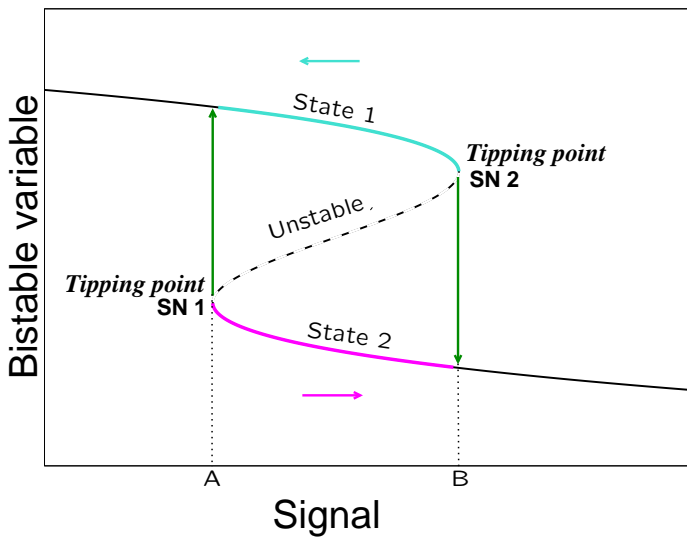


Figure 1.1. A schematic signal-response curve, or bifurcation diagram, for a typical bistable system with hysteresis. A combination of two saddle-node bifurcations leads to the phenomenon of bistability where in a certain interval of the control parameter, two stable states co-exist with an unstable one in-between. Bistable systems can be driven to change states by external variables. The bistability interval exists for a signal between $S = A$ and $S = B$; if the signal can only take values in that interval $[A, B]$ the system cannot switch: we call such signal *sub-threshold*.

1.1.1 Thresholds: tipping points

In Fig. 1.1, $SN1$ and $SN2$ are tipping points: once crossed, a regime shift occurs, which may be impossible to reverse, in case there isn't a strong enough - or controllable enough - forcing. Hence, the detection of early-warning signs of the approximation of tipping points has become a key goal [6] in various areas like the climate [5], ecosystems [7], epileptic seizures [8] or finance [9] where a regime change could lead to dramatic consequences.

A related challenge is how to control the shifts. The prototypical, normal form, model for a bistable unit is given by:

$$\frac{dx}{dt} = ax - bx^3, \quad (1.1)$$

where a and b are positive constants.

We can describe the relaxation to one of two stable states using the concept of a potential [10]: left to itself, the system will be in one of the states of lowest energy (Fig. 1.2).

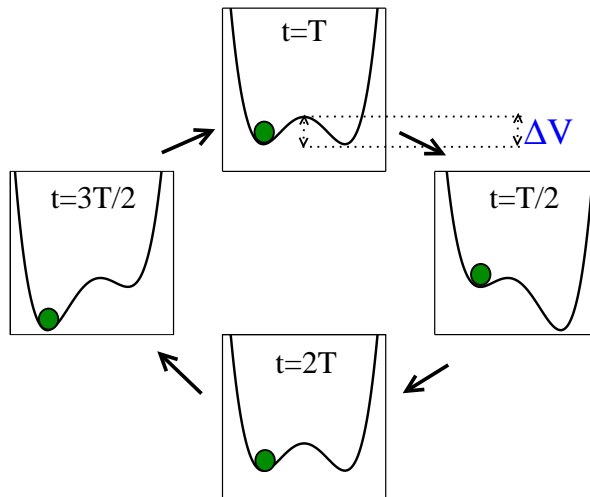


Figure 1.2. The mechanical depiction of a bistable system imagines a ball rolling into two different valley basins. A periodic subthreshold signal with period $T = 2\pi/\Omega$ alternately lowers or raises one of the potential wells without destroying them: as a consequence the ball cannot cross to the other well.

Eq. 1.1 is then written as a relaxation into a potential, $\frac{dx}{dt} = -\frac{\partial V}{\partial x}$, where the potential is

$$V(x) = -a\frac{x^2}{2} + b\frac{x^4}{4} \quad (1.2)$$

with the minima located at $x_o = \pm\sqrt{a/b}$ and the barrier height being $\Delta V = a^2/4b$.

In order for the particle to cross the barrier there needs to be an increase of energy, coming from an external source. We think about thresholds when we think about some forcing that can drive the system through it. Forced by a time-dependent signal, let's say a periodic one, the Eq. 1.1 becomes:

$$\frac{dx}{dt} = -\frac{\partial V'}{\partial x} = ax - bx^3 + A \sin(\Omega t), \quad (1.3)$$

where A is the amplitude of the signal, Ω its frequency, and the new potential $V'(x) = -a\frac{x^2}{2} + b\frac{x^4}{4} - Ax \sin(\Omega t)$. Fig. 1.2 illustrates the effect of a weak signal. The potential is modulated by a *sub-threshold* signal, with its minima being alternately raised or lowered relative to the potential barrier, without losing bistability: this means the system behaviour is basically indifferent to perturbations, as there are only small intra-wells oscillations.

It looks like the only way to force a bistable system to switch states is to find a strong enough driving. A main topic in this thesis concerns what to do in case this is not possible.

1.2 Nonlinear oscillators

Bistable systems only oscillate between two states when they are subjected to a sufficiently strong external periodic forcing. But oscillations are so widespread in Nature - circadian clocks, the beating of the heart, seasonal cycles, and many others [11] - that there arises the need to model intrinsic oscillatory systems.

The simplest oscillator model - a linear harmonic oscillator - has an amplitude that depends on initial conditions, since linearity requires that if $\vec{x}(t)$ is a solution, so is $A\vec{x}(t)$. This strongly limits its domain of applications, as a variety of natural systems - like a beating heart - needs to oscillate with a steady amplitude. In contrast, nonlinear oscillators can have an intrinsic amplitude that is robust to perturbations. A paradigmatic example of a nonlinear oscillator is a model [12] proposed in 1927 by the Dutch engineer Balthasar van der Pol when studying electrical circuits to model the beating of the heart. The van der Pol equation is:

$$\ddot{x} = -x + \mu(1 - x^2)\dot{x}, \quad (1.4)$$

where μ is a positive constant called the nonlinearity parameter, and $\mu(1 - x^2)$ is the position-dependent nonlinear damping term that distinguishes it from the linear oscillator. The left panels of Fig. 1.3 illustrate the trajectories that result from this model.

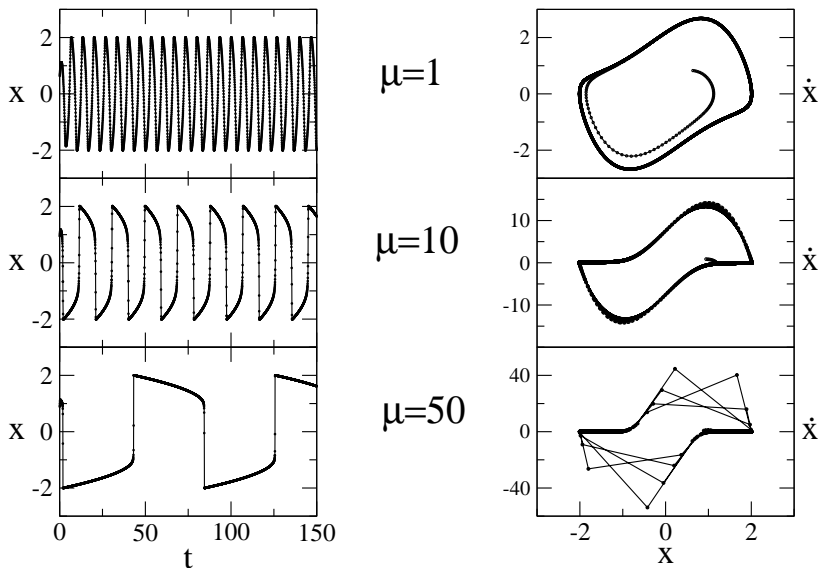


Figure 1.3. Trajectories (left) and corresponding limit cycles (right) for several values of μ . Note that while the period grows with μ , the amplitude remains the same. In the last case of large $\mu = 50$ the transitions between the slow branches are so fast as to be discontinuous, while as μ decreases the trajectories become more similar to an undamped linear oscillator, that is recovered when $\mu = 0$.

For $|x| > 1$ the damping term is negative while for $|x| < 1$ it is positive, which results in the damping down of large amplitude oscillations and pumping up of small ones. This leads to stable oscillations, reflected in asymptotically stable closed trajectories on a phase plane, now called limit cycles, as illustrated in Fig. 1.3. We also note that there is a clear distinction between a fast and a slow motion, and that the period increases with μ (Fig. 1.3): this is expected since for larger μ the damping is amplified and the oscillator spends more time in a slow branch when the damping term is positive and less time moving to the other slow branch when the damping is negative.

We can put the analysis on a firmer ground by noting that the van der Pol oscillator is a special case of a Liénard system [11, 13], as described by the equation $\ddot{x} = f(x)\dot{x} + g(x)$. By Liénard theorem, these systems have a stable limit cycle surrounding the origin of the phase space provided the following conditions are satisfied:

- $g(x)$ is an odd function and positive for positive x : it is like a restoring force.
- $f(x)$ and $g(x)$ are differentiable for all x ,
- there is an odd function $F(x) = \int_0^x f(u)du$ that has exactly one positive zero at $x = a$, is negative for $0 < x < a$ and positive/non-decreasing for $x > a$, and $F(x) \rightarrow \infty$ as $x \rightarrow \infty$: damping is negative at small x and positive at large x .

In case of the van der Pol oscillator, $g(x) = x$, $f(x) = \mu(x^2 - 1)$ $F(x) = \int_0^x \mu(u^2 - 1)du = \mu(x^3/3 - x)$, and $a = \sqrt{3}$.

We can write the van der Pol equation 1.4 in a two-dimensional form that highlights a fast and a slow motion, using the Liénard transformation $y = x - x^3/3 - \dot{x}/\mu$:

$$\begin{cases} \dot{x} &= \mu(x - \frac{1}{3}x^3 - y) \\ \dot{y} &= \frac{1}{\mu}x. \end{cases} \quad (1.5)$$

It is sometimes difficult or impossible to find explicitly the solutions of a system, and that is specially true when the system is non-linear. The behaviour of two-dimensional nonlinear models can be visualised by means of phase-plane portraits, that offer a geometrical tool to understand qualitatively how systems evolve. The x-nullcline is the curve where $\dot{x} = 0$ and it is given by the cubic curve $y = x - \frac{1}{3}x^3$ as illustrated in Fig. 1.4, while the y-nullcline - the curve where $\dot{y} = 0$ - is given by $x = 0$ and is simply the y-axis. Their intersection at the origin of the (x, y) plane corresponds to an unstable point. Far from the cubic nullcline, when $x - \frac{1}{3}x^3 - y \sim 1$, we have $\dot{x} \sim \mu$ while $\dot{y} \sim \frac{1}{\mu}$; thus the trajectory is basically horizontal and the system is moving fast between the slow branches. When $x - \frac{1}{3}x^3 - y \sim \mu^2$ then both \dot{x} and \dot{y} are $\sim \mu^{-1}$ and the system crawls along a slow branch. Then the process repeats itself, as illustrated in Fig. 1.4. The entire process corresponds to a limit cycle.

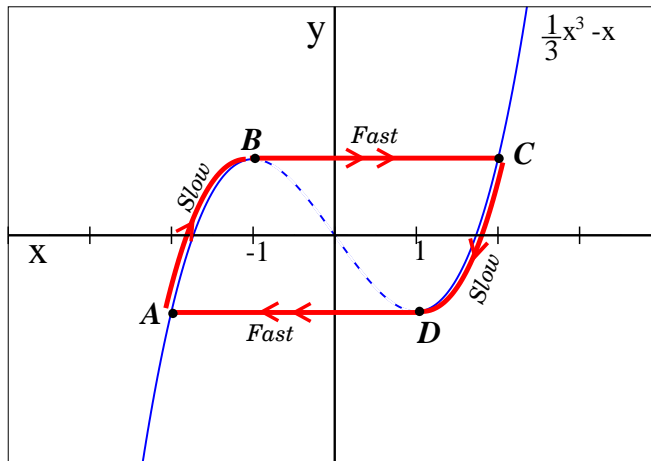


Figure 1.4. Phase portrait of the van der Pol oscillator in Liénard (x, y) variables. The two time scales are a defining characteristic of relaxation oscillators, referring to the slow dynamics or relaxation along the slow branches. The blue curve depicts the x-nullcline and the red curve the limit cycle.

For large μ we can neglect the time spent on the fast branches $B - C$ and $D - A$ (Fig. 1.4). Then we can calculate the period from the time travelling on the slow branches, and make explicit the dependence of the

period of oscillations on μ , that we observe on Fig. 1.3:

$$T_{AB} = \int_A^B dt = \int_{-2}^{-1} \frac{dy}{dx} \frac{dx}{dy} dt = \mu \int_{-2}^{-1} (1 - x^2) \frac{1}{x} dx = \mu \left(\frac{3}{2} - \ln 2 \right). \quad (1.6)$$

Since, for symmetry reasons, $T_{AB} = T_{CD}$, the total period is $T \approx \mu(3 - 2 \ln 2)$, neglecting the time spent in the fast motion regions T_{BC} and T_{DA} .

It is useful to have this kind of dependence in mind when we examine in Chapter 6 the response of a system of van der Pol oscillators to an external signal, since, as we will see, the response of the system depends on its period and therefore on μ .

1.2.1 Spatial and temporal thresholds

We saw in Section 1.1 that an external periodic signal modifies the potential wells in a bistable system. A forced bistable system oscillates with the external signal frequency: if the signal is weak, it oscillates within a well, and only if the signal is strong enough - *suprathreshold* - will it be able to induce inter-well oscillations (Fig. 1.5).

When we think of nonlinear oscillators, an additional requirement for an *influential* signal is that its frequency is close to the oscillator intrinsic frequency (Fig. 1.5). In the case of a strong enough signal and close enough frequency, nonlinear oscillators can become synchronised with the driving signal [11], adjusting their frequency to the driving frequency (middle panel in Fig. 1.6). Van der Pol [12] thought that the heartbeat could be modelled as a relaxation oscillator, and he was interested in understanding how its rhythm could be stabilised in case of irregular beating (arrhythmias). His studies on entrainment by an external signal were meant to mimic the heart being driven by a pacemaker, and became the first systematic study of synchronisation [11, 14]. This is a type of synchronisation - where the van der Pol oscillator interacts with an external forcing whose frequency is not affected by the interaction - that will concern us mostly in the thesis (Chapter

6). However, we should note that van der Pol oscillators with different individual frequencies are able to mutually synchronise, which is a characteristic that sets them apart for linear oscillators that are thus inadequate to model systems that exhibit collective synchronised oscillations.

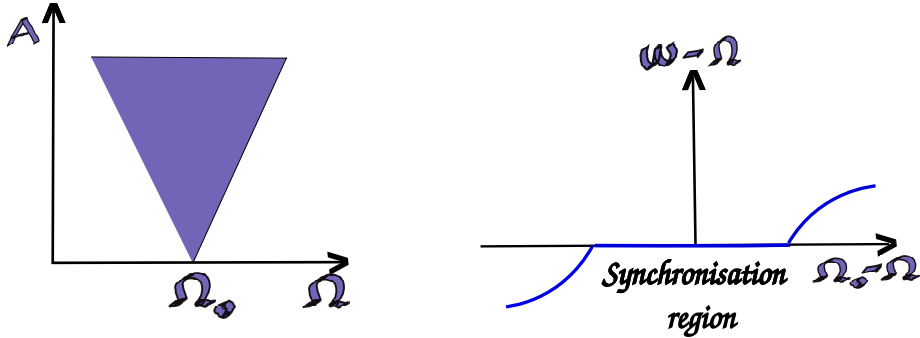


Figure 1.5. Left: Schematic view of a generic Arnold tongue - the region of parameters strength A and frequency Ω of the external force where synchronisation occurs, for an oscillator with frequency Ω_0 . Right: Dependence of the observed frequency ω on the external one (at a constant amplitude of forcing) exhibits a synchronisation plateau.

When driven by an external forcing, the van der Pol oscillator can display several types of behaviours, apart from synchronisation. A related phenomenon to entrainment is quasiperiodicity (upper panel in Fig. 1.6), that occurs when the forcing strength is fairly low. The intrinsic frequency of the oscillator competes with the forcing frequency resulting in a time-varying frequency and amplitude. Also, since the inclusion of a signal introduces another dimension in the system, it can lead to chaotic trajectories for some parameters, as seen on the lower panel of Fig. 1.6. In fact, in 1927 van der Pol and van der Mark reported [15] that an "irregular noise" was heard at certain driving frequencies between the natural entrainment frequencies, in what is now recognised as one of the first experimental observations of deterministic chaos.

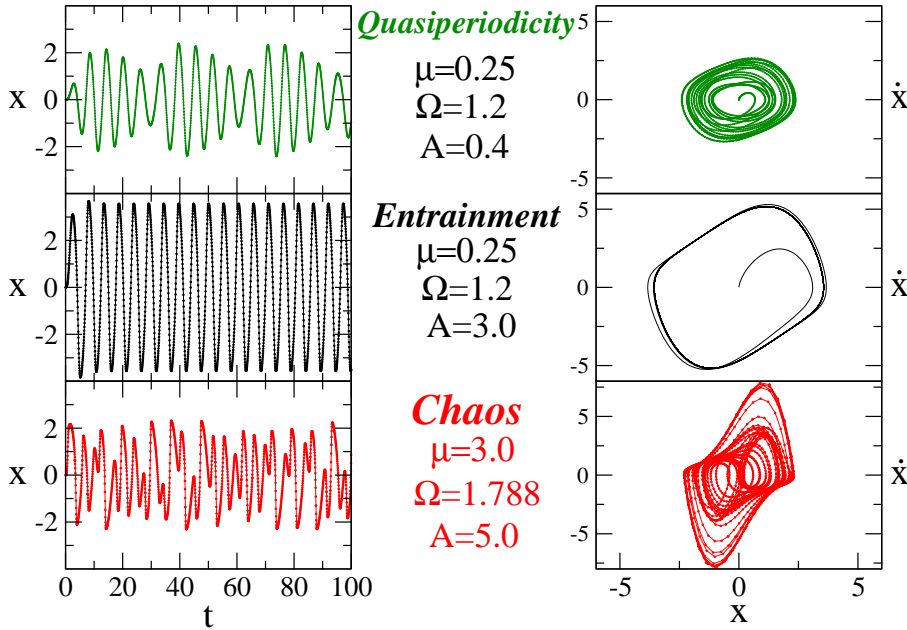


Figure 1.6. The reaction of the van der Pol oscillator to an external forcing depends on the strength of the forcing, on its amplitude, and on how close the driving frequency is to the oscillator frequency.

While the threshold in a bistable system is a kind of spatial threshold, here we have additionally a temporal threshold, and the challenge is to widen the range of frequencies that can be entrained. When signals are fast they need to be strong enough to overcome the positive damping term, and when they are slow, they need to be able to postpone the jumping between slow branches, so they coincide with its period. We will return to this question on Chapter 6.

1.3 Excitable systems

Excitable systems share with nonlinear relaxation oscillators the existence of fast and slow time-scales. The difference is that instead of jumping between different states, when perturbed beyond a given threshold they make a long

excursion in the phase space before returning to the original rest state. During that excursion time, there is an interval, called the refractory period, where the system is relatively indifferent to perturbations.

These systems [16] appear near a bifurcation from a rest state to a limit cycle, and are useful to model [17] certain chemical reactions, lasers, biological tissues, forest fires, or - which is the classical example - neurons that operate by communicating with other neurons when a signal exceeding a given threshold results in a neuron *firing*.

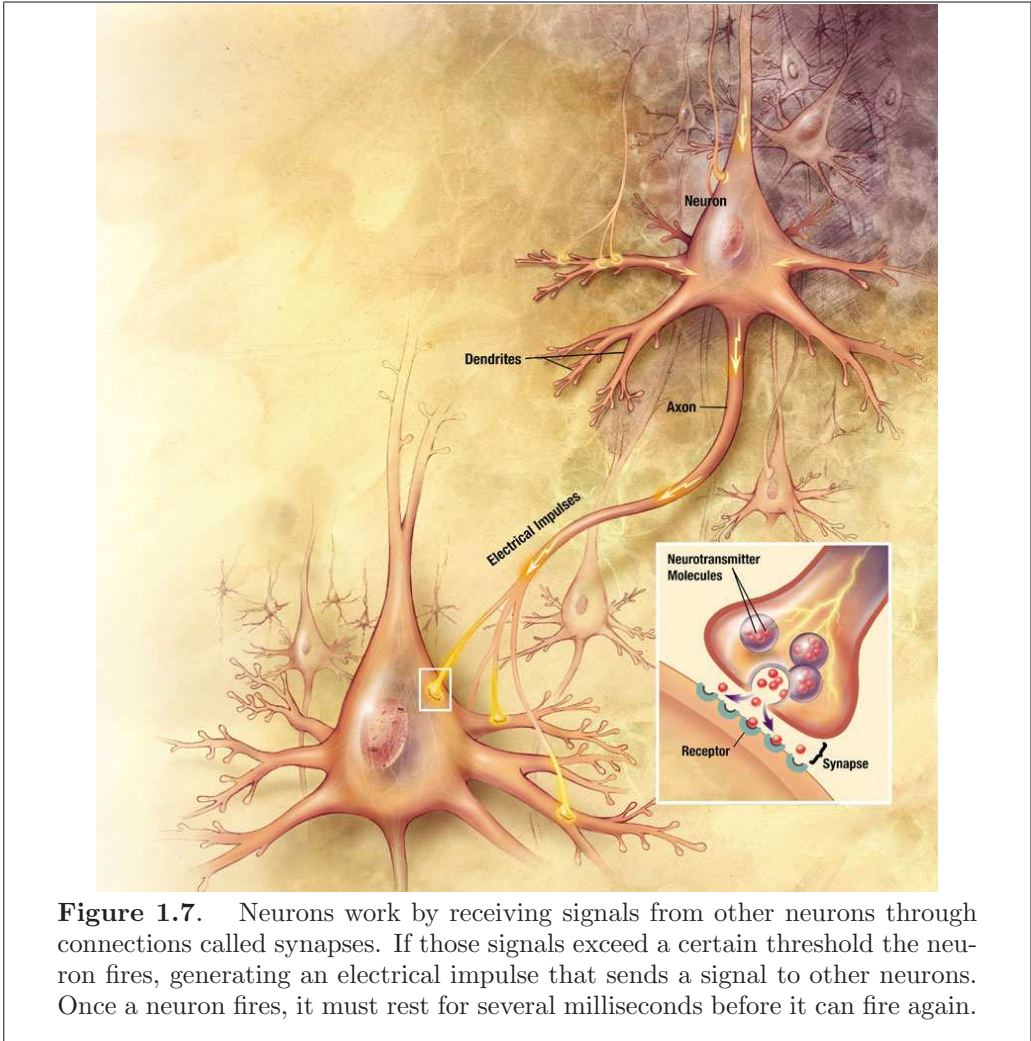


Figure 1.7. Neurons work by receiving signals from other neurons through connections called synapses. If those signals exceed a certain threshold the neuron fires, generating an electrical impulse that sends a signal to other neurons. Once a neuron fires, it must rest for several milliseconds before it can fire again.

In this section, we will introduce the basic characteristics of two types of excitable systems, by choosing the simplest examples, focusing in particular on their threshold or threshold-like behaviour.

1.3.1 Active rotator

A limit cycle - an isolated closed trajectory - is usually [17] the path followed by an excitable unit during its firing state, while it is making an excursion on the way back to the rest state. The existence of limit cycles requires two dimensions, which can be harder to analyse. A way to circumvent this problem is to describe the dynamics by a single phase variable, which is generally a good option because the amplitude of the trajectory of a limit cycle is usually less affected by interactions [17] than its phase.

Let us consider an *active-rotator* $\phi(t)$ [18], whose dynamics is given by;

$$\dot{\phi} = \omega - \sin \phi \tag{1.7}$$

For $\omega \leq 1$ the system is excitable and the fixed points are $\pm \arcsin \omega$, corresponding to a stable point at $\arcsin \omega$, and an unstable one at $-\arcsin \omega$. When $\omega = 1$ the stable node collides with the saddle and a limit cycle is born. At this point, for $\omega > 1$, the system becomes oscillatory with a frequency $\sqrt{\omega^2 - 1}$. This is a prototypical example of a system that exhibits a saddle-node bifurcation on an invariant circle [19].

It is useful to rewrite the dynamics as a potential equation, $\dot{\phi} = -\frac{\partial V(\phi)}{\partial \phi}$ with the potential $V(\phi) = -\omega\phi - \cos \phi$ (Fig. 1.8). We are interested in the excitable regime, where a perturbation can induce a spike if it is large enough to surpass the distance between the saddle-node and the stable point that constitutes a threshold. That distance depends on the value of ω , becoming smaller as ω grows, which is why we observe in Fig. 1.8 that a weak perturbation can lead to repetitive firing when $\omega = 1$ but not when $\omega = 0.7$. Finally, for $\omega = 1.1$, the threshold has disappeared and the system is oscillatory: a periodic driving can only change the firing frequency.

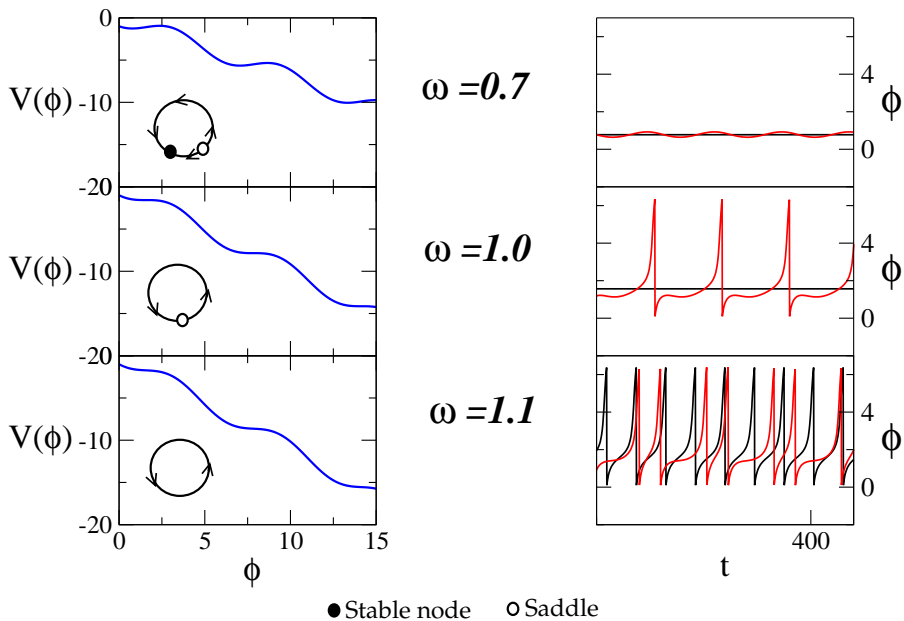


Figure 1.8. The panels on the left show the potential in blue and the limit cycles in black, and the panels on the right show the corresponding trajectories in case the system is unperturbed (black lines) or perturbed (red line) by a periodic signal. The regime of the active rotator depends on the frequency ω . When $\omega \leq 1$ the system is in the excitable regime and a perturbation can induce a spike (red line) if it is strong enough. When $\omega > 1$ the system is oscillatory and the periodic forcing can modify the frequency of oscillations.

1.3.2 The FitzHugh-Nagumo model

This model [20, 21] was proposed as a simplification of the more realistic Hodgkin-Huxley model for neurons, by modifying the van der Pol system 1.5. The FitzHugh-Nagumo equation is:

$$\begin{aligned} \dot{x} &= x - \frac{1}{3}x^3 - y + I, \\ \dot{y} &= \frac{1}{\tau}(x + a - by). \end{aligned} \quad (1.8)$$

where a and b are parameters and the constant τ is responsible for the separation of time scales: for $\tau \gg 1$ the y variable is slow and the x variable

is fast. I plays the role of an injected current. Fig. 1.9 illustrates the nullclines of the system, given by the cubic black curve and the straight red line. As always, the intersection of nullclines corresponds to a fixed point, and the point of intersection depends on how strong I is. In case the intersection occurs in the middle branch of the cubic curve, the equilibrium is unstable. When the current I increases beyond a critical point, an oscillation appears, modelling the firing of a neuron (Fig. 1.9). This scenario - a limit cycle that appears through the destabilisation of a fixed point - is called a Hopf bifurcation [19].

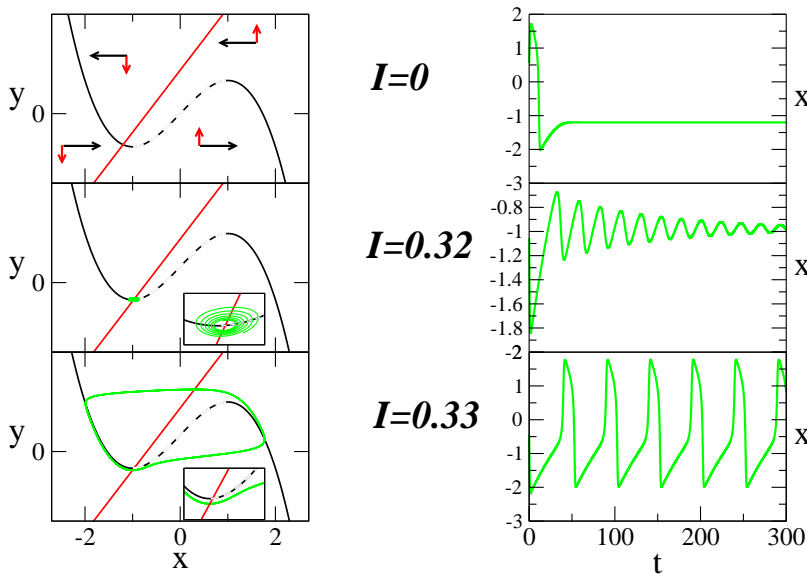


Figure 1.9. When $I = 0.33$ the y -nullcline intersects the middle branch of the x -nullcline. The fixed point becomes unstable leading to repetitive spiking. We used $a = 0.7$, $b = 0.8$ and $\tau = 13$, so that $\dot{x} \sim 10\dot{y}$ and x is the fast variable. Compare the figure with the van der Pol where a similar picture is observed.

1.3.3 Hard and soft thresholds

Studying neuronal firing patterns, Hodgkin identified two types of excitable behaviours [22], that are associated with the bifurcations they undergo [23, 16]: a saddle-node bifurcation on an invariant circle, and a Hopf bifurcation. The first case, corresponding to the active rotator, is called a Class I excitable

system, and the second case, corresponding to the FitzHugh-Nagumo, is a Class II excitable system ¹.

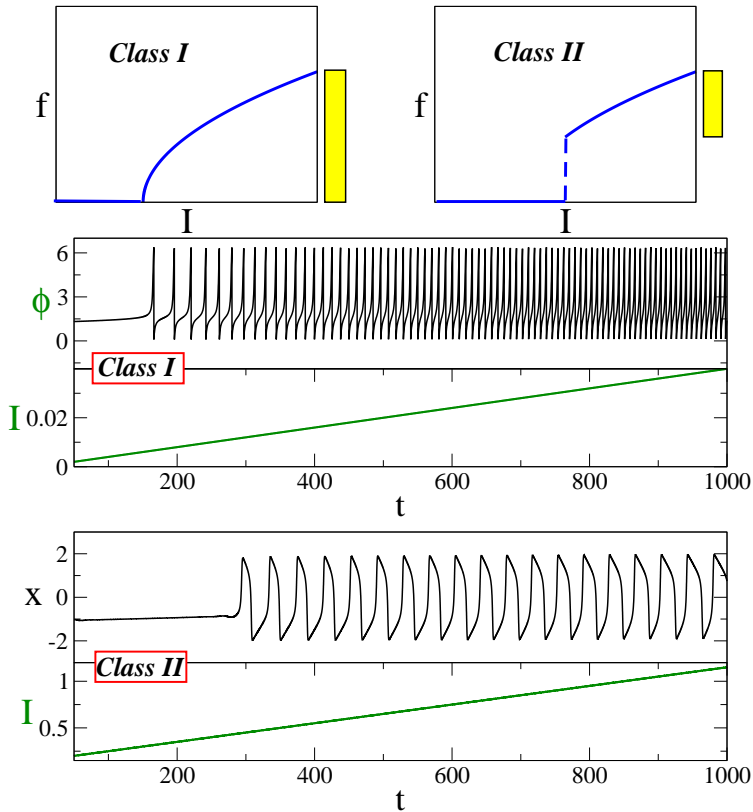


Figure 1.10. Upper panels: Schematic representation of the dependence on the frequency of oscillations f on the external perturbation I , illustrating the difference between the two types of excitable systems. Left: in a Class I excitable system the firing frequency increases with the applied current, while the frequency of a Class II (right) excitable system is relatively insensitive to the strength of the forcing. Lower panels: The different dependency of the firing frequency on the intensity of the current I is the signature of the two classes of systems.

Those two classes of excitable system display different reactions to a perturbation, that are illustrated in Fig. 1.10. The case of *Class I* excitable

¹Yet a third class consists of excitable systems that are unable to exhibit repetitive spiking unless the injected current is very strong [16]

systems is shown in the upper left panel: in these systems the trajectory slows as the critical point is reached - a phenomenon known as critical slow down - thereby allowing for oscillations with arbitrarily slow frequency, that increases with the applied current I . On the right upper panel, we show the case of *Class II* excitable systems: at the bifurcation point oscillations with non-zero frequency appear, and the frequency is relatively insensitive to the value of the current I . Therefore, the range of frequencies with which a Class I excitable system can fire is considerably larger than that of a Class II. (Fig. 1.10, yellow bar).

Besides the different dependencies on the firing frequency on the forcing, the two classes of excitable systems have different types of thresholds. The response of Class I model to a forcing shows an all-or-nothing behaviour: either there is a firing with a given amplitude, or there is a decay back to the stable point. In this sense, Class I models have a real threshold, whose value is given by the distance between the saddle and the node. In contrast, the amplitude of response of Class II models depends on the strength of the perturbation. For weak pulses $I = I_0\delta(t - t_0)$ of the injected current the system exhibits small-amplitude spikes, when trajectories follow the unstable middle branch for some time, as observed in Fig. 1.11. Class II systems are said to have a *soft* threshold. Nevertheless, they have a critical point that can be well described as a threshold, where the sensitivity to perturbations is much higher (see Fig. 1.9).

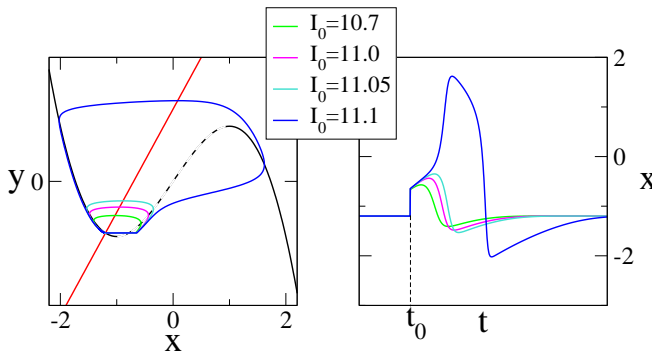


Figure 1.11. The figure illustrates the absence of all-or-none firings in the FitzHugh-Nagumo model, that doesn't have a clear threshold. On the left panel we show the phase portraits and on the right panel the corresponding spikes resulting from some values of the strength of the pulse $I_0\delta(t - t_0)$. Parameters: $a = 0.7$, $b = 0.8$ and $\tau = 13$.

1.4 Sociophysics models

Up until now we have reviewed models whose main inspiration lied outside Physics domains: the van der Pol oscillator models the beating of the heart and neurons are the classic prototype of excitable systems. The different Natural sciences can find a common framework in nonlinear dynamical systems studies, and this is an uncontroversial statement. We will take a step further now, to venture into sociophysics models, and more specifically opinion formation models.

In this era of heavy specialisation, where the frontiers between sciences are carefully guarded by departments, official curricula and titles, it is easy to forget that there has never been impermeable borders between the natural and social sciences [24], nor each discipline is without internal divergences.

A recent area where the cooperation between natural and social sciences has been successful is complex network studies [25, 26, 27, 28], and an area that has always benefited from contributions from both fields is Statistics [29, 30]. In fact, when the social sciences began to emerge as separate academic disciplines in the nineteenth century, the first systematic studies consisted in a large part on statistical measurements of various social processes, looking for the natural sciences to provide a model for empirical inquiry, free of religious dogma or prejudices.

The use of statistics is part of the wider positivist philosophy of science, that rejects speculation in favour of measurable empirical facts and cause-effects relations. However, this standpoint encompasses a wide variety of practices. Comte [31] (1798 - 1857) - arguably the first western philosopher of Science - was a major proponent of positivism that still didn't agree that different objects of studies should be studied with exactly the same tools, and didn't appreciate such an heavy reliance on Statistics. He sought to clarify the boundaries and methods of different sciences, and advocated for a hierarchical unity of science, in the sense that each science should encompass the methods of the one that appeared before, and go a step further in a ladder whose ultimate destination was a to establish a Sociology capable of coordinating the whole of knowledge and use it to further social progress. Among the sciences, two stood up for signalling a transition to a more perfect way of knowledge: Astronomy as the first science that was free

of metaphysical contaminations, and Biology as concerned with an organic whole, as Sociology should be. His ideas are clear in this quote [31]:

The first step to be taken in forming a positive philosophy is to classify the sciences. The first great division we notice in natural phenomena is the division into inorganic and organic phenomena. Under the inorganic we may include the sciences astronomy, physics, chemistry; and under the organic we include the sciences biology and sociology.

Comte

The recent discipline of Sociophysics [32, 33, 34, 35], in particular the formulation of opinion models, is part of the broad mosaic of complexity sciences [36], stressing the idea that a meaningful structure can emerge out of different elementary interactions, without any external coordination. The appearance of complexity science has in a sense promoted Physics - a branch of Physics - to an organic science, driving it closer to the interests of Sociology and Biology.

The micro/macro question - can a macroscopic structure emerge out of individual interactions between people with different opinions without external coordination? Is there some mesoscopic ingredient? - is an outstanding problem that touches upon issues like free will and the capacity of people to construct the social world, and in this sense it is related to the agency/structure question debated by major modern sociologists, in particular in Europe [37, 38, 39].

The construction of an opinion model requires the following basic building blocks.

1. The **parameters** that characterise each agent. In the simplest case the only attribute that characterises agents is an opinion. It can be either discrete or continuous, and uni- or multi-dimensional. As additional features agents can have different resistance/willingness to change, thresholds of interaction, etc...
2. The definition of an **interaction network**. Agents can interact via some particular topology, chosen independently of the opinions, or the formation of a link can depend on the opinions in confrontation.

3. The **outcome of an interaction**. Do opinions drift apart or do agents compromise? Do they follow the majority as long as it is a big majority, or do they follow a random neighbour?

4. The **update rule**. Are the opinions of all agents updated in the same step? Is the update sequential or synchronous?

Just by playing with these options, it looks trivial to construct a wide variety of models, and in fact the number of models is vast. [32, 34, 35]

However, the basic tenant of complexity is that a model is more than the sum of its parts, so that interesting and unexpected results can appear from different details. In this regard, the recourse to agent-based models is an useful tool where sometimes the tension between the preference for the elegance of minimalist models and the realism of very detailed ones is manifested, which also carries a decision about the goals of research. The contribution of Physics lies on its experience in this area, allowing it to discard all irrelevant details, for instance using insights learnt from several variations of the Ising model.

Models can be grouped in two big families, according to whether they consider that the opinion can take a finite set of values, or that it is a continuous real variable [40, 41, 42]. As examples of the models that treat opinions as continuous we can cite the Deffuant *et al.* [41] and the Hegselmann-Krause [42] models, and as examples of discrete models there is the Sznajd model [43] and several Ising-type variations.

For the sake of concreteness, and since we will return to them later in the thesis, we will review below two models. The first is a discrete model where agents change their opinion to adopt the majority opinion, which implies a simple kind of a threshold: we change opinions as long as a high enough number of neighbours have a different opinion. The second model is a continuous-opinion model where agents only interact with others as long as their opinions differ less than a given threshold.

1.4.1 A discrete model

A minimalist model of opinion formation [44], that incorporates the essential ingredients of opinion formation under the presence of an external forcing can represent the possible values of opinions in terms of two options (yes/no), and an interaction rule among neighbours that is a majority rule.

Additionally, we include an external signal in the model, modelling advertising, representing external factors that in a real society also affect opinion evolution, like political propaganda, advertising, or even a changing biological or economical environment.

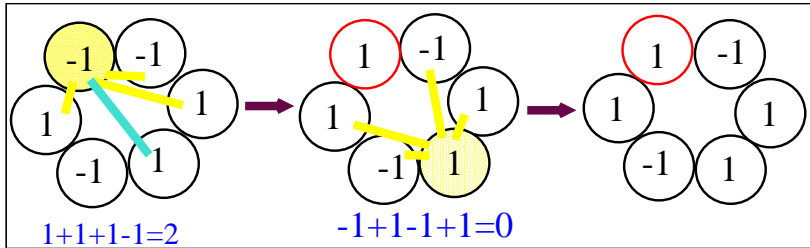


Figure 1.12. A process by the majority rule. The first yellow agent looks at its neighbours: three regular (yellow links) and an additional random link (blue), and adopts the sign of the majority. The second yellow agent doesn't change because the opinions of its neighbours are equally divided.

Let us consider a population of N individuals, which, at a given time t , can adopt one of two possible values, $\mu_i = \pm 1$, and evolve according to the following dynamical rule: at time t one of the variables, say μ_i , is chosen at random. The value of this variable is updated according to:

$$\mu_i(t + \tau) = \begin{cases} \text{sign} \left[\sum_j \mu_j(t) \right] & \text{w.p. } 1 - |a \sin(\Omega t)|, \\ \text{sign} [\sin(\Omega t)] & \text{w.p. } |a \sin(\Omega t)|, \end{cases} \quad (1.9)$$

(w.p. stands for “with probability”). In both cases, if the expression within square brackets is equal to zero, the variable does not change: $\mu_i(t + \tau) = \mu_i(t)$. The first case represents a weighted “majority-rule” in which the opinion of the individual is determined by the sign of average opinion of the

other agents j he interacts with. The second case represents the effect of an external forcing of frequency Ω – the intensity $a < 1$ determines the rate at which the signal influences the dynamics of the variable μ_i . The choice of the time step $\tau = 1/N$ defines the unit of time as N updates.

In the global coupling case and $a = 0$, the only possible outcome of these rules is an absolute consensus, whose value ± 1 depends on initial conditions. Again we encounter a bistable effective potential, where the depth of the potential well is related to the number of units that share the corresponding opinion. Unless the probability of interacting with the external signal is very high, there isn't any chance of being able to adjust to environmental changes. Thus the idea to introduce some kind of disorder, as we will see in Chapter 4.

1.4.2 A continuous model

The Deffuant *et al.* model [41] was introduced in the context of a proposal about improving agri-environmental policies in the European Union. A central assumption of the model is that agents only interact if their difference in opinion is not greater than a given threshold, the so-called *bound of confidence* ϵ . This homophily assumption [45, 46] intends to take into account social psychology concepts like cognitive dissonance or just the confidence in one's own opinion.

We consider that an agent i , taken from a set of $i = 1, \dots, N$ agents, holds at time t an opinion x_t^i expressing on a numerical scale his degree of agreement on a particular topic. Opinions are a continuous real variable that can take values on the interval $[0, 1]$: values close to 0 indicate a large degree of disagreement, and values close to 1 a large degree of agreement with the topic in question. At time $t = 0$, the opinions are independently drawn from a uniform random distribution in the interval $[0, 1]$. At time t two individuals, say i and j , are randomly chosen. If their opinions are closer than the bound of confidence ϵ , $|x_t^i - x_t^j| < \epsilon$, they become closer by an amount proportional to their initial difference:

$$x_{t+\tau}^{i(j)} = x_t^{i(j)} + \mu(x_t^{j(i)} - x_t^{i(j)}), \quad (1.10)$$

The parameter μ mainly determines the rate of convergence, and it is often taken to be $\mu = 0.5$, in which case agents compromise by adopting the same position.

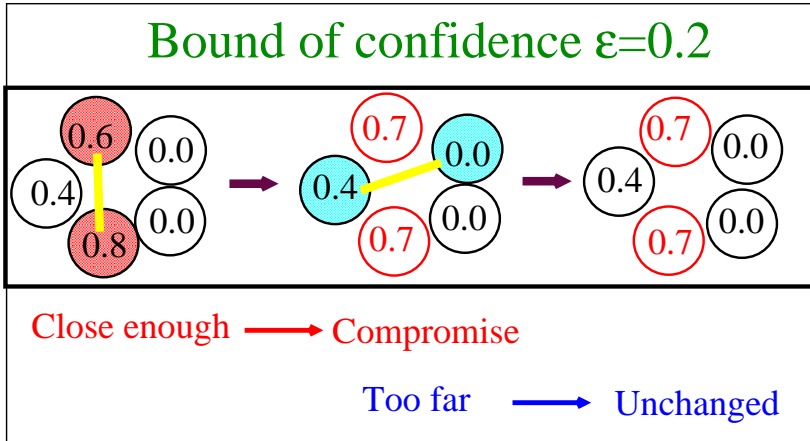


Figure 1.13. A sketch of the Deffuant *et al.* rules, given a bound of confidence $\epsilon = 0.2$. The last configuration with 3 final groups can not evolve any more because the groups can not interact: their opinions differ by more than the bound of confidence.

The major result of the Deffuant *et al.* model is that when the bound of confidence is low, we assist to a fragmentation of society into several non-interacting clusters, each one having a different opinion.

This conclusion can be reached using one of the two basic approaches to analyse the model: either to do agent-based Monte Carlo simulations considering a given number of agents, or take the $N \rightarrow \infty$ limit by considering density-based dynamics by means of a master equation [47, 48], which is a traditional statistical physics tool. The model does not evolve deterministically, since at any given time the interacting individuals are randomly chosen. Therefore, a given state X has to be described probabilistically, and the changes of its probability $P(X, t)$ at time t depend on the transition probability from one state to another. Or:

$$\frac{dP(X, t)}{dt} = \sum_{X'(\neq X)} [w(X|X'; t)P(X', t) - w(X'|X; t)P(X, t)] \quad (1.11)$$

where the flow from X' into X is assumed to be proportional to the probability $P(X', t)$ of state X' and to the transition rate $w(X|X'; t)$ from X' to X . This assumption that the transition rates depend only on the previous state of the system is applicable to the Deffuant *et al.* model, which is a Markov process.

The analysis of the master equation for the Deffuant *et al.* model was the approach followed in [47], whose main conclusions we briefly review below. Assuming with loss of generalisation that $\mu = 0.5$, $\epsilon = 1$ and opinions can take values in the interval $[-\Delta, \Delta]$, the authors [47] began by the definition of the fraction of agents $P(x, t) dx$ whose opinion lies in the range $[x, x + dx]$ at time t . The distribution $P(x, t)$ evolves according to the master equation:

$$\begin{aligned} \frac{\partial}{\partial t} P(x, t) &= \int \int_{|x_1 - x_2| < 1} dx_1 dx_2 P(x_1, t) P(x_2, t) \\ &\times \left[\delta \left(x - \frac{x_1 + x_2}{2} \right) - \delta(x - x_1) \right]. \end{aligned} \quad (1.12)$$

This dynamical rule conserves the total mass $M_0 = \int P(x, t) dx$ and the mean opinion $M_1 = \int x P(x, t) dx$, and the goal is to determine the nature of the final state $P_\infty(x) \equiv P(x, \infty)$. The authors [47] find that when the range of opinions Δ is large enough the distribution of opinions evolves into several non-interacting clusters, with the final distribution consisting of a series of groups at locations x_i with masses m_i :

$$P_\infty(x) = \sum_{i=1}^p m_i \delta(x - x_i) \quad (1.13)$$

This basically agrees with the simulation results, and in Fig. 1.14 we illustrate the bifurcation diagram showing the location of clusters in the

limit density versus the continuum of values of the bound of confidence ϵ . The diagram results from the integration of the master equation [47], with a transformation of variables as $\Delta = \frac{1}{2\epsilon}$, since in simulations it is usually the bound of confidence ϵ , and not the range of opinions Δ that varies and appears in plots, as we will see later in the thesis in Chapter 5.

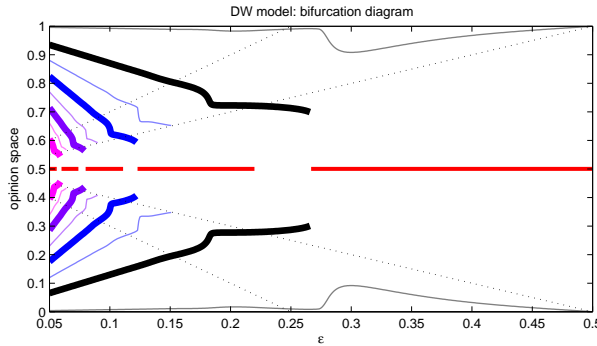


Figure 1.14. Bifurcation diagram of the Deffuant *et al.*, after a numerical analysis of the master equation of the model [47]. Figure reproduced from reference [40].

The numerical Monte-Carlo simulations don't necessarily agree exactly with the results of the master equation, due to finite-size fluctuations inherent in simulations. For instance, the minor clusters at the extremes and between major clusters that we observe in Fig. 1.14 often don't appear in agent-based simulations due to the small number of agents. This calls for the need to develop analytical methods that can take into account the fact that in social issues neither the infinite size [49] nor the asymptotic time limit usually make much sense.

The Deffuant *et al.* model has been modified by testing variations against all the major options. There are many possible extensions to this model: for instance, we can modify the underlying network of interaction [50], adopting some co-evolution rule; we can soften the bound of confidence [51], assume heterogeneous bounds of confidence [52], or add noise [48].

We can also modify the homophily assumption, or include repulsive interactions. The homophily hypothesis - the idea that individuals have a tendency to associate with those with whom they share more characteristics

- is a basic assumption of the model proposed by Axelrod [45], a mathematician (B.A) that upon turning into a political scientist (PhD) inspired many of present day sociophysics endeavours. Closely related to homophily, is the assumption that when individuals interact, their opinions have a tendency to converge. Some of the most well-known classical sociological theories [37,38], on the other hand, have conflict, negotiation or reflexivity at their core and for them order is not equated with a state of absolute consensus, but rather with some form of structure. In fact, the homophily assumption, although it has some grounding in social studies [46], it is not all empirically justified universally; and Axelrod's question [45] *If people tend to become more alike in their beliefs, attitudes, and behaviour when they interact, why do not all such differences eventually disappear?* should be read as *In case people tended to become more alike in their beliefs, attitudes, and behaviour when they interact, wouldn't all such differences eventually disappear?*

In recent proposals of opinion formation models, namely in modifications of the Deffuant *et al.* model, there has been interest in including the possibility of growing apart as a result of interaction, by adding *repulsive links* according to some rule. Jager *et al.* [53] interpret the bound of confidence as a latitude of acceptance of opinions, implying a willingness to move closer to those with whom we have some affinity and, accordingly, they define a latitude of rejection. Drawing upon a social judgement theory, they assume that opinions get farther apart if their difference is greater than a given threshold. A somewhat similar reasoning was behind some recent modifications of opinion models to incorporate repulsive links [54,55]. However, the confidence bound can also be interpreted as simply a threshold for interaction, with no further implications on its outcome. Huet *et al.* [56] apply the concepts of dissonance theory by considering two dimensions. The rejection/attraction disposition on one dimension is conditioned by the disagreement/agreement in another dimension. Regardless of their repulsive or attractive disposition, agents only interact if their opinions are close enough, the reasoning being that if an agent has an *a priori* rejection feeling towards someone, they feel uncomfortable if their positions are too close.

Still, the reasons for rejection being the outcome of interaction are many, and do not confine themselves to the opinions in confrontation, in one or another dimension. Rejection can result from a rational discussion,

when people realise that even though they share the same opinion, they do it for contradictory reasons, or from the desire to distinguish oneself from some individuals, to define a social status. In the present thesis, in Chapters 4 and 5, we model those many possible reasons as random, without considering another dimension, and we will show how they affect the reception to external messages. This topic, the influence of mass media, has also been the focus of several studies [57, 58], some of which addressed specifically the influence of disorder in the form of noise or diversity on the efficient spreading of propaganda [44, 59, 60]. The idea that disorder can enhance the transmission of information may look strange, and in next chapter we will tell how this idea originated.

2

Ordering role of disorder

To understand what we mean by disorder, imagine an ensemble of many units. In case they are identical, evolve under exactly the same environmental conditions, and are coupled in such a way as to induce a convergence of behaviour, they will obviously follow together the same evolution.

But in real Nature, systems live in a noisy environment. Furthermore, the existence of identical units is a mathematical abstraction, and the presence of repulsive links is not unusual. Surprisingly enough, some type of order can be enhanced by all these three types of disorder. A system needs to adapt itself to a changing environment, and some systems have some kind of threshold, as we saw in the last Chapter 1. When those systems are subjected to a sub-threshold forcing, they cannot display a significant response.

In this chapter we are going to show how disorder can help, by raising the signal above the detection level and therefore enhance the adaptation to the environment. Specifically, we will present the phenomenon of stochastic resonance and diversity induced resonance, by which noise or diversity can enhance the response to an external forcing.

2.1 Stochastic resonance

In what follows, we will present the main idea of stochastic resonance by illustrating the basic mechanism in both a bistable and an excitable system. For thorough reviews, see [61,62,63,64]. But first it is useful to clarify what is meant by *noise*.

The implementation of diversity involves the definition of what can be diverse and a choice of the type of diversity distribution [65]. Also, the inclusion of competitive interactions implies decisions about the underlying network and the type of repulsion and coupling. However, the terms diversity and repulsive links are straightforward - even if their implementation is not.

Noise is a more ambiguous concept that entered the scientific arena at the beginning of the XX century. As it is often the case of scientific concepts, it did so at almost the same time by different independent routes. In 1900 Louis Bachelier presented his PhD thesis *Théorie de la Spéculation* [66], on modelling prices fluctuations in the French Stock Market. Arguing that prices fluctuations were a sequence of uncorrelated random events that should be described probabilistically, he formulated an equation for the drift of prices that introduced the concept of random walk - a term that was to be coined 5 years later by Pearson [67]. That same 1905 year, a foundational paper by Einstein [68] marked the entrance of noise in Physics. Certainly unaware of Bachelier work, he arrived at a similar formalisation, though his interests were quite different: the same equation governing the drift of prices could be applied to the drift of microscopic particles in water ¹.

Shortly after Einstein's paper, in 1908, Langevin developed an alternative approach interpreting the fluctuations of the position as the result of two forces: a viscous resistance plus a fluctuating force independent of velocity. While the viscous resistance follows Stokes law, the fluctuating force depends on random factors and its time average is zero. The equation that describes the motion of a particle is:

¹Unfairly as it may be, the history of Science doesn't record who had the first idea, but those who are considered to have had a lasting impact, at a given moment. As the history of *noise* is being rewritten, names like Thiele or Sutherland are coming to occupy its place as earlier or contemporary proponents of some concepts [69]

$$m\ddot{x} = -\gamma\dot{x} + \alpha\zeta(t) \quad (2.1)$$

where the stochastic term $\zeta(t)$ satisfies the properties of being zero on average and uncorrelated, or: $\langle \zeta(t) \rangle = 0$ and $\langle \zeta(t_1)\zeta(t_2) \rangle = \delta(t_2 - t_1)$

These formalisations came to place noise at the heart of many phenomena as a label for what we don't know, since it is too fast and complicated, and the efforts in the following decades were devoted to formalise, describe, and when possible control, confine and predict the action of noise, still considered mostly as an unavoidable nuisance.

That changed in 1981 with the discovery of the phenomenon of *stochastic resonance* [70,71]. This is a somehow counterintuitive effect arising from the cooperation between deterministic dynamics and dynamical disorder or noise. By this effect, a system's coherent response to a weak signal can be optimally amplified by an intermediate level of noise. Initially proposed to explain the periodicity of ice ages, [70,71], it has broadened its focus to include a vast amount of systems and situations, in particular in biological settings [72].

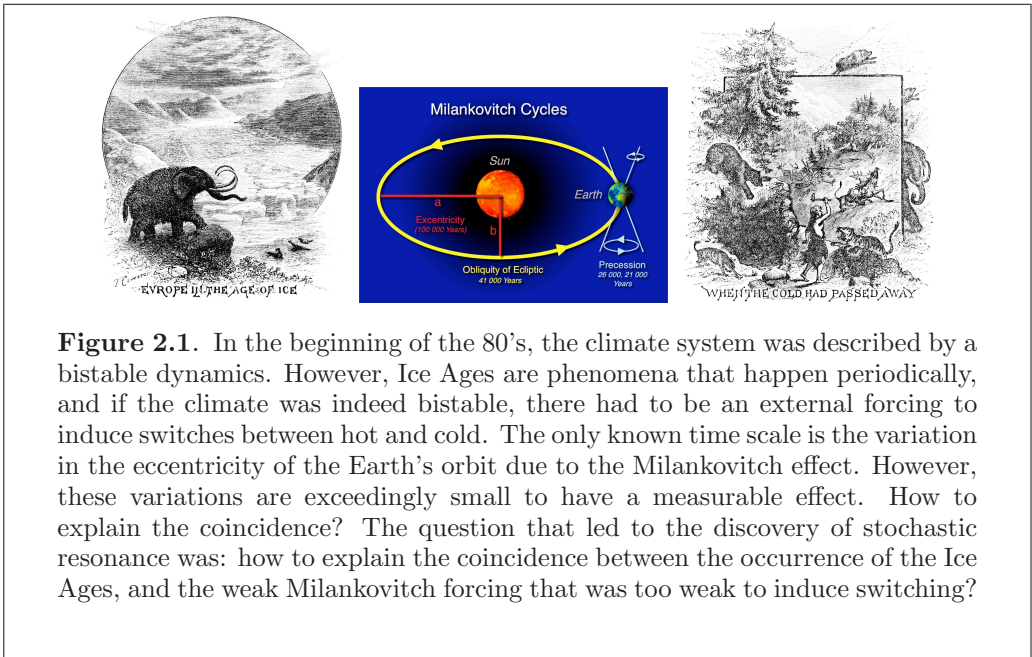


Figure 2.1. In the beginning of the 80's, the climate system was described by a bistable dynamics. However, Ice Ages are phenomena that happen periodically, and if the climate was indeed bistable, there had to be an external forcing to induce switches between hot and cold. The only known time scale is the variation in the eccentricity of the Earth's orbit due to the Milankovitch effect. However, these variations are exceedingly small to have a measurable effect. How to explain the coincidence? The question that led to the discovery of stochastic resonance was: how to explain the coincidence between the occurrence of the Ice Ages, and the weak Milankovitch forcing that was too weak to induce switching?

2.1.1 Stochastic resonance in a bistable system

The typical mechanism of stochastic resonance involves a bistable system and a matching of time scales that occurs at intermediate levels of noise: the half-period of the forcing, and the residence time inside a potential well, that depends on noise according to Kramers rate.

Noise is traditionally introduced to represent the unknown, since noise are fast random variations, whatever their origin. Therefore, we introduce noise in Eq. 1.3 (with $a = b = 1$) that describes a forced bistable dynamics and see what happens. The standard model that exhibits stochastic resonance is given by a Brownian particle moving in a bistable potential driven by a weak periodic forcing.

$$\frac{dx}{dt} = x - x^3 + A \sin(\Omega t) + \sqrt{D} \eta(t) \quad (2.2)$$

where $\eta(t)$ is a Gaussian random variable with mean $\langle \eta(t) \rangle = 0$ and correlation $\langle \eta(t) \eta(t') \rangle = \delta(t - t')$, and D is the noise strength.

Noise will lead to transitions between the two wells and in case its strength is small compared with the height of the potential barrier, the rate depends on the noise strength D , according to Kramer's rate [73, 74], given by:

$$W = \frac{\sqrt{|\ddot{V}(0)| |\ddot{V}(1)|}}{2\pi} \exp\left(\frac{-2\Delta V}{D}\right), \quad (2.3)$$

where the dots denote double differentiation with respect to x and ΔV is the energy difference between the maximum of the potential at 0 and the potential minimum at 1.

When we introduce a periodic signal, the potential becomes modified as $V'(x) = -\frac{x^2}{2} + \frac{x^4}{4} - Ax \sin(\Omega t)$, and if $Ax \ll \Delta V$, the potential is unable to destroy bistability (Chapter 1).

As the potential changes, the transition rate becomes accordingly modulated. Since Kramers formula is formulated for a time independent potential, this holds for the case where the external signal frequency is sufficiently

low - $\Omega \ll W$ -, which is known as the *adiabatic limit* of the time dependent case.

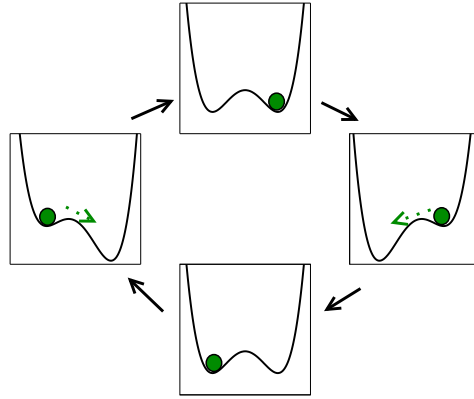


Figure 2.2. A schematic illustration to explain the mechanism of stochastic resonance. The potential wells represent stable attractors, and the ball, the state of the system. The periodic signal introduces a bias in the shape of the potential, deepening one of the potential wells in turn. The ball moves from a well to the other under the action of noise (the dashed arrow) when the barriers are lowered, that is, every half-period.

In Fig. 2.2 we illustrate the basic mechanism of stochastic resonance. If the level of noise is too low, there will be just a few hopping between the two wells (Fig. 2.3, a). When the noise is too high, the system behaviour will be completely aleatory, with random hopping between the two states. The simple, yet surprising, idea that underlies stochastic resonance is that between these two extremes, there exists a level of noise for which the cooperation between noise and forcing is optimal. This was observed in the numerical experiments of the original works [70, 71], and was finally understood in 1989 [75] as corresponding to a matching between the two time scales involved: the half-period of the forcing, and the mean residence time τ , that, being on average the inverse of Kramer's rate - $\langle \tau \rangle = 1/W$ - depends on the level of noise. [73] When that happens, the period of oscillations between the climate states matches the period of the signal, as seen in Fig. 2.3, b) and c).

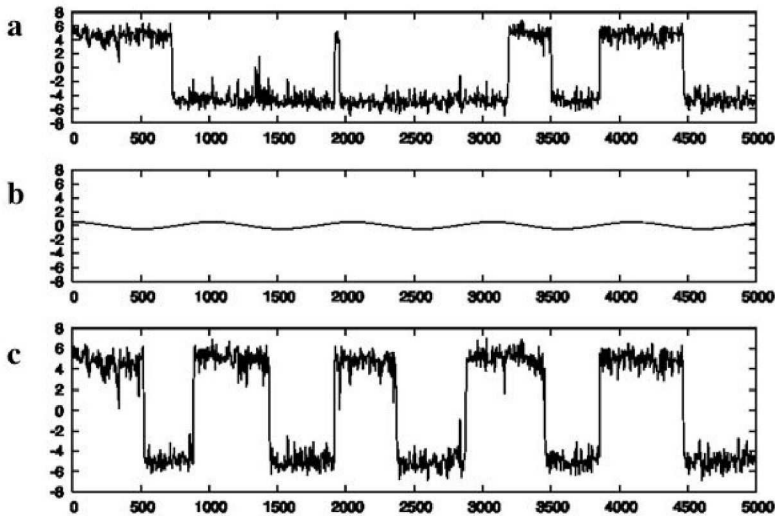


Figure 2.3. The small periodic forcing synchronises the random switching from one state to the other. Source: R. Benzi, *Stochastic Resonance: from climate to biology*, eprint arXiv:nlin/0702008, 2007.

2.1.2 Excitable systems

Even though the idea of stochastic resonance was developed with bistability in mind, the example above has shown the phenomenon to be rooted in three basic ingredients: 1) a system with a threshold 2) a weak subthreshold signal and 3) noise. In fact, the scope of stochastic resonance has developed well beyond its original proposal, and has found some of the most interesting applications in biological settings [72], and most notably in neuronal contexts [76, 77], usually modelled as excitable systems (Section 1.3).

Both bistable and excitable systems have a threshold that can be surpassed by noise at a given time-scale [78]. The signal periodically modulates the threshold (Fig. 2.4), while a noisy excitable system can leave the rest state with a noise-induced rate, doing it more easily when the threshold is smaller.

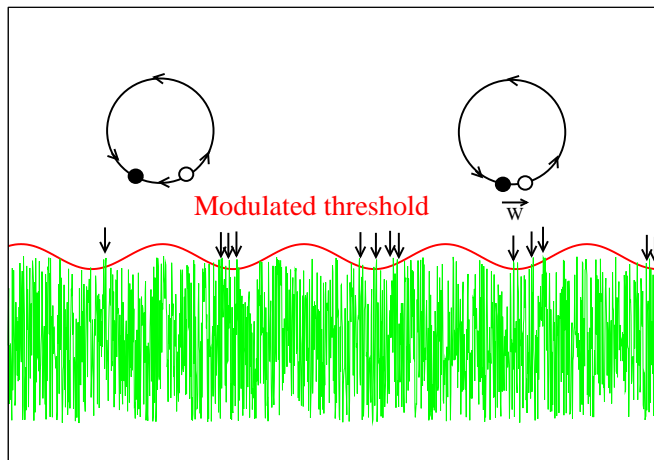


Figure 2.4. A schematic illustration of the basic mechanism of stochastic resonance in an excitable system. The threshold, given by the distance between the stable state (black circle) and saddle (white circle), is modulated by the signal. The arrows signal the times where the noise (represented in green) is able to surpass the threshold and induce a firing.

Instead of counting transitions between states, the response of the system is given by a train of pulses that happen when the modulated threshold (see Fig. 2.4) is crossed:

$$x(t) = \sum_i \delta(t - t_i), \quad (2.4)$$

There are two differences in the response relative to the bistable case. On one hand, the firing events get synchronised with the period of the signal, not with the half-period. When noise surpasses the level of the periodic modulated threshold (Fig. 2.4) a pulse is emitted. Since this happens every period of the signal, the relevant time matching is between the noise-induced transition rate W and the period of the signal.

Another difference [79] with respect to stochastic resonance in the standard bistable model is that we notice a double peak in the response. This effect has been called *double stochastic resonance* and has its origins in the fact that even in the absence of an external signal noise can induce a frequency of oscillations in excitable systems [17]. When the signal frequency

matches the noise-induced eigenfrequency a resonance occurs.

2.2 Measures

A number of measures have been proposed to indicate (Fig. 2.5) the optimal response as a function of the noise level, such as the signal-to-noise ratio [80], the residence time distribution [81], information theoretic measures [82,83], or the spectral power amplification [84].

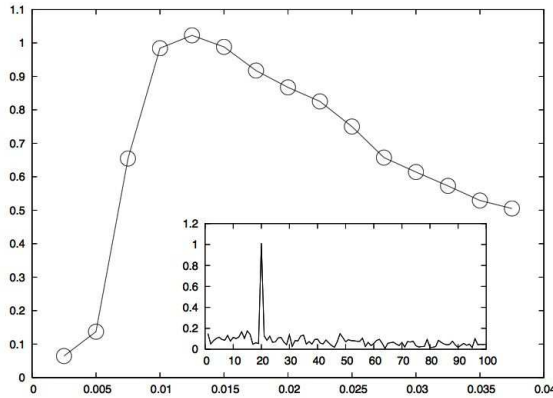


Figure 2.5. The figure illustrates a good measure of stochastic resonance, that shows a maximum for a given value of D , in the x-axis. Namely, it shows the the power spectrum evaluated at the signal frequency for different values of the noise amplitude D . In the inset we show power spectrum $P(\omega)$ for the optimal noise amplitude: at the signal frequency, this measures exhibits a peak. Source: R. Benzi, Stochastic Resonance: from climate to biology, eprint arXiv:nlin/0702008, 2007.

In the case of a periodic signal, a good measure of stochastic resonance should exhibit a peak for the value of noise at which $x(t)$ is oscillating with the signal frequency. Therefore, it is natural to start with computing the **power spectrum** $P(\omega)$:

$$P(\omega) = \frac{1}{2\pi t_{max}} \left| \int_0^{t_{max}} dx(t) e^{-i\omega t} \right|^2 \quad (2.5)$$

The phenomenon of stochastic resonance manifests itself in a peak of the power spectrum at the signal frequency Ω , for an optimal level of noise.

If we want to quantify the phenomenon against various levels of noise, we can, from the power spectrum, calculate the **signal-to-noise-ratio** (SNR) as:

$$SNR = \frac{P(\Omega)}{P_N(\Omega)}, \quad (2.6)$$

where $P(\Omega)$ is the output power spectrum evaluated at the signal frequency Ω , and $P_N(\Omega)$ is the power spectrum of the noisy background.

In general, the contribution to the power spectrum of the intra-well motion - the fact that potential minima vary with the time-dependent signal - is negligible with respect to the power of the switching events between the wells. For a vanishing noise strength the power $P_N(\Omega)$ tends to zero, as the system can no longer transition between the wells. Meanwhile, the $P(\Omega)$, although small, is finite due the contribution of the intra-well motion. Therefore, the SNR diverges. We can avoid this divergence by digitalising the signal and neglecting the intrawell motion, or then we can simply use another measure of resonance.

A measure that doesn't suffer from the divergence problem is the **spectral power amplification factor** [84], defined as the ratio of the output to input power at the corresponding driving frequency. This measure assumes that asymptotically the response of the system will oscillate with the frequency Ω of the signal, being given by $\langle x(t) \rangle_a = \bar{x} \cos(\Omega t - \phi)$. The spectral power amplification R is:

$$R = \frac{P(\Omega)}{P_S(\Omega)} = 4A^{-2} |\langle e^{-i\Omega t} x(t) \rangle|^2 \quad (2.7)$$

where $\langle \dots \rangle$ is a time average. R is roughly proportional to the amplitude of the oscillations of $x(t)$, and since it depends on the driving period it can be related to the synchronisation between output and input.

A more direct way to quantify the degree of synchronisation with the signal is to simply compute the **distribution of residence times** in the wells in case of bistable systems, or in the stable state in case of the excitable system. In the adiabatic limit and in the unforced case the distribution of the time spent on a metastable or rest state decays exponentially with t ,

reflecting the random switches induced by noise. A periodic signal leads to a superposition of Gaussian-like peaks over the envelope of the exponentially-decreasing distribution. The center of each peak is located at $T_n = (n-1)T_\Omega$, where T_Ω is the signal period and $n = 1, 2, 3, \dots$. At the optimal level of noise where stochastic resonance is observed there is an enhancement of the peak corresponding to the signal half-period in the case of bistable systems or to the period in the case of excitable systems, which means that the system leaves the rest state with the periodicity of the signal.

In real life, many signals are not periodic [85] and measures based on the Fourier spectra are not so relevant or applicable. In such cases, we can use **information theoretic measures** such as the Fisher information.

As mentioned before, the concept of stochastic resonance has triggered a wide extension of studies and applications well beyond climate studies, in such diverse areas as lasers [80], SQUIDS [86], or neurons [76], just to mention a few [61], and it has been found to play a role even in systems well beyond the traditional setting of a bistable system subjected to a periodic signal, to include excitable [87] or monostable [88] systems, non-periodic forcing [85], etc.

Another, more recent, related line of research considers the role that other types of disorder, such as quenched noise (identified with heterogeneity or disorder), can play in producing a resonance effect in systems with many units. Tessone *et al.* [89,90] have shown that in generic bistable or excitable systems, an intermediate level of diversity in the individual units can enhance the global response to a weak signal. This will be the subject of the next section.

It was shown in reference [89] that diversity or heterogeneity, in the form of quenched disorder, can play the same constructive role of noise as a signal amplifier. The optimal diversity doesn't preclude the existence of two stable states in the unperturbed system, but changes its position and the height of the potential barrier that separates them. The region of optimal response coincides with a degradation of order, and the optimal response corresponds to an increase in the amplitude of oscillations, and not to a matching between two time scales.

The authors [89] considered two prototypical examples of a bistable

and an excitable system, and in what follows we will look into more detail at the bistable example, as the excitable case follows a similar reasoning.

2.3 Diversity induced resonance

As in the last section, we will review the effects of diversity in the response of a forced bistable model.

Instead of a single unit, let us consider an ensemble of N globally coupled bistable systems, whose dynamics is given by

$$\dot{x}_i = x_i - x_i^3 + a_i + \frac{C}{N} \sum_{j=1}^N (x_j - x_i) \quad (2.8)$$

where $x_i(t)$, $i = 1, \dots, N$ is the position of the i -th unit at time t and C is the coupling strength. Diversity is related to the dispersion in the distribution of the parameter a_i that controls the relative stability of each individual bistable state. We assume that the a_i 's follows a probability distribution function $g(a)$ that satisfies $\langle a \rangle = 0$, $\langle a_i a_j \rangle = \delta_{ij} \sigma^2$, where the standard deviation σ measures the diversity.

We will be interested in the macroscopic variable $X(t) = \frac{1}{N} \sum_{i=1}^N x_i(t)$, the average position of the units. In the globally coupled case considered here, the coupling amongst units appears only through this macroscopic quantity:

$$\dot{x}_i = CX + (1 - C)x_i - x_i^3 + a_i \quad (2.9)$$

Averaging eq.(2.9) over all units, we obtain

$$\dot{X} = X - \frac{1}{N} \sum_i x_i^3 \quad (2.10)$$

As we see, diversity is no longer present in an explicit form in this equation. We recover its influence when we express [91] the position of each unit in terms of a deviation δ_i from the average position as $x_i = X +$

δ_i . Introducing the variance of the deviations $M = \frac{1}{N} \sum_i \delta_i^2$, we relate disorder and diversity when we compute the value of M by averaging over the probability distribution of a_i , as $M(t) = \int da g(a) [x(t; a) - X(t)]^2$.

If we assume that δ_i are distributed according to an even distribution, or, alternatively, that δ_i is small and we can neglect the third moment, we get, using eq. (2.10), the equation for the macroscopic variable X that describes a bistable system.

$$\dot{X} = X(1 - 3M) - X^3. \quad (2.11)$$

The effective potential is given by

$$V(X) = -\frac{X^2}{2}(1 - 3M) + \frac{X^4}{4}. \quad (2.12)$$

and the equilibrium points are at $X_{\pm} = \pm\sqrt{1 - 3M}$.

As M increases, the system goes from bistable to monostable, passing through a region of bistability that is characterised by a lower barrier height and an approximation of the two potential wells, as shown in Fig. 2.6. The influence of diversity on the response of the system to a weak external signal can already be guessed. If $M = 0$, the units are completely ordered and a weak signal can only induce small oscillations inside a well, as explained in the previous chapter. When disorder is too high, namely for $M > 1/3$, the potential becomes monostable and the response consists of small oscillations within that potential well. By contrast, at an intermediate level of the disorder M the potential is still bistable, but the potential barrier starts to decrease (Fig 2.6, thereby turning the signal supra-threshold. Therefore, an optimal response appears for an intermediate level of diversity: the desirable consequence of lowering the barrier, and the not so desirable consequence of approximating the potential wells. For a given signal, the balance is achieved when the barrier is low enough for the signal to become supra-threshold and the potential wells are still sufficiently distant to elicit a big amplitude of oscillations. Fig. 2.7 illustrates the coincidence between the transition order-disorder and an increase in the response of the system that is at the heart of the phenomenon.

The effect translates itself in an increase in the amplitude of oscillations of the macroscopic variable (depicted in bold line in the Fig. 2.8). When there isn't any disorder (upper panel Fig. 2.8) all the units execute small oscillations within a well. When diversity is too high (lower panel in the same figure) the units manifest all types of disorganised behaviour: some remain within one of the wells, while others jump between the two: the end result is that the average position oscillates around zero. It is in the middle panel of Fig. 2.8 that the optimal diversity enables an almost synchronised hopping between the two wells.

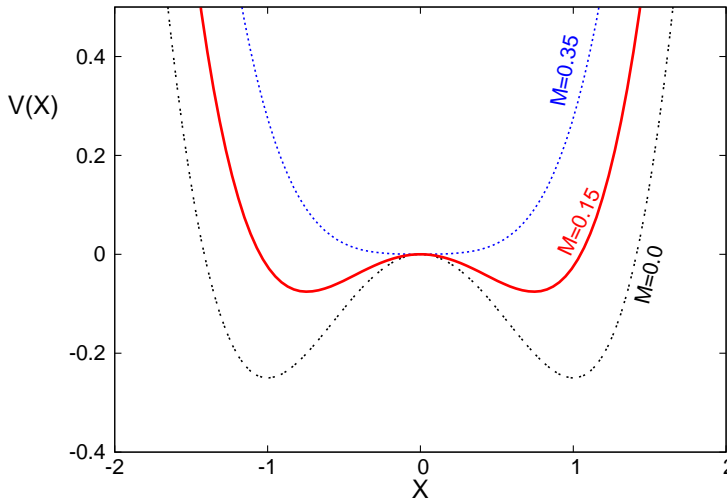


Figure 2.6. The variation of the potential shape as disorder increases. For an intermediate level of disorder, the potential is still bistable, but the wells are closer and the barrier is lower. The optimal level of disorder corresponds to a balance between a desirable low barrier and a not so desirable approximation of the wells.

Whereas in the case of stochastic resonance in a single unit system the optimal noise is the one for which the rhythm of the system matches the frequency of the signal, here the optimal diversity is the one that amplifies the amplitude of oscillations, because once the stable states are reached, the only source of movement in the system is the external forcing, and any oscillation happens at its rhythm.

Therefore, a convenient measure of resonance evaluates the amplitude

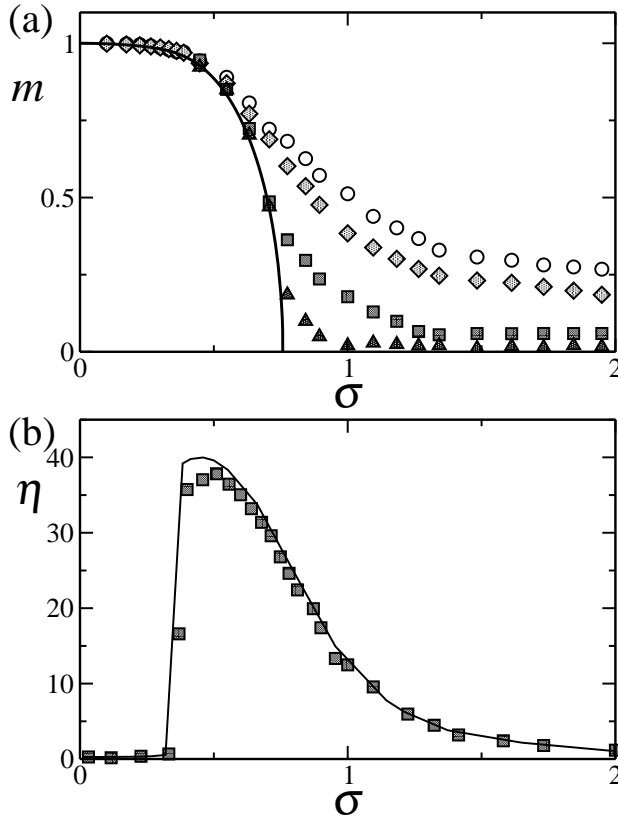


Figure 2.7. The resonance peak (lower panel) appears close to an order-disorder transition (upper panel). Source: [90].

of oscillations at the frequency of the signal. As a way of quantifying the coherence of the global response to a periodic forcing $A \sin(2\pi t/T)$, we chose the spectral amplification factor R , defined as the ratio of the output to input power at the corresponding driving frequency Ω [84]:

$$R = 4A^{-2} |\langle e^{-i2\pi t/T} X(t) \rangle|^2 \quad (2.13)$$

where $\langle \dots \rangle$ is a time average, and $X(t)$ is the global response (system's magnetisation): $X(t) = \frac{1}{N} \sum_{i=1}^N x_i(t)$.

Large values for R indicate that the global variable $X(t)$ follows the external forcing, while small values of R indicate a small influence of the

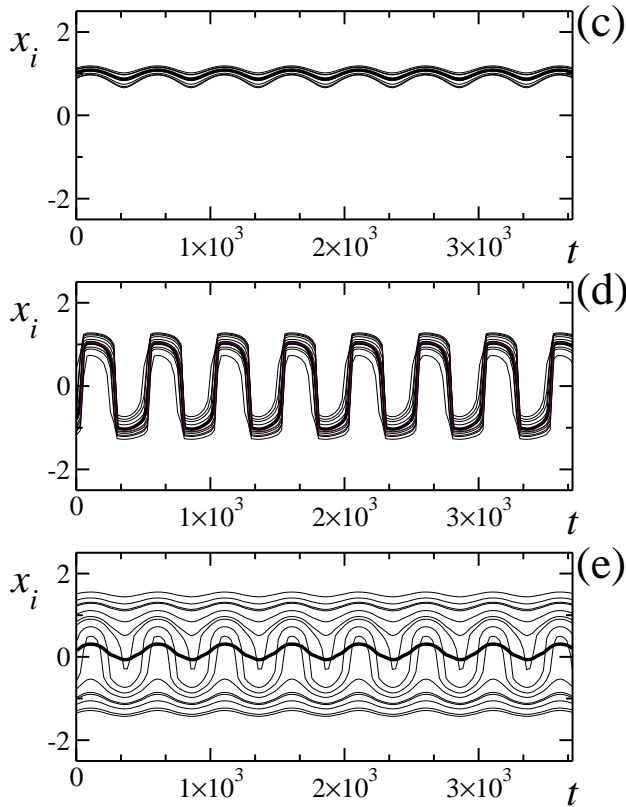


Figure 2.8. The resonance corresponds to an increase in the amplitude of oscillations (middle panel). Source: [90].

forcing on the global variable. R is roughly proportional to the amplitude of the oscillations of $X(t)$: if $R < 1$, then the amplitude of the response is less than that of the signal, and vice versa for $R > 1$.

2.4 Is diversity required at all?

The previous section was called *diversity induced resonance*, and the microscopic explanation of the resonance relies on diversity itself, namely, on the assumption that diversity assures that there will always be some units that

can respond to the forcing. When the units are identical (and both states are equally stable for all units) the signal is sub-threshold and, because of the coupling, all units remain in the same state. As diversity increases, the signal becomes, for half of its period, supra-threshold for some of the units and forces those units to jump from their less stable state to the other. In the other half of the period, the signal becomes supra-threshold for a different set of units. The units which follow the signal pull the other units, to whom they are attractively coupled, and the collective effect is that a significant fraction of the units is able to respond to the external forcing.

Most interestingly, any source of disorder that fulfills very generic requirements such as leading to symmetric deviations around the average position of the system, should lead to the same resonance effect. Thus, disorder induced resonance provides a theoretical framework that can encompass a wide range of different sources of disorder, including noise in extended systems.

And yet we saw that macroscopically the relevant parameter that optimises the response is the parameter M , that simply measures disorder in the position of the units, whatever its origin. In fact, in the derivation of Eq 2.11 the only assumption was that either the deviations from the mean field are so small that the third moment can be neglected, or, alternatively, that they follow an even distribution. Not only does this make sense in the particular case of an evenly distributed diversity parameter a_i , but it is also applicable to a wide range of situations that don't imply any diversity. In general this loss of entrainment can also be induced by noise (in the case of extended stochastic resonance [92, 93]), competitive interactions, irregular network of connectivity or by some other source.

To better compare the effects of stochastic and diversity induced resonance, we focused here on a bistable system like we did in the last chapter, but we stress that the same diversity induced resonance effect has been found in different types of systems, such as excitable systems [89], or linear oscillators [94].

Along these lines, the role of the heterogeneous complex network topology in the amplification of external signals has been addressed in [95], and Chen et al. [96] have shown how structural diversity enhances the cellu-

lar ability to detect extracellular weak signals. The interplay between noise and diversity in an ensemble of coupled bistable FitzHugh-Nagumo elements subject to weak signal has been considered in [97]. The role of diversity in heterogeneous excitable media was considered in [98] where the author demonstrates that diversity in a parameter can cause the emergence of global oscillations from individually quiescent elements in a system of van der Pol-FitzHugh-Nagumo elements.

But generic as it is, the assumption of an even distribution or small deviations from the mean field is not universally applicable. It cannot apply, for instance, when we assist to the formation of many metastable states in discrete systems, which can happen when there is frustration due to the presence of repulsive interactions. Does this mean that the disorder induced by competitive interactions is not suitable to get optimal responses, or does it lead to responses with different characteristics? The remainder of the thesis will be devoted to the resolution of this question.

Part II

Original Research

The presence of both repulsive and attractive interactions is not unusual in systems with many units. The existence of inhibitory and excitatory connections in the brain neurons, or a society with friends and enemies are examples of such systems. The emergence of a coherent behaviour in the absence of forcing and in the presence of repulsive links was treated in [99]. There it was shown that one can obtain a more coherent behaviour, in the form of synchronised pulsing, by adding an optimal amount of long-range repulsive couplings in a mixture of excitable and oscillatory units described by the Hodgkin-Huxley model. In the same reference, a similar improvement of the internal coherence in an Ising model with a simple majority-like dynamics in the presence of long-range repulsive links was also shown. Also in [100], an intermediate amount of repulsive links was found to trigger collective firing in an ensemble of active-rotators [18] in the excitable regime. The combined effects of noise and variability in the synchronisation of neural elements has been studied in [101], while reference [102] unveils the general mechanism for collective synchronised firing in excitable systems arising from degradation of entrainment originated either by noise, diversity or other causes.

Additionally, as mentioned before, the fact that people's opinions can diverge as a result of interaction is a topic of increasing interest.

In this Part of the thesis, we will show how these repulsive links that are present in so many systems can enhance the reception to an external forcing.

3

The ϕ^4 model

Focusing on a double-well model, Perc *et al.* [103] studied the combined effect of dynamic and static disorder, where static disorder was either diversity, the presence of competitive interactions, or a random field. Namely, they showed that the random presence of repulsive bonds decreases the level of noise warranting the optimal response.

It is the purpose of this work to show that competitive interactions can actually replace -not merely enhance- noise in its constructive effect. We will see that competitive interactions can replace noise or diversity in their constructive effect. We focus on the generic globally coupled bistable system, and show that the addition of an intermediate fraction of repulsive links can increase the sensitivity to an external forcing. In particular, we numerically demonstrate that the response of the macroscopic variable to an external signal, is optimal for a particular proportion of repulsive links. Furthermore, we show that a resonance also occurs for other system parameters, like the coupling strength and the number of elements. Resorting to a spectral analysis of the Laplacian [104] matrix, we locate the amplification region, and unveil the mechanism of resonance.

The outline of this chapter is as follows: in section 3.1 we will introduce the model; we show that there is an amplification and discuss how the amplification mechanism is related to a break of stability in section 3.2; and how we can predict the resonance peaks in section 3.3; Conclusions are

drawn in section 3.4.

3.1 The bistable model

We consider the same system of N globally-coupled bistable units described by real variables $s_i(t)$, $i = 1, \dots, N$ under the influence of a periodic forcing.

$$\frac{ds_i}{dt} = s_i - s_i^3 + \frac{C}{N} \sum_{j=1}^N J_{ij}(s_j - s_i) + A \sin(2\pi t/T), \quad (3.1)$$

where t is the dimensionless time, C measures the coupling strength amongst the different units and $A \sin(2\pi t/T)$ is a periodic external signal with amplitude A and period T .

The interaction matrix J_{ij} reflects the presence of attractive and repulsive interactions between the units. More specifically, we adopt the following values at random:

$$J_{ij} = J_{ji} = \begin{cases} -1, & \text{with probability } p, \\ 1, & \text{with probability } 1 - p. \end{cases} \quad (3.2)$$

The single-element case, $N = 1$, with added noise is the prototypical double-well potential system for which stochastic resonance was first considered. The case without repulsive interactions, $p = 0$, can still be described globally by a bistable potential (see next section) and, in the presence of noise, has been widely studied as a model case for stochastic resonance in extended systems [70]; it has also been considered, in the presence of a random field, as a prototypical example for the diversity-induced resonance effect [89]. For $p > 0$, the coexistence of attractive and repulsive interactions is characteristic of a wide class of spin-glass-type systems [105].

We will focus on the macroscopic variable $S(t) = \frac{1}{N} \sum_i s_i(t)$, and use as a measure of response the spectral power amplification factor [84], defined as the ratio of the output to input power at the corresponding driving frequency:

$$R = 4A^{-2} \left| \langle e^{-i2\pi t/T} S(t) \rangle \right|^2 \quad (3.3)$$

where $\langle \dots \rangle$ is a time average.

3.2 Signal amplification

It is convenient to analyse first the structure of the steady-state solutions for the system of equations (3.1) in the non-forced case, $A = 0$. The dynamics is relaxational $\frac{ds_i}{dt} = -\frac{\partial V}{\partial s_i}$ [106], being

$$V(s_1, \dots, s_N) = \sum_{i=1}^N \left[-\frac{s_i^2}{2} + \frac{s_i^4}{4} + \frac{C}{4N} \sum_{j=1}^N J_{ij} (s_i - s_j)^2 \right] \quad (3.4)$$

the Lyapunov potential. Therefore, the stable steady states are the configurations (s_1, \dots, s_N) which are absolute minima of V . If there are no repulsive links, $p = 0$, the Lyapunov potential has just two equivalent minima at $s_i = +1$ or $s_i = -1$, $\forall i = 1, \dots, N$ and, hence, the macroscopic variable will reach the stable asymptotic values $S = +1$ or $S = -1$, depending solely on the initial conditions. Thus we have a typical situation of bistability. As p increases, the absolute minima depart from $S = \pm 1$ and, furthermore, new metastable minima of V appear. The dynamical equations (3.1) may or may not get stuck in one of these minima, depending on initial conditions and the particular realisation of the coupling constants J_{ij} . We have used throughout the paper random initial conditions drawn from a uniform distribution in the $(-1, 1)$ interval, although we have observed the same type of phenomenology when using other random, but still symmetric, distributions such as truncated Gaussian or the Johnson family of distributions.

From our simulations we compute numerically the probability distribution $P(S)$ of the final values of S reached during the dynamical evolution for different realisations of the coupling constants J_{ij} and initial conditions. This is plotted in Fig. 3.1. We can observe a second-order phase transition as the average value $\langle |S(t)| \rangle$ vanishes for $p > p_c \approx 0.44$. One can interpret these results in terms of an effective potential $V_{\text{eff}}(S) \equiv -\ln P(S)$ which has two equivalent absolute minima at $S = \pm S_0(p)$, where $1 > S_0(p) > 0$ for $0 < p < p_c$, and one absolute minimum at $S = 0$ for $p \geq p_c$. The effective potential V_{eff} presents many relative minima for all values of $p > 0$, especially in the critical region $p \approx p_c$, a typical situation for the spin-glass models [105].

We now turn on the forcing $A > 0$ and study the system response,

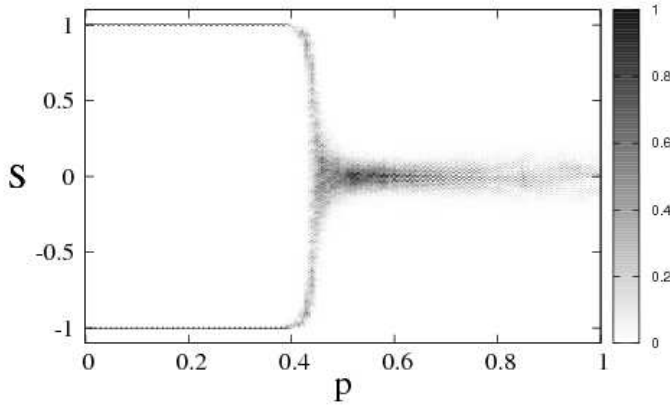


Figure 3.1. We plot in a gray scale the stationary probability distribution $P(S)$, in the absence of external signal $A = 0$, coming from numerical simulations of Eqs. (3.1). For better viewing, the distribution has been rescaled by its maximum value at each p . The data show that at $p < p_c \approx 0.44$ the system presents two equivalent absolute maxima for $P(s)$, while there is only one absolute maximum for $p > p_c$. We note, however, that there are many relative maxima for all values of p , specially around the region $p \approx p_c$. Other parameter values are: $N = 200$, $C = 8$. The probability has been computed after averaging over 1000 realisations of the couplings J_{ij} and initial conditions drawn from a uniform distribution in the interval $(-1, 1)$. For the numerical integration we used a fourth-order Runge-Kutta method with a time step $\Delta t = 0.1$.

as measured by the spectral power amplification factor R defined above, Eq. (3.3). Consider first the case $p = 0$. For a small, sub-threshold, amplitude A the macroscopic variable $S(t)$ will just execute small oscillations of amplitude proportional to A around the stable values $S = +1$ or $S = -1$. As A increases beyond the threshold value $A_o \approx 0.4$ the amplitude of the forcing is large enough to induce large jumps of the macroscopic variable from $S \approx -1$ to $S \approx +1$ and vice versa. This change of behaviour at A_o appears as a sudden increase in the value of R , as shown in the inset of Fig. 3.2. As the same inset shows, similar behaviour is observed for $0 < p \lesssim p_c$: the response shows a sudden increase for a particular value of the amplitude A and then decreases monotonically. For $p > p_c$, the response is very small and almost independent on the value of A .

More interesting, and the main result, is the dependence of R on the probability p of repulsive links, main plot in Fig. 3.2. We note that there is an optimal probability of repulsive links that is able to amplify signals whose amplitude would be sub-threshold in the case $p = 0$, i.e. $A < A_o$. For suprathreshold signals, $A > A_o$, the presence of repulsive links does no longer lead to enhanced amplification. As shown in the figure, the optimal value for amplification is close to the critical value p_c signalling the transition from bistability to monostability in the non-forced case. The optimal amplification as a function of p can clearly be observed in Fig.(3.3) which shows representative trajectories for $p = 0$ (small oscillations around the value $S = +1$), $p = p_c$ (large oscillations between $S \approx +1$ and $S \approx -1$) and $p = 1$ (small oscillations around $S = 0$).

The existence of an optimal value of the fraction of repulsive p for which signal amplification is maximum is somehow reminiscent of the stochastic resonance phenomenon. There are some important differences, however. While in stochastic resonance, the response R shows a maximum as a function of period, resulting from the matching between Kramers' rate and the forcing half-period, in our case the same optimal disorder p amplifies responses to signals of every period, as shown in Fig. 3.4. When the signal is slow enough, the system has time to respond to the fuller extent, going to the absolute extrema of the potential, and the amplification factor reaches a constant value, see inset of Fig. 3.4.

It is possible to reinterpret these results in terms of the effective po-

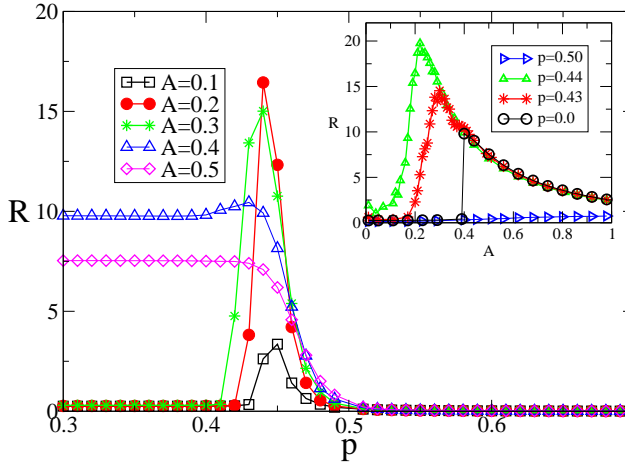


Figure 3.2. Spectral amplification factor R versus probability of repulsive links p . Inset: the influence of the amplitude A of the external forcing on the response R . For suprathreshold amplitudes, $A \gtrsim 0.4$, R decreases with A due to the denominator A^2 in the definition of the spectral amplification factor R . $T = 300$, N and C as in Fig. 3.1.

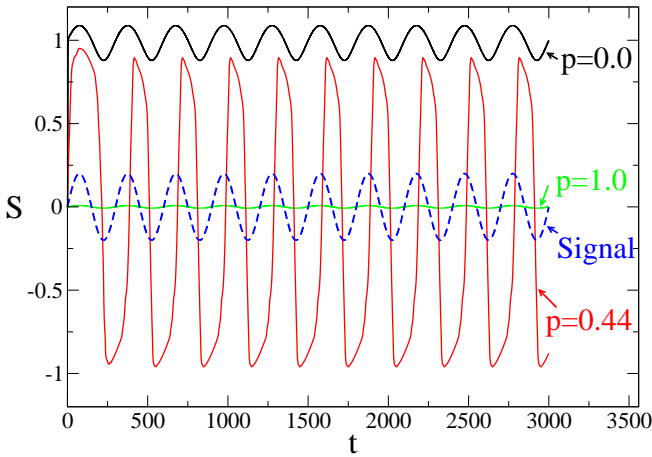


Figure 3.3. Representative trajectories of the macroscopic variable $S(t)$. Note the large amplitude of the oscillations in the intermediate case $p = 0.44$. The “signal” is the periodic function $A \sin(2\pi t/T)$. Values of N , C and T as in Fig. 3.2, $A = 0.2$.

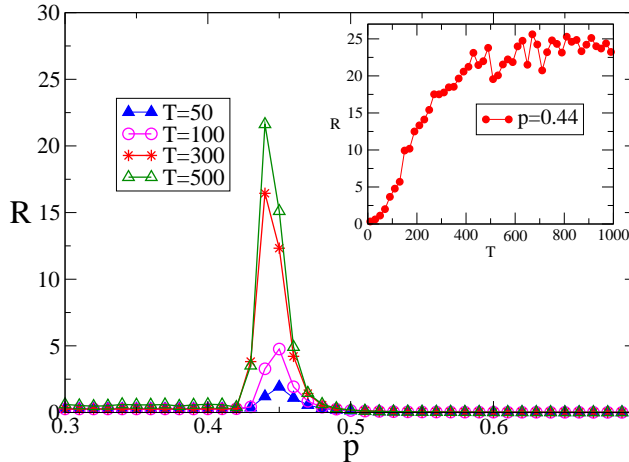


Figure 3.4. The influence of the signal period T on the response R . In the inset, we see the response R reaches a constant value for slow enough signals. Values of N , C and A as in Fig. 3.1.

tential $V_{\text{eff}}(S)$ introduced above. The periodic forcing can be seen, approximately, as a periodic modulation to the potential $V_{\text{eff}} - S \cdot A \sin(2\pi t/T)$. As discussed above, the effect of the repulsive links is such that $V_{\text{eff}}(S)$ changes from bistable at $p = 0$ to having many metastable minima at $p \approx p_c$ and a single absolute minimum for $p > p_c$. Hence, the deep potential barrier separating the $S = \pm 1$ solutions for $p = 0$ lowers under the effect of the repulsive links. As a consequence, the modulation induced by the periodic forcing is now large enough, and the global variable is then able to oscillate from the minimum $+S_0(p)$ to $-S_0(p)$ and vice versa. As p approaches p_c a more complicated scenario appears. In this region the effective potential presents already a rich structure with many metastable minima in the non-forced case. Those minima can be modified or even disappear by the effect of the periodic modulation. It is particularly illustrative to compare the responses to a suprathreshold signal of amplitude $A = 0.4$ in the case $p = 0$, and to a signal of amplitude $A = 0.2$ (which would be subthreshold in the case $p = 0$) at the optimal fraction of repulsive links $p = p_c$. In both cases, the amplitude of the oscillations is approximately the same, as the system makes large excursions from $S \approx -1$ to $S \approx +1$ and vice versa. However, the shape of the oscillations is rather different, as shown in the upper panel

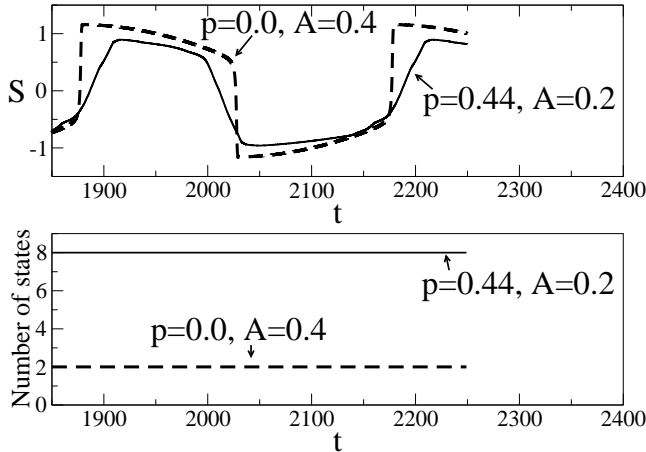


Figure 3.5. We amplify some representative trajectories (upper panel), and count the number of states through which the system moves in each trajectory (lower panel). Values of T , N and C as in Fig. 3.2.

of Fig 3.5. In the $p = 0$ case, the transition from one minimum to the other is rather fast (vertical portion of the dashed line), while in the case $p = p_c$, the transition is slower as the system seems to be spending more time in intermediate states.

To determine what those differences reveal about the underlying effective potential, we have used a method [107] that allows us to detect the number of states a system visits from an analysis of its time series. A typical example is shown in the lower panel of Fig. 3.5. We only detect two states in the global variable S when $p = 0$, corresponding, as expected, to the modulated bistable potential. By contrast, the slight irregularities in the trajectory for $p = 0.44$, hardly visible by eye, correspond to several very shallow potential wells. The system evolves through many states at the optimal probability of repulsive links, as shown in the lower panel of Fig 3.5. This image explains why signals of every amplitude and period can be amplified for $p \approx p_c$. In this case, the system can access the many intermediate states, covering a distance proportional to T and A , in case of very fast or very weak signals.

The previous results show that the disorder induced by an intermediate

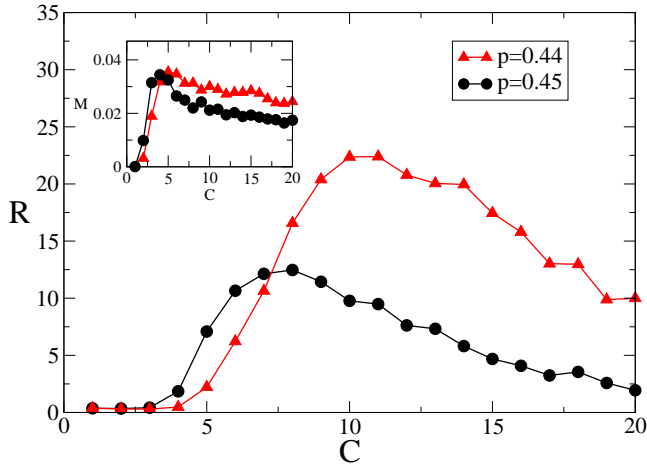


Figure 3.6. Coupling-induced resonance. Main plot: the response R shows a maximum as a function of coupling constant C . As shown in the insert, the same maximum appears as a function of the localisation measure M , see section 3.3. Values of N , T and A as in figure 3.1 and $K = 0.2$ in the insert.

level of repulsive links is an essential ingredient to get an optimal response to the external forcing. This can be explained as, in the absence of forcing, the metastable states correspond to a wide distribution for the values of s_i 's. When the forcing is turned on, some units will be responsive to the signal, and then they will pull others which are positively coupled to them. This basic mechanism is further highlighted by the observation of a resonance behaviour with both the coupling constant C and the number of units N .

The resonance with C and some representative trajectories are displayed in Figs. 3.6 and 3.7, respectively. In the weak coupling limit, the units behave basically as independent from each other and, as the signal amplitude A is subthreshold for a single variable, the overall response is small. In the large coupling limit, the interaction term is too big to allow an unit that could first follow the signal to depart from the influence of its neighbours.

The resonance with the number of units N and some representative trajectories is presented in Figs. 3.8 and 3.9. Since fluctuations in the number of repulsive links decrease with N , a larger system requires a greater fraction

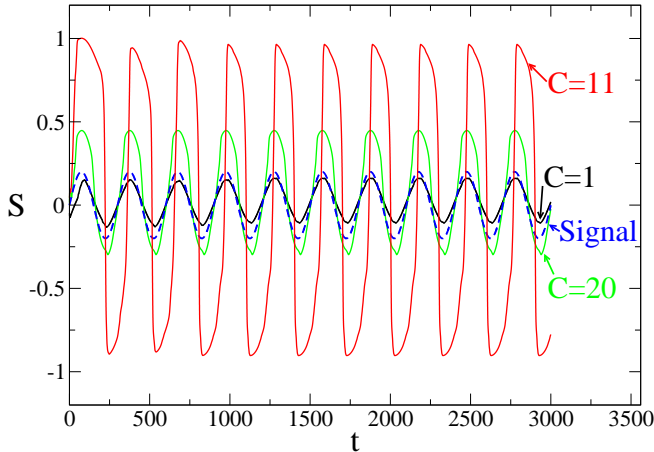


Figure 3.7. Coupling-induced resonance, as revealed by the resonant trajectory at optimal $C = 11$. Values of N , A and T as in Fig. 3.1.

of repulsive links to achieve the same level of disorder than a smaller system. As a consequence, the response of a larger system is best amplified at a higher probability of repulsive links. As the fraction of repulsive links must not exceed the fraction of positive ones, there can be a limit on how large can a system be, to be able to amplify a signal. The same behaviour, focusing on the number of neighbours was found in a previous study of an Ising-like network model [108].

3.3 Spectral analysis

We have already commented that the optimal probability of repulsive links drives the system to a glassy phase. Anderson [109, 110] has proposed a connection between a glass and a delocalisation-localisation transition, relating the existence of many metastable states with a localisation of modes. From this proposal, we retain the idea to work in the eigenspace of the interaction matrix, and to look for the fraction of repulsive links where mode localisation becomes significant. This approach has the virtue of not only identifying the steady states, but also to shed light onto how the reaction to perturbations is sustained and spreads along the system, depending on

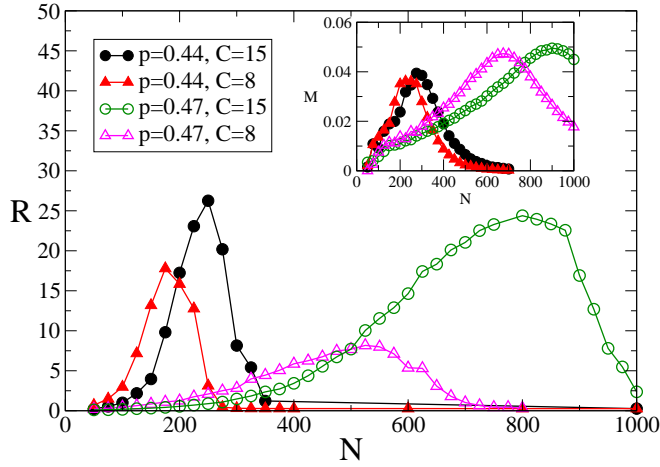


Figure 3.8. System-size induced resonance. Main plot: the response R shows a maximum as a function of the number of units, that follows the same pattern as the maximum M ($K = 0.2$) (inset). Since N decreases the influence of a single neighbour, and C increases it, when the coupling intensity is larger, the optimal system size increases. Values of T and A as in Fig. 3.1.

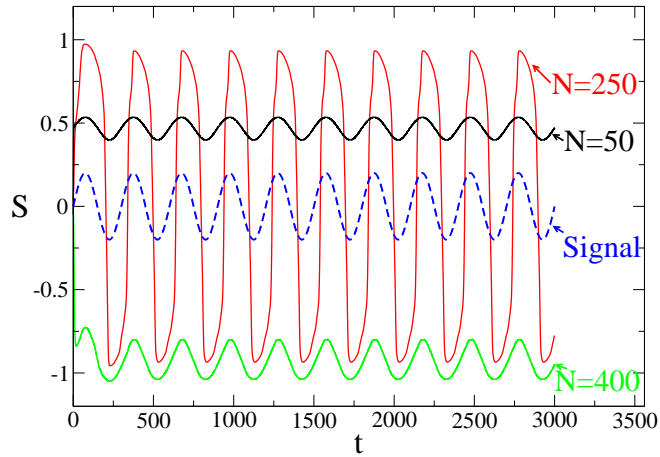


Figure 3.9. System size induced resonance, as revealed by the resonant trajectory at optimal $N = 250$. Values of T , A and C as in Fig. 3.1.

the fraction of repulsive links. In this manner, we hope to locate the region where multistability is expected, and also to understand the mechanism of response to external perturbations.

Following [103], let us define the eigenvalues Q_α and (normalised) eigenvectors $e^\alpha = (e_1^\alpha, \dots, e_N^\alpha)$ of the Laplacian matrix [104] J'_{ij} :

$$J'_{ij} = J_{ij} - \delta_{ij} \sum_{k=1}^N J_{kj}, \quad (3.5)$$

$$\sum_{j=1}^N J'_{ij} e_j^\alpha = Q_\alpha e_i^\alpha. \quad (3.6)$$

The effect of the competitive interactions can be described by the so-called participation ratio of eigenvector e^α , defined as $\text{PR}_\alpha = 1 / \sum_{i=1}^N [e_i^\alpha]^4$. It quantifies the number of components that participate significantly in each eigenvector. A state α with equal components has $\text{PR}_\alpha = N$, and one with only one component has $\text{PR}_\alpha = 1$. When $\text{PR}_\alpha = 1$ on a fraction f of elements, and 0 elsewhere, then $\text{PR}_\alpha = f$, which justifies its name. More precisely, we will define “localised” modes as the ones whose participation ratio is less than $0.1N$. Our first observation (Fig. 3.10) is that at the optimal region p there is a significant fraction of positive eigenvalues, and, of those, a significant fraction of the corresponding eigenstates are localised. In this region, we will neglect the coupling between different modes. This approximation allows us to look in more detail at what happens at the optimal region, and in particular at the effect of the coupling strength C and the number N of elements.

Let us focus first on the unforced system ($A = 0$), to see how the presence of the disorder induced by the repulsive links affects a state configuration. We assume each unit i is initially at a given state s_i^o , chosen from a random symmetric distribution and split the variables in the steady state as $s_i = s_i^o + x_i$, being x_i the deviation from the initial condition. We express x_i in the eigenbasis of the J'_{ij} matrix:

$$x_i = \sum_{\alpha=1}^N B_\alpha e_i^\alpha, \quad (3.7)$$

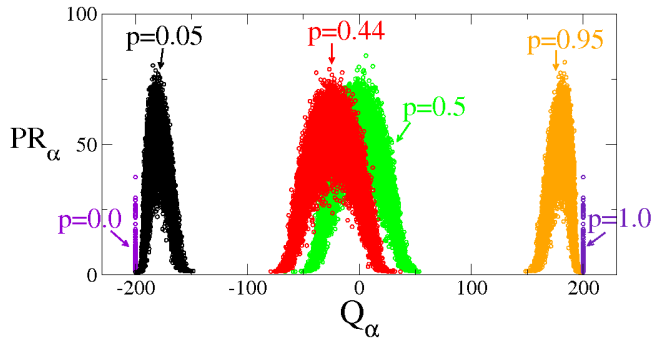


Figure 3.10. The participation ratio PR_α is a measure of localisation; it estimates the number of eigenvectors components contributing to the Q_α eigenvalue. The eigenvalues at both ends of the spectrum are localised for intermediate levels of disorder. $N = 200$, results after 1000 independent runs.

Expanding Eq. (3.1) for $A = 0$, multiplying the resulting equation by e_i^α , summing over all elements i , and approximating averages of the product of initial conditions and eigenvectors by the product of their individual averages (e.g. $\sum_{i=1}^N s_i^o e_i^\alpha \approx \sum_{i=1}^N s_i^o \sum_{i=1}^N e_i^\alpha = 0$), we obtain:

$$\sum_{\beta, \gamma, \eta} F^{\beta\gamma\eta\alpha} B_\beta B_\gamma B_\eta + \left(K - C \frac{Q_\alpha}{N} \right) B_\alpha = 0, \quad (3.8)$$

where

$$F^{\beta\gamma\eta\alpha} = \sum_{i=1}^N e_i^\beta e_i^\gamma e_i^\eta e_i^\alpha, \quad (3.9)$$

$$K = \frac{3}{N} \sum_{i=1}^N (s_i^o)^2 - 1. \quad (3.10)$$

Neglecting coupling between modes leads to $F^{\beta\gamma\eta\alpha} = 1/PR_\alpha$ if $\alpha = \beta = \gamma = \eta$ and $F^{\beta\gamma\eta\alpha} = 0$ otherwise. We then obtain the following equation for the amplitude of the α -th mode:

$$B_\alpha^3 + PR_\alpha \left(K - C \frac{Q_\alpha}{N} \right) B_\alpha = 0. \quad (3.11)$$

According to this approximation, unless $Q_\alpha > \frac{KN}{C}$, the amplitude B_α of the mode α is zero, and any small perturbation vanishes. Otherwise, the mode is said “open” and B_α takes one of the values:

$$B_\alpha = \pm \sqrt{\text{PR}_\alpha \left(C \frac{Q_\alpha}{N} - K \right)}. \quad (3.12)$$

For intermediate amounts of disorder, some open modes begin to appear. The final state of an unit is $s_i = s_i^o + \sum_{\alpha=1}^N B_\alpha e_i^\alpha$, and when the initial conditions are random and the open modes α are localised, the system reaches many metastable states, given all the possible combinations of individual states. For this reason, we want to locate a transition to a region with a significant number of localised modes.

To concretise, we define a measure M of localisation:

$$M = \frac{N_L^2}{N_O N}, \quad (3.13)$$

where N_O is the number of modes α whose associated eigenvalue Q_α is greater than $\frac{KN}{C}$, and N_L is the number of those modes which, in addition, are localised, i.e. $\text{PR}_\alpha < 0.1N$.

Recalling the definition of K (Eq. (3.10)), we see its value is related to a choice of initial conditions, by the variance of s_i^o . Since we expect multistability to emerge when the initial distribution is more or less uniform, we present results in Fig. 3.11 for values of $K \approx 0$.

At moderate levels of disorder, the localised nodes appear on the tails of the spectra, Fig. 3.10. We confirm that the optimal probability of repulsive links coincides with a maximal localisation of open modes in that region, as identified by the peak in M (Fig. 3.11).

In a particular metastable state, the units are randomly distributed, more concentrated near one of the potential wells. Observing the results in Fig. 3.11 for $K \gtrsim 0$, we see that we recover the dependence on C , and that the peak in M still coincides with the optimal probability region. The enhanced responsiveness to an external signal can thus be understood as a consequence of mode localisation. Since units can be in different positions, some will be able to answer the signal, and then - since the overall coupling

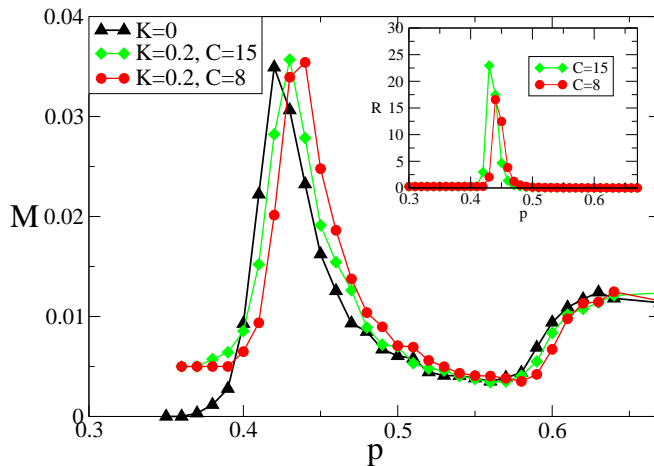


Figure 3.11. Measure of localisation M : close to the optimal region there is an increase in the fraction of localised open eigenstates. The small dependence of M with K and C is as expected. Parameters: $N = 200$. Inset: $A = 0.2$, $T = 300$.

is attractive - pull the others. This is done in an incremental fashion, as confirmed by the localised reaction to perturbations.

The same analysis is valid when we plot M as a function of C or N . We notice a peak in M and accordingly the dependence of the response on C (Fig. 3.6) and N (Fig. 3.8) shows a maximum for intermediate values (insets Fig. 3.6 and Fig. 3.8). When C is small, even if the modes are open, their amplitude B_α is weak, Eq. (3.12). A high fraction of repulsive links, increasing the number of open modes, can overcome this situation to a certain degree, allowing for resonances at a smaller coupling strength.

3.4 Conclusions

In this work, we have analysed the response to a weak period signal, of a model composed by bistable units coupled through both attractive and repulsive links.

Our main result is that the system collective response is enhanced by the presence of an intermediate fraction of repulsive links. Hence, com-

petitive interactions are taken as a source of disorder, as an alternative to previous studies where disorder was induced by noise [61] or diversity [89], and a similar amplification was verified.

We have chosen a very generic double-well model, and have shown that the optimal disorder is the one that destroys the ordered system bistability. The resulting multistable effective potential allows for the amplification of very weak or fast signals. There is not a need to match specific levels of disorder with specific frequencies. Having the optimal disorder, the system becomes more sensitive to external signals of every kind. Furthermore, we have shown that varying the number of elements or the coupling strength in an ensemble of coupled bistable elements can improve the sensitivity to an external forcing. These various ways to increase sensitivity make the phenomenon less dependent on a fine tuning of the proportion of repulsive links, which can be a positive feature in practical applications. Apparently, when the system size becomes very large, it is difficult to get a resonance effect, unless we increase the coupling strength by many times. Arguably, this difficulty can be overcome by other types of network settings [100].

Finally, we have shown that the location of the resonance peaks can be predicted by a spectral analysis of the Laplacian matrix. In heuristic terms [104], the positive eigenvalues of the Laplacian can be seen to express the contribution of the coupling term to the vulnerability of the system to perturbations. We conclude that the location of the amplification region, for a given system size and coupling constant, is reasonably independent of the particular dynamical system. In broad terms, it corresponds to the point where the positive eigenvalues of the Laplacian matrix become localised, signalling a transition to a region where perturbations can accumulate in an incremental manner. The more precise location would depend on the particular dynamical system by means of a condition on open modes.

Competitive interactions are widespread in nature, notably in biological systems. In those systems and others, there has been some studies highlighting their role in achieving a coherent behaviour in the absence of forcing: increasing synchronisation [99] or enabling a collective firing [100]. In the present study, we saw they can also help to enhance perception, something that can be potentially relevant in sensory systems.

4

A discrete bistable model

We study an Ising model in a network with disorder induced by the presence of both attractive and repulsive links and subjected to a periodic subthreshold signal. By means of numerical simulations and analytical calculations we show that the global response of the system reaches a maximum value for a given fraction of the number of repulsive interactions. The model can represent a network of spin-like neurons with excitatory and inhibitory couplings, or a simple opinion spreading model [99, 44], which is the language we will adopt throughout most of the time in this chapter. In this context, attractive/repulsive links represent friends and enemies.

4.1 Noise and diversity

Let us recall the model presented in subsection 1.4.1. We concluded that the depth of the potential well where the population is entrapped is estimated by (half) the number of people that shares our opinion, it seems like a good idea to break consensus a little, by the introduction of some form of disorder. In case individuals are somehow different, we can anticipate that a consensus will be harder to reach. Tessone *et al.* [59] changed the interaction rule 1.9 to dilute the social pressure of the neighbours by taking into account individual preferences or biases towards one of the opinions. In their model [59], the rule 1.9 is replaced by:

(i) Select randomly one individual i . Its opinion at time t is modified as :

$$\mu_i(t + dt) = \text{sign} \left[\frac{1}{k_i} \sum_{j \in n(i)} \mu_j(t) + \theta_i \right]. \quad (4.1)$$

The parameter θ_i represents the individual preference and is drawn from a probability distribution $g(\theta)$, which satisfies $\langle \theta_i \rangle = 0$, $\langle \theta_i \theta_j \rangle = \delta_{ij} \sigma^2$. According to this, the agent i only adopts the average opinion in its neighbourhood $n(i)$ if this average opinion overcomes its preference θ_i .

By resorting to numerical simulations and a mean-field approximation, the authors [59] found that there exists an optimal value of the diversity σ for which the response to a weak forcing takes a maximum value, and that the mechanism is in everything identical to the diversity induced resonance effect described in Chapter 2.

Yet another earlier attempt [44] to aid the propagation of the signal involved the introduction of noise. Kuperman and Zanette [44] used the model 1.9 and included noise as a certain probability to change randomly from one opinion to another. In the context of opinion formation models, noise might represent flicker emotions, free will, or some other external factor [48]. The main point is that now agents can change in a random fashion, not taking into consideration any known factor in the model. Their aim [44] was to uncover the influence of the network topology on the stochastic resonance effect, thus building a bridge between stochastic and disorder induced resonance. Namely, they observed that when the interaction network is regular, the unperturbed system reaches a paramagnetic phase, and that the introduction of some random long range interactions is necessary for the existence of a ferromagnetic state, and as a consequence a bistable situation.

Being interested in stochastic resonance, they turned their attention to this bistable situation enabled by small world networks, finding that as the probability of small world increases, so does the potential depth and as a consequence the strength of the signal needed to invoke a response. Although they didn't elaborate on it in detail, they hint at the possibility of another type of disorder induced resonance, when mentioning the possibility that very weak forcing could get a response when the population is restricted

to local interactions, by the diffusive propagation that could be enabled by the paramagnetic phase. As we will see in the rest of this chapter, this can in fact be achieved by any kind of network as long as we include a mixture of attractive and repulsive links.

4.2 Model

We consider a set of N spin-like (Ising) dynamical variables $\mu_i(t)$ which, at a given time t , can adopt one of two possible values, $\mu_i = \pm 1$. We will sometimes use the language of a magnetic system, but our aim is quite general and these states can represent, for instance, two different opinions (in favour/against) about a topic, the state of a neuron (firing/not firing), or several other interpretations [99, 44]. The variables are located on the nodes of a given network whose links represent interactions. We assign a weight ω_{ij} to the link connecting nodes i and j and consider only the symmetric case $\omega_{ij} = \omega_{ji}$ (or an undirected network). According to the discussion above, we let the weights take positive or negative values: $\omega_{ij} = 1$ or $\omega_{ij} = -\kappa$ with $\kappa > 0$. The neighbourhood of node i is the set $V(i)$ of nodes j for which a connecting link between nodes i and j exists.

The spin variables evolve according to the following dynamical rule: At time t one of the variables, say μ_i , is chosen at random. The value of this variable is updated according to:

$$\mu_i(t + \tau) = \begin{cases} \text{sign} \left[\sum_{j \in V(i)} \omega_{ij} \mu_j(t) \right] & \text{w.p. } 1 - |a \sin(\Omega t)|, \\ \text{sign} [\sin(\Omega t)] & \text{w.p. } |a \sin(\Omega t)|, \end{cases} \quad (4.2)$$

(w.p. stands for “with probability”). In both cases, if the expression within square brackets is equal to zero, the variable does not change: $\mu_i(t + \tau) = \mu_i(t)$. The first case represents a weighted “majority-rule” in which the state of the spin is determined by the sign of its *local field* $h_i(t) = \sum_{j \in V(i)} \omega_{ij} \mu_j(t)$. The second case represents the effect of an external forcing of frequency Ω – the intensity $a < 1$ determines the rate at which the signal influences the dynamics of the variable μ_i . The choice of the time step $\tau = 1/N$ defines the unit of time as N updates. We consider both regular lattices

(with k neighbours) and random networks of the small-world type. The latter are constructed according to the algorithm proposed by Watts and Strogatz [111]. Denoting by q the rewiring probability (percentage of short-cuts), the limit $q = 1$ corresponds to a random Erdős/Rényi-type network, $q = 0$ is a regular ring-network and intermediate values of q define a small-world network. We have also considered a square lattice in which a node is linked to the $k = 8$ nodes of its Moore neighbourhood. In each case, links are assigned a strength $-\kappa$ with probability p or a strength 1 with probability $1 - p$. In the case of a random network, the number of links (degree) k_i of node i is a random variable with probability P_{k_i} and average $\langle k_i \rangle = k$. Denoting by k_i^+ and k_i^- respectively the number of positive and negative links of node i , its degree is $k_i = k_i^+ + k_i^-$ and $\langle k_i^+ \rangle = (1 - p)k$, $\langle k_i^- \rangle = pk$.

It is worth noticing that, from the formal point of view, the majority-rule is equivalent to a heat-bath stochastic dynamics in the limit of zero temperature [112]. The Hamiltonian is $\mathcal{H} = -\sum_{\langle i,j \rangle} \omega_{ij} \mu_i \mu_j$ (the sum runs over all pairs of neighbours) and the majority-rule always leads to a configuration with less or equal energy. If all the weights ω_{ij} are positive, the ground states are $\mu_i = +1$ or $\mu_i = -1$, $\forall i$, and these ground states are reached independently of the initial condition. If there is a fraction of negative links, the system is of the spin-glass family. The (in general unknown) ground state can have many metastable configurations nearby and the use of the majority-rule may trap the system in one of them.

As a way of quantifying the coherence of the global response to the forcing, we chose the spectral amplification factor R , defined as the ratio of the output to input power at the corresponding driving frequency [84], as mentioned in Section 2.2:

$$R = \left\langle \frac{4}{a^2} \left| \langle\langle \mathbf{m}(t) e^{-i\Omega t} \rangle\rangle \right|^2 \right\rangle, \quad (4.3)$$

where $\langle\langle \dots \rangle\rangle$ is a time average, $\mathbf{m}(t)$ is the global response (system's magnetisation):

$$\mathbf{m}(t) = \frac{1}{N} \sum_{i=1}^N \mu_i(t), \quad (4.4)$$

and $\langle \dots \rangle$ is an ensemble average over network realisations, initial conditions and realisations of the dynamics.

4.3 Simulation results

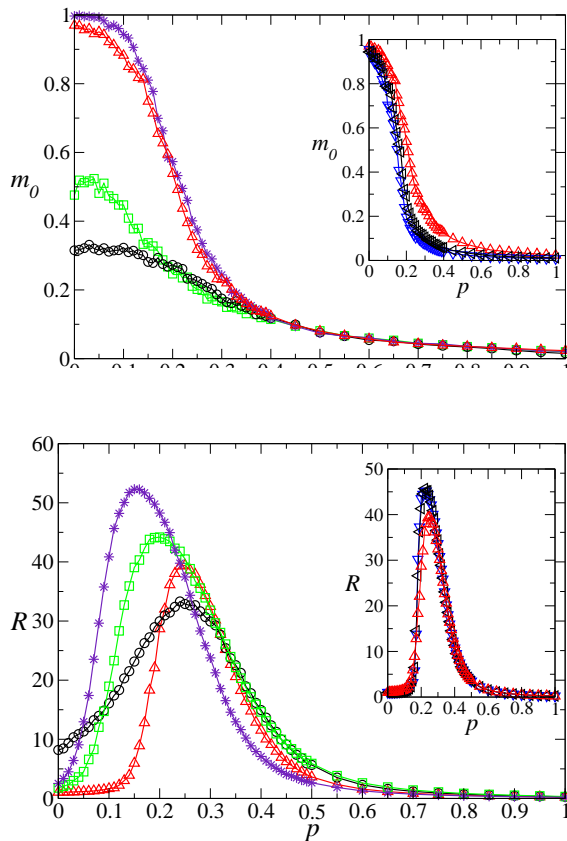


Figure 4.1. The coincidence between resonance and order-disorder transition region. Upper panel: Modulus of the average magnetisation as a function of the probability of repulsive links. In the regular networks, the existence of metastable states reveals itself in a smaller magnetisation at $p = 0$. Lower panel: Spectral amplification factor R versus probability of repulsive links p . Parameters are: $a = 0.15$, $\Omega = \frac{2\pi}{100}$, $\kappa = 1$. In the main graph, $N = 100$ and symbols correspond to topologies: ring with $k = 10$ neighbours (\circ), square lattice with $k = 8$ neighbours in the Moore neighbourhood (\square), and random networks with average number of neighbours $k = 10$ and rewiring probability $q = 0.2$ ($*$) and $q = 1$ (\triangle). In the inset, we chose the random network with $q = 1$, $k = 10$, and different curves correspond to sizes $N = 100$ (\triangle), 500 (\triangleleft), and 1000 (∇).

The main result is that there is a resonance effect, a maximum of the amplification factor R , at an intermediate value of the probability of repulsive links p , as shown in Fig. 4.1, and that the resonance region coincides with an order-disorder transition. In our case, the degradation of order has its origin in the increasing importance of the inhibitory connections. This is clearly seen in Fig.4.1, upper panel, where we plot the standard order parameter m_0 as a function of the probability p of inhibitory links. The optimal probability for resonance p_c (location of the peak of Fig.4.1) is found near the phase transition between the ferro and paramagnetic regions.

The existence of this maximum is also visible when looking at the amplitude of the oscillations of the global variable $m(t)$ – Fig.4.2. For small p , $m(t)$ oscillates with a small amplitude (of order a) around a value close to either $+1$ or -1 . As p increases, one clearly notices that the amplitude increases dramatically and $m(t)$ oscillates around 0. As p increases even further, the amplitude of the oscillations decreases but the global variable still oscillates around 0. This resonance effect appears for all lattices considered, regular or random, for all values of the rewiring probability q .

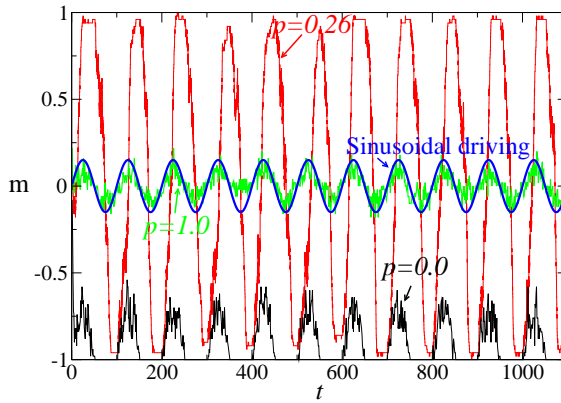


Figure 4.2. Evolution of magnetisation in time (random network, $q = 1$, $k = 10$). Other parameters are: $N = 100$, $a = 0.15$, $\Omega = \frac{2\pi}{100}$, $\kappa = 1$.

The existence of this order-disorder transition and its relation to the resonance effects are reproduced by a simple mean-field theory that we de-

velop in some detail in the next section.

4.4 Mean-field approach

At each time step the magnetisation $\mathbf{m}(t)$ may change due to the modification of a single variable μ_i . The following relation holds exactly for the ensemble average $m(t) = \langle \mathbf{m}(t) \rangle$:

$$Nm(t + \tau) = Nm(t) + \langle \mu_i(t + \tau) - \mu_i(t) | \{\mu(t)\} \rangle \quad (4.5)$$

where $\{\mu(t)\} = (\mu_1(t), \dots, \mu_N(t))$ denotes the particular realisation of the μ_i variables and $\langle \dots | \dots \rangle$ denotes a conditional ensemble average. By identifying $\tau = 1/N$ and rearranging we get:

$$\frac{m(t + \tau) - m(t)}{\tau} = \langle \mu_i(t + \tau) - \mu_i(t) | \{\mu(t)\} \rangle = -m(t) + \langle \mu_i(t + \tau) | \{\mu(t)\} \rangle \quad (4.6)$$

We now identify the left hand side as the time derivative and use the dynamical rules given by Eq.(1.9) to write:

$$\begin{aligned} \frac{dm(t)}{dt} &= -m(t) + |f(t)| \langle \text{sign}[f(t)] | \{\mu(t)\} \rangle + \\ &\quad (1 - |f(t)|) \left\langle \text{sign} \left[\sum_{j \in V(i)} \omega_{ij} \mu_j(t) \right] \middle| \{\mu(t)\} \right\rangle \end{aligned} \quad (4.7)$$

where we have used the notation $f(t) = a \sin(\Omega t)$. Since the forcing $f(t)$ is independent of the state $\{\mu\}$, then $\langle \text{sign}[f(t)] | \{\mu(t)\} \rangle = \text{sign}[f(t)]$. Moreover $|f(t)| \text{sign}[f(t)] = f(t)$. For the last term of the right hand side of this equation we use the mean-field approximation:

$$\sum_{j \in V(i)} \omega_{ij} \mu_j(t) \approx \left[\sum_{j \in V(i)} \omega_{ij} \right] \cdot m(t) \quad (4.8)$$

where we replace the value $\mu_j(t)$ by the average value $m(t)$.

Now $\sum_{j \in V(i)} \omega_{ij} = k_i^+ - \kappa k_i^- = k_i^+(1 + \kappa) - k_i \kappa$, and the mean-field approximation can be rewritten as:

$$\begin{aligned} \left\langle \text{sign} \left[\sum_{j \in V(i)} \omega_{ij} \mu_j(t) \right] \middle| \{ \mu(t) \} \right\rangle &= \\ (-1) \cdot \text{Prob} \left([k_i^+(1 + \kappa) - k_i \kappa] m(t) < 0 \right) &+ \\ (+1) \cdot \text{Prob} \left([k_i^+(1 + \kappa) - k_i \kappa] m(t) > 0 \right) & \\ = 1 - 2 \text{Prob} \left([k_i^+(1 + \kappa) - k_i \kappa] m(t) < 0 \right) & \\ \equiv G(m(t)) & \end{aligned} \quad (4.9)$$

from where we obtain the desired mean-field equation:

$$\frac{dm(t)}{dt} = -m(t) + f(t) + (1 - |f(t)|)G(m(t)) \quad (4.10)$$

The function $G(m)$ can be easily computed in terms of the cumulative probability function F_{k_i} of the binomial distribution of the number of positive links, given that the total number of links is k_i . This is precisely defined as:

$$F_k(x) = \sum_{k^+ < x} \binom{k}{k^+} p^{k-k^+} (1-p)^{k^+}. \quad (4.11)$$

In the case $m > 0$,

$$\begin{aligned} \text{Prob} \left([k_i^+(1 + \kappa) - k_i \kappa] m(t) < 0 \right) &= \\ \text{Prob} \left(k_i^+ < \frac{k_i \kappa}{1 + \kappa} \right) &= F_{k_i} \left(\frac{k_i \kappa}{1 + \kappa} \right), \end{aligned} \quad (4.12)$$

while, for $m < 0$,

$$\begin{aligned} \text{Prob} \left([k_i^+(1 + \kappa) - k_i \kappa] m(t) < 0 \right) &= \\ \text{Prob} \left(k_i^+ > \frac{k_i \kappa}{1 + \kappa} \right) &= 1 - F_{k_i} \left(\frac{k_i \kappa}{1 + \kappa} \right). \end{aligned} \quad (4.13)$$

By averaging over the distribution of the number of neighbours, we get:

$$G(m) = \text{sign}(m) \sum_{k_i} P_{k_i} \left[1 - 2F_{k_i} \left(\frac{k_i \kappa}{1 + \kappa} \right) \right] \quad (4.14)$$

P_{k_i} being the probability that a node has k_i links. Within the spirit of the mean-field approximation we assume that all nodes have the same number of links $k_i = k$ and replace the above formula by:

$$G(m) = \text{sign}(m) \left[1 - 2F_k \left(\frac{k\kappa}{1 + \kappa} \right) \right]. \quad (4.15)$$

In case of no forcing, $f(t) = 0$, the equilibrium value m_0 of the magnetisation satisfies $m_0 = G(m_0)$. A standard analysis of this equation predicts a phase transition separating a regime of non-zero stable solutions $\pm m_0 \neq 0$ from a regime in which the only solution is $m_0 = 0$. The coexistence line is $m_0 = 1 - 2F_k \left(\frac{k\kappa}{1 + \kappa} \right)$ and the critical point occurs at $F_k \left(\frac{k\kappa}{1 + \kappa} \right) = 1/2$. In Fig.4.3 we plot the equilibrium magnetisation m_0 as a function of the probability p for fixed k . It is clear from this figure that the mean-field approximation reproduces the loss of order that arises as the proportion p of negative links increases, although the precise location of the transition point is not well reproduced.

In Fig.4.3, lower panel, we plot the amplification factor computed after a numerical integration of Eq.(4.10). Qualitatively, the results agree with those of simulations presented in the previous section: there is a resonance effect, i.e. the response shows a maximum as a function of p . The maximum value is reached for a value p_c , close to that signalling the order-disorder transition. Furthermore, it can be noticed that the size of the amplification region, defined as the set of values of p for which $R > 1$, is similar to the size of the transition region, defined roughly as the set of values of p for which the magnetisation satisfies $m(p) < 0.5$ and the maximum is achieved at a value of p such that $m(p) \approx 0.2 - 0.3$. As the average number of neighbours k increases, the size Δp of this region decreases as $k^{-1/2}$ and it disappears in the limit $k \rightarrow \infty$. Since the relative dispersion in the number of positive links also scales as $\sigma[k^+] / \langle k^+ \rangle \sim k^{-1/2}$, one is tempted to attribute the existence of the resonance to the existence of such a dispersion, a fact already stressed in the study of synchronised oscillations induced by diversity [100]. This is supported by a modified version of the mean-field approach in which the dispersion is strictly equal to 0. This can be achieved by using in (4.15) the probability distribution that would arise if all nodes had the same number k_i^+ of positive links, namely $F_k(x) = 0$ if $x < pk$ and $F_k(x) = 1$ if $x > pk$.

As shown in Fig.4.3, in this case the amplification region has disappeared altogether.

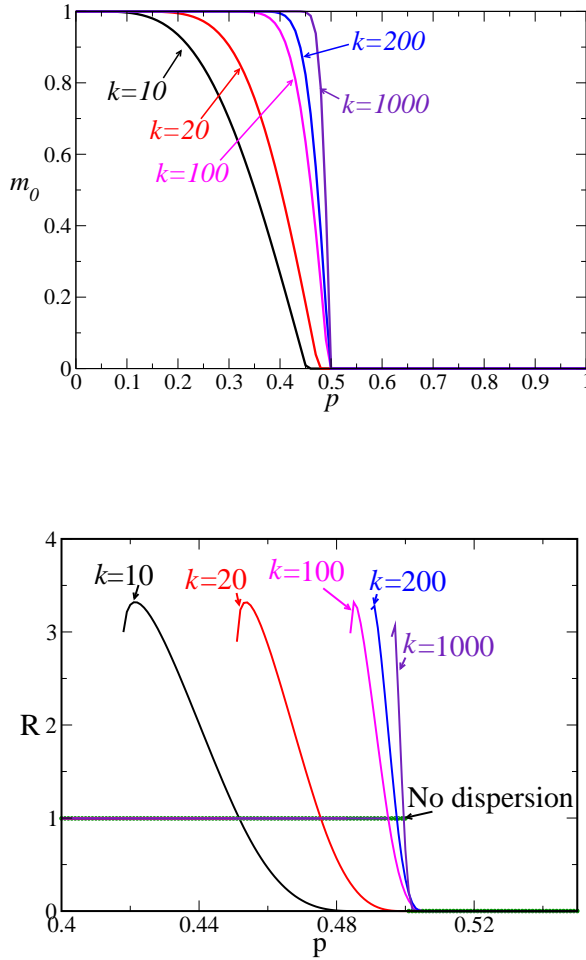


Figure 4.3. Upper panel: Modulus of the average magnetisation as a function of the probability of repulsive links according to the mean-field theory for $\kappa = 1$. Lower panel: Spectral amplification factor versus probability of repulsive links according to the mean-field theory for $a = 0.15$, $\Omega = \frac{2\pi}{100}$, $\kappa = 1$.

However, it should be noted that the response in the transition to the

amplification region is not continuous in this mean field case. There is a jump at a value p_* , such that $R(p \rightarrow p_*^-) = 1$ but $R(p \rightarrow p_*^+) > 1$. As discussed later, this discontinuity arises because, in the mean field scenario, the dynamics is governed by a bistable potential. The onset of amplification corresponds to the system being able to jump the potential barrier.

4.5 Mechanism

4.5.1 Microscopic point of view

We now give an explanation of some features of the observed resonance from a microscopic point of view, i.e. analysing the evolution of individual values of μ_i .

According to the rules (4.2), a chosen node takes the sign of the external signal with a probability $|a \sin(\Omega t)|$, independently of the current system configuration. To enhance resonance, there are two necessary requirements after a node has changed its state: to maintain the perturbation in the next time steps, and to spread it to its neighbours. The crucial issue is then how the local configuration of nodes and links helps (or hinders) this ordering process.

To spread a perturbation, it would be an advantage to have all-attractive couplings; however, to maintain its state, the node cannot be too constrained by its neighbours. With a high homogeneity of the neighbours states and a positive connection with all of them, a perturbed spin would likely be forced to go back to its original state next time it is selected. At the other extreme, when all its connections are negative, a perturbed node is also very much constrained by the state of its neighbours, the local field being maximal for a local anti-ferromagnetic ordering. At an intermediate level of positive and repulsive connections, we have the optimal state. It has a capacity to spread a perturbation to the whole network, but constrains minimally a node that has been perturbed. Due to the combination of attractive and repulsive links, the local field around a node is close to zero. Therefore, if a node changes its state, it possibly won't be forced to return to its previous position after consulting with its neighbours. On the other hand, it is easy to

spread a perturbation: if a node had previously a zero local field, after one neighbour has changed, the balance is broken, and it has to align with that neighbour, if the connection is positive.

To illustrate this point we monitored the system's response when the signal is switched on and off, at regular intervals. The goal is to see to what extent perturbations spread after the signal is switched off. These perturbations take the following form: during one unit of time (N updates), taken at regular intervals, the dynamics is such that the randomly chosen nodes adopt the $\mu=1$ state, with probability $A = 0.15$. As shown in Fig. 4.4, those perturbations die out almost immediately for $p \approx 0$ or $p \approx 1$ and only for $p \approx p_c$ are the perturbations able to spread during a finite amount of time.

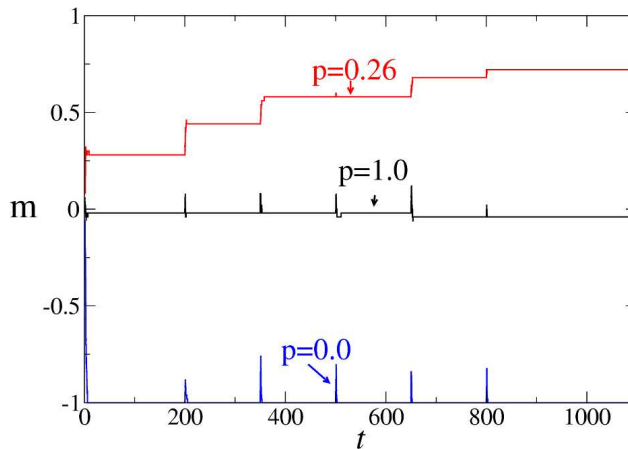


Figure 4.4. This image suggests that the step-by-step response we propose is a reasonable mechanism. Their outreach of the perturbations depends on the probability of repulsive links. At the optimal probability $p = 0.26$, the net effect of perturbations accumulates, but after the signal is switched off they don't continue spreading to the whole network.

This microscopic picture will help us to understand some of the observed features. For example, in Fig. 4.5 we show that the amplification region Δp decreases when the number of neighbours k increases, whereas p_c tends to 0.5. Both facts agree qualitatively with the predictions of the

mean-field theory. It is clear that for large k the condition of a local field close to zero can only be satisfied for a probability of repulsive links near 0.5. This is easily illustrated when one considers the case of p far from 0.5 and a uniform magnetisation (at the peak of a signal's cycle). Getting a local field close to zero when the connectivity is high requires many neighbours flips. Since the unit to be updated is chosen randomly at each time step, it is likely that a unit is chosen twice before enough of its neighbours have been perturbed. On the other hand, $p = 0.5$ is the upper limit for the amplification region, because a majority of positive links is necessary to have perturbation spreading. As the proportion of repulsive links approaches 0.5, more neighbours have a negative connection and they will exert, when perturbed, an influence opposite to the signal.

Note that for the resonance to disappear we need formally the limit $k \rightarrow \infty$. In a finite network, the maximum value is $k = N - 1$ and, as shown in Fig. 4.5 for $N = 201$ and $N = 1001$, the resonance does not disappear completely even for the maximum connectivity.

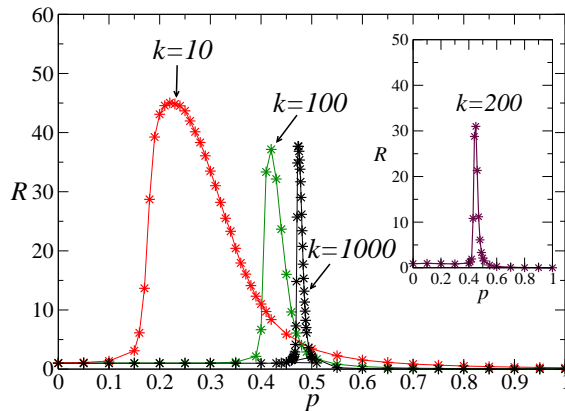


Figure 4.5. Spectral amplification factor versus probability of repulsive links for a random network with $q = 1$, $a = 0.15$, $\Omega = \frac{2\pi}{100}$, $\kappa = 1$. Main graph uses $N = 1001$ while the inset shows the case $N = 201$.

As we did in the mean-field treatment, and in order to isolate the influence of competitive interactions from the disorder induced by the dispersion

in the number of links, we also present in Fig. 4.6 results from random networks when all nodes have exactly the same number of neighbours k and the same proportion p of repulsive links [113]. At variance with the previous results, an almost total reduction of the amplification region can be achieved even for finite values of N , for large enough k . This shows that diversity in the number of positive links is an important ingredient for the robustness of the resonance effect, although that effect doesn't require in general that diversity.

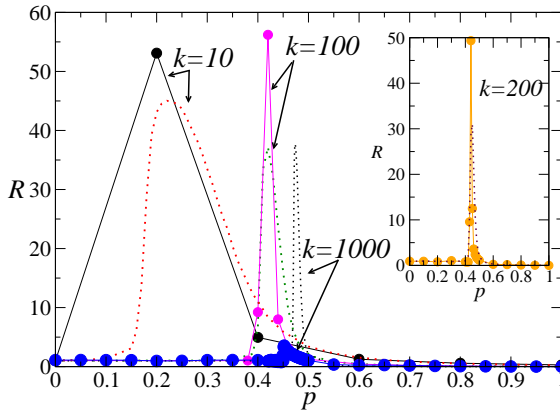


Figure 4.6. Spectral amplification factor versus probability of repulsive links for a “no-dispersion” network in which all sites have the same number of positive and negative links. Due to the particular way the network is constructed [113], only values of $p = k/N$ where the total number of neighbours per site, k , is an even integer number are allowed. Parameters are $N = 1001$, $a = 0.15$, $\Omega = \frac{2\pi}{100}$, $\kappa = 1$ (main graph) and $N = 201$ (inset). Note that the amplification region shrinks as k increases. For comparison, we also include as dotted lines the results of Fig.4.5.

Why does dispersion matter? The precise mechanism is hard to grasp, but it is certainly related to a degradation of order at local level. To decrease the chance of having perturbed neighbours driving several units in the direction opposite to the signal, there have to be many nodes with a clear majority of positive links. But as we saw above – assuming every node had the same number of negative links – those units require many neighbours flips, to maintain their local field close to zero. However, if the nodes

are heterogeneous, an unit with a lower than average number of repulsive links can profit from those neighbours that have many negative connections to other nodes. Since those are more susceptible to changes, their presence decreases the local field, thereby diminishing the need for many neighbours updates. This result confirms the importance of diversity in making the phenomenon more robust, but also shows that we can have an amplification even without diversity.

4.5.2 Macroscopic point of view

In this subsection, we consider the explanation of the resonance from the macroscopic point of view, i.e. we look at the behaviour of the collective variable (magnetisation) $m(t)$. We assume that the dynamics of this macroscopic variable in the no-forcing case, $f = 0$, can be described in terms of relaxation in a potential function $V(m)$. The absolute minima $\pm m_0$ of the potential give the rest states which are separated by a potential barrier ΔV . This picture has proved to be valid in other problems with diversity in the parameters [89] and it certainly holds in the mean-field limit where, according to the previous section, the dynamical equation is $\frac{dm}{dt} = -\frac{dV}{dm}$ with a potential given by:

$$V(m) = \frac{m^2}{2} - M(p)|m| \quad (4.16)$$

with $M(p) = 1 - 2F_k\left(\frac{k\kappa}{1+\kappa}\right)$ running from $M(0) = 1$ to $M(1) = -1$. Fig. 4.7, upper panel, illustrates the effect of repulsive links on the shape of the potential, according to the mean field predictions. There are two minima of the potential, $m_0 = \pm M(p)$ for $M(p) > 0$, and a single minimum $m_0 = 0$ for $M(p) < 0$, or $p > p_c$, the critical point. For small p the barrier separating the two minima is high and it can not be overcome by the effect of the weak forcing $f(t)$. The only effect of the forcing is a small oscillation around one of the minima (chosen by the initial conditions). As p increases, the two minima of the potential get closer to each other and the barrier separating them decreases such that, at a particular value of p the forcing is able to overcome the barrier and $m(t)$ oscillates between the two minima $\pm m_0$. As p crosses the critical value p_c , the two minima merge at $m_0 = 0$, the barrier

disappears and the effect of the forcing is reduced again to small oscillations around a single minimum.

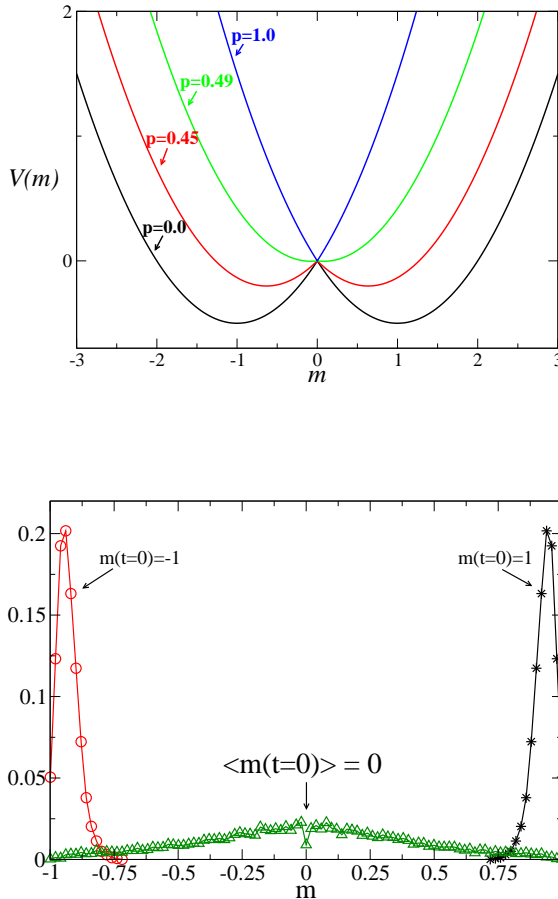


Figure 4.7. Comparison between the stable states predicted by mean field and simulations. Upper panel: the effective potential defining the relaxational dynamics according to Eq. 4.16, for different values of the probability of repulsive links p . We considered the case of $k = 100$. Lower panel: Distribution of stable states at the optimal probability $p_c = 0.25$ in the case of an unforced random network with $q = 1$, $N = 100$, $k = 10$, $\kappa = 1$ starting from three different initial conditions: all spins equal to $+1$ (data set indicated as $m(t = 0) = 1$), all spins equal to -1 ($m(t = 0) = -1$) and spins take randomly the value ± 1 ($\langle m(t = 0) \rangle = 0$).

To apply this potential image beyond the mean-field approximation we need to include an important modification. As discussed before, the energy landscape is that of a spin-glass with many metastable states and two absolute minima $\pm m_0$. As a consequence, in the no-forcing case, the final state reached depends strongly on initial conditions. This is illustrated in figure 4.7, lower panel, where we plot the probability distribution of the final magnetisation. If the initial state is the ordered state $\mu_i = +1$ (resp. -1) $\forall i$, the final magnetisation is peaked near $m = 1$ (resp. -1). If the initial state adopts $\mu_i = \pm 1$ randomly, then the final magnetisation is peaked around $m = 0$. This reflects the existence of many barriers separating the metastable states from the absolute minima of the potential. When the forcing is introduced, it has to be able to overcome all these intermediate barriers. The final image is that of a particle moving in a “rugged” potential. As p increases, the height of those barriers decreases and the forcing is able to explore a larger fraction of the configuration space, but not necessarily leading to trajectories ending in the absolute minima of the potential. This can be seen in figure 4.8 where we show the effect of a forcing weaker than that used in Fig.4.2. The magnetisation oscillates around a mean value that drifts with time. If we enlarge the period of the forcing – Fig. 4.8, lower panel – the oscillations become wider and the system has now enough time to reach the equilibrium minima close to $m_0 = \pm 1$.

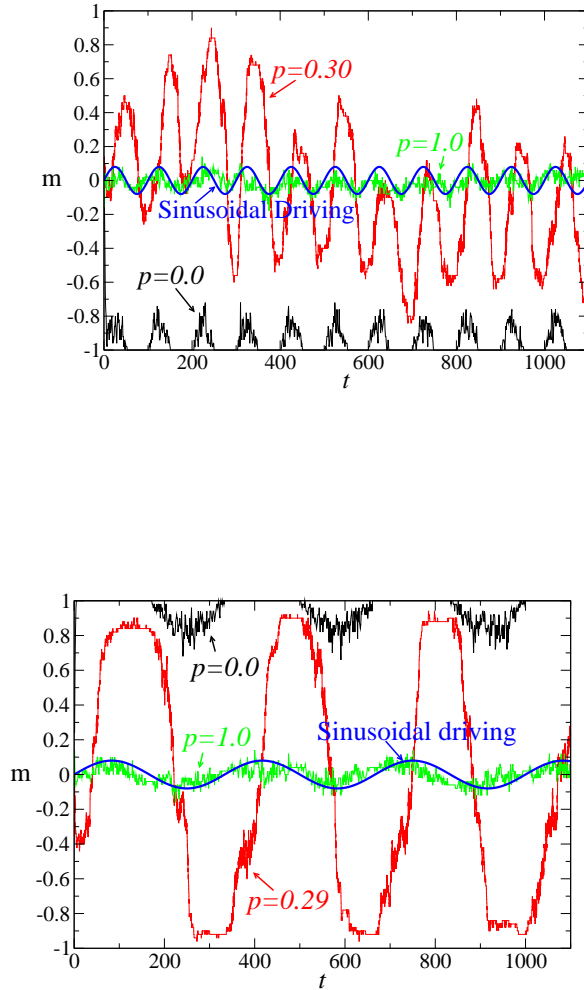


Figure 4.8. Upper panel: Evolution of the magnetisation following a weak signal $a = 0.08$, $\Omega = \frac{2\pi}{100}$, in the case of a random network, $q = 1$, $k = 10$, $\kappa = 1$. The extreme values of the magnetisation coincide with the points where the driving value changes sign, they don't take always the same value. This nonstationarity is explained by the influence of the random factors in our model. According to the proposed mechanism, the system walks in multi-steps (Fig. 4.4). The amplitude of the response depends on random factors, such as the sequence of perturbed nodes and their different local fields and connectivities. When the signal is weak and fast, these random factors influence the amplitude of the response, which explains the nonstationarity. Lower panel: Same as Fig.4.8 for a slower forcing $\Omega = \frac{2\pi}{333.3}$. If is sufficiently slow, many nodes are perturbed, and at the end the system is able to display the maximum possible response and reach the points $m = \pm 1$.

The origin of the discrepancy in the results of simulations and mean field lies in the approximation 4.8. When we consider an annealed version, where disorder is not correlated in time, we can recover a bistable potential as it is predicted by the mean field. In the annealed version, the neighbourhood is fixed but the relationship matrix w_{ij} is redefined randomly at each time step. In fact, this version could be more accurate to represent, for instance, plasticity in the brain, or a society without personal prejudices: here people are not always opposed to the position of the same neighbours. Another option is to allow for a transient time, when the connectivity changes randomly, and then freeze the connections. This transient time with annealed disorder is a way of averaging over the distributions of repulsive links, thereby making the system less dependent on initial conditions. This scenario might model a society where a diffusive animosity finally crystallises into entrenched positions of friends and enemies, or in another context, the known fact that brain plasticity is higher in initial stages. Even though the microscopic mechanism of resonance is the same in all the three scenarios, the macroscopic picture is somewhat different. In the temporarily annealed scenario, the bimodal distribution of stable states in Fig. 4.9 suggests a bistable nonlinear dynamics. We don't show here the annealed disorder case, because it looks similar to Fig. 4.9. However, there is a difference: in the annealed disorder scenario the system oscillates randomly between the potential wells, whereas in the temporarily annealed case, usually (not always...) a stable state is reached when the population is not being forced by an external signal. Comparing the lower panel of Fig. 4.9 with the upper panel of Fig. 4.8 we observe that the response to very weak fast signals is much more pronounced when the relationship matrix changes with time.

Just like the introduction of diversity in the number of repulsive links made the response more robust against changes in the number of elements, so does the introduction of some kind of stochastic disorder make the system more sensitive to weaker signals.

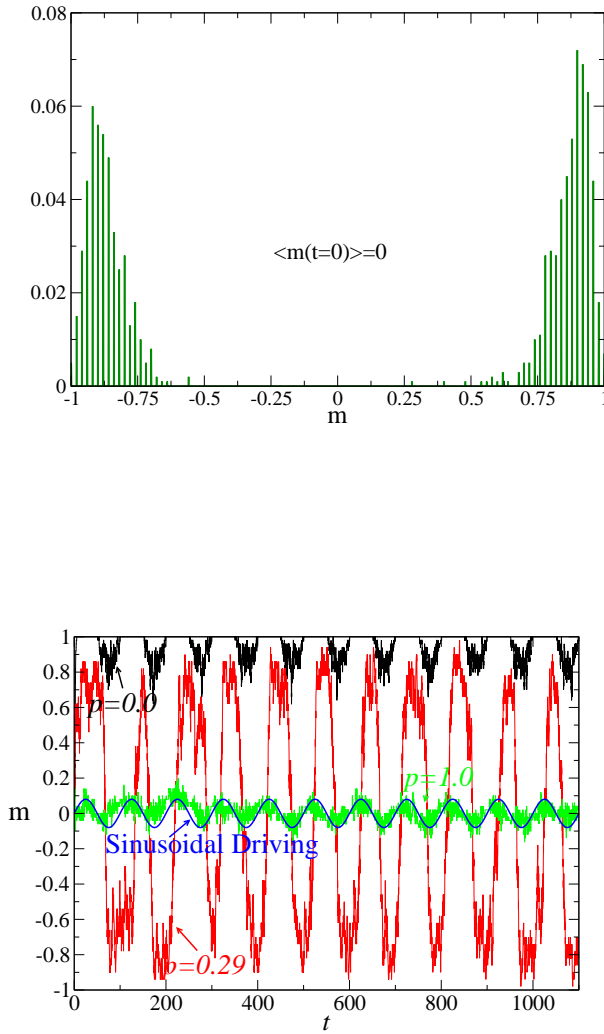


Figure 4.9. The influence of annealed disorder. Upper panel: Distribution of stable states at the optimal probability $p_c = 0.26$ in the case of an unforced random network with $q = 1$, $N = 100$, $k = 10$, $\kappa = 1$ starting from random initial conditions ($\langle m(t = 0) \rangle = 0$). Lower panel: Evolution of the magnetisation following a weak signal $a = 0.08$, $\Omega = \frac{2\pi}{100}$, in the case of a random network with annealed disorder in the interaction matrix, $q = 1$, $k = 10$, $\kappa = 1$.

4.6 Conclusions

We have used Monte Carlo simulations and analytical (mean field) calculations to investigate the response of a system of two-state units, with both attractive and repulsive interactions and majority-rule dynamics, to a weak periodic signal. For both regular and random networks, we have found that competing interactions can enhance the system response – a kind of “divide and conquer” strategy. In each case, a resonance was found for an optimal percentage of negative links which depends on the model parameters. Applications include opinion dynamics and neuron networks but the model is generic enough to predict that the same type of effect can be found in other systems. We have carried out a detailed analysis for an opinion model first introduced by Zanette and Kuperman [44] but we want to stress that the “microscopic” details of the model are not essential for the resonance phenomenon. In fact, we have considered other models with modified versions of the updating rules and still the same main results hold. For instance, instead of a sinusoidal time dependent probability of following either the external signal or the weighted majority, we have tried a constant probability a . The dynamical rules are then modified to:

$$\mu_i(t + \tau) = \begin{cases} \text{sign} \left[\sum_{j \in V(i)} \omega_{ij} \mu_j(t) \right] & \text{w.p. } 1 - a, \\ \text{sign} [\sin(\Omega t)] & \text{w.p. } a, \end{cases} \quad (4.17)$$

Another modification considers that the effect of the external influence is a factor to be considered simultaneously with the majority rule. In this case, the updating rule becomes:

$$\mu_i(t + \tau) = \text{sign} \left[\frac{1}{k_i} \sum_{j \in V(i)} \omega_{ij} \mu_j + a \sin(\Omega t) \right] \quad (4.18)$$

In both modified versions we have confirmed our main result, namely that there exists a value of the probability of repulsive links p for which the response adopts a maximum value.

We have discussed in some detail the microscopic mechanism for the amplification. We argued that the flexibility of the system to follow the

external signal requires that the *local field* seen by each unit is kept close to zero and analysed how this condition might be achieved in some parameter limits.

A macroscopic analysis, in terms of a relaxation dynamics in a bistable potential, is able to explain the mean-field results. It is difficult to use this description beyond the mean field treatment, due to the presence of many metastable configurations. Because of their presence, a large response, corresponding to oscillations around (symmetrical) absolute minima can be obtained for a sufficiently slow forcing.

There are studies that point to the role network topology plays in synchronisation or response to stimuli [114]. Analysing the effect of coupling strength, degree distribution and other network characteristics on the coherent response may shed some light on how the mechanism can be optimised.

5

Mass media reception in a continuous opinion model

This chapter focus on the effect of repulsive interactions on the adoption of an external message in an opinion model. With a simple change in the rules, we modify the Deffuant *et al.* model to incorporate the presence of repulsive interactions. We will show that information receptiveness is optimal for an intermediate fraction of repulsive links. Using the master equation as well as Monte Carlo simulations of the message-free model, we identify the point where the system becomes optimally permeable to external influence with an order-disorder transition.

5.1 Introduction

The discrete model we considered in the previous chapter suggested that a society where its members interact via some repulsive links increases its receptivity to an external message for an intermediate probability of repulsive links. Still, the model is very generic, and perhaps too vague. Therefore, we will now study a more established representation of opinion formation. Carletti *et al.* [58] study the conditions for an efficient spreading of propaganda in the Deffuant *et al.* model, and find that when the interaction threshold is small, propaganda can only have local effects. In this work, we show this

is not the case under the presence of repulsive links: when agents prefer to have different opinions than some of their neighbours, consensus can be built around an external message, even in close-minded societies.

In the previous bistable systems, the individual units have some stable states that can only be left or accessed by overcoming a barrier that a weak signal alone is not enough to surpass. Disorder cooperates with the signal by inducing collective switches at the signal rhythm between the stable states.

The novelty of the present study lies on the identification of a comparable phenomenon - an optimal response to a message resulting from the presence of disorder - in a system that does not have the usual ingredients. An agent can adopt any opinion on an interval, not having an intrinsic preferred state. But as a result of the collective dynamics, opinions can be fragmented into several non-interacting groups [41], some of which will be beyond the message's threshold of interaction. As we will see, it is the presence of repulsive links that enables agents to reach the basin of interaction of the signal.

In the rest of the chapter, after defining the model and the corresponding parameters, we present and analyse the results and summarise our main conclusions.

5.2 Model

We consider that an agent i , taken from a set of $i = 1, \dots, N$ agents, holds at time t an opinion x_t^i expressing on a numerical scale his degree of agreement on a particular topic. The opinions take values on the interval $[0, 1]$: values close to 0 indicate a large degree of disagreement, and values close to 1 a large degree of agreement with the topic in question. At time $t = 0$, the opinions are independently drawn from a uniform random distribution in the interval $[0, 1]$. We assign a weight ω_{ij} to the link connecting agents i and j and consider the symmetric case $\omega_{ij} = \omega_{ji}$ (or an undirected network). The weights take randomly positive or negative values: $\omega_{ij} = 1$ with probability $(1 - p)$ or $\omega_{ij} = -1$, with probability p .

The model is based on the rules introduced by Deffuant *et al.*: At time

t two individuals, say i and j , are randomly chosen. If their opinions are closer than the bound of confidence ϵ , $|x_t^i - x_t^j| < \epsilon$, they converge or diverge as

$$x_{t+\tau}^{i(j)} = x_t^{i(j)} + \mu\omega_{ij}(x_t^{j(i)} - x_t^{i(j)}), \quad (5.1)$$

where the parameter μ mainly determines the speed of convergence or divergence. We will adopt from now on the value $\mu = 0.5$, which minimises the transients. Note that as a consequence of repulsive interactions, this evolution rule could allow opinions to leave the interval $[0, 1]$. To keep x_t^i in the interval $[0, 1]$, we impose the extra adsorbing boundary conditions: if $x_{t+\tau}^i < 0$, $x_{t+\tau}^i = 0$, and if $x_{t+\tau}^i > 1$, $x_{t+\tau}^i = 1$. By taking $\tau = 1/N$, we define the usual unit of Monte Carlo time as N updates.

To model the effect of advertising we add the rule that every T/τ agent-agent interactions, the entire population interacts simultaneously with an external message, or signal, S . That is, for every individual i , if $|x_t^i - S| < \epsilon$,

$$x_{t+\tau}^i = x_t^i + \mu(S - x_t^i), \quad (5.2)$$

where S is a constant in the interval $[0, 1]$.

Note that the original Deffuant *et al.* model [41] with propaganda [58] is recovered when $p = 0$.

5.3 Results

Figure 5.1 shows the simulations results for the number of agents whose opinion coincides with the propaganda - the “followers”. We start our analysis by noting that the time evolution proceeds much slower when there is a combination of positive and repulsive links, compare $p = 0.30$ with $p = 0$ and $p = 1$. We would reach asymptotically a steady state in the limit $t \rightarrow \infty$. However, we have decided not to focus on those asymptotic values since we argue that they can have no practical interest, as no social interaction can persist for an infinite time. Instead, all time average results of this paper refer to averages in the latest 20% of the time, or $t \in [11200, 14000]$, an

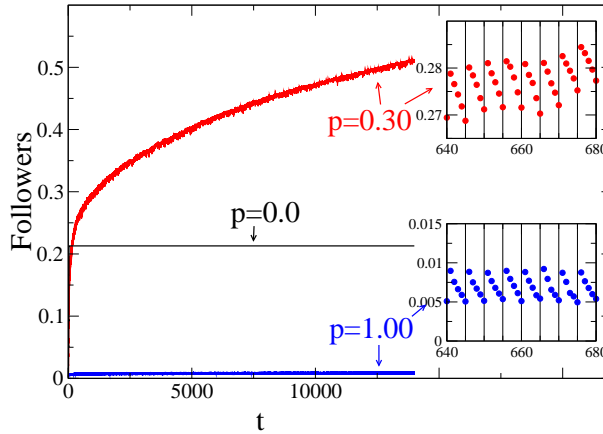


Figure 5.1. Time evolution of the fraction of followers. $\epsilon = 0.1$, $S = 0.1$, $N = 10^3$, $T = 5$. In the insets, we have a closer view of the $p = 0.3$ and $p = 1.0$ cases. The vertical lines show the times where the signal was acting, and hence the number of followers increases. Averages over 100 runs.

arbitrary choice, but we note that the qualitative results do not depend on the chosen time interval.

In Fig. 5.2 we plot the average fraction of followers, as a function of the probability of the repulsive links p and the bound of confidence ϵ . For a given p , the adoption of the external message depends on the period T of the signal, and on the the bound of confidence ϵ . As noticed in [58] for the $p = 0$ case, when ϵ is sufficiently large, namely for $\epsilon > 0.28$, the message can spread to all agents. In contrast, when all interactions are attractive and ϵ is small - a “close-minded society”, where agents only interact with others whose opinion is very close - the message cannot convince the entire population [58]. For $\epsilon < 0.28$ and in the absence of advertising, opinions are fragmented into several major groups [40] that don’t interact with each other. Since some of the clusters will be outside the propaganda basin of attraction, the external message can only have local effects [58]. In this region, the presence of a fraction of repulsive links is crucial for the message to spread to the entire population, as seen in Fig. 5.2. We also observe that a low-frequency signal (Fig. 5.2, b)) can not convince the entire population when there is a significant fraction of repulsive links, a point to which we will return later (Fig. 5.4).

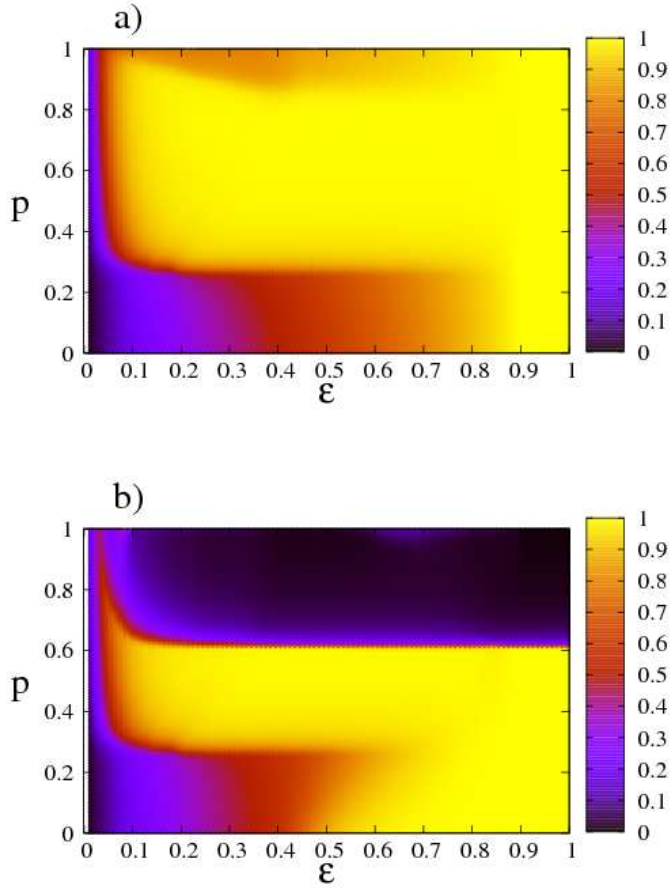


Figure 5.2. Density plot of the fraction of followers as a function of the probability of repulsive links p and the bound of confidence ϵ for messages of a) high frequency ($T = \tau = 0.001$) and b) low frequency ($T = 1$). The plots are the results of averages over 100 runs in the case $S = 0.1$ (extreme message) and $N = 10^3$. Similar results are obtained for other values of S and N , namely for $S = 0.5$ (moderate message) for both $N = 200$ and $N = 10^3$.

Interestingly, the fraction of repulsive links where consensus around the signal starts to build, $p \approx 0.30$, is remarkably independent on the specific characteristics of the message, like its frequency and value. This suggests that we must explore the effect repulsive interactions have on the system in the absence of signal, to find out what changes at that probability that can help the adoption of any kind of propaganda. In Fig. 5.3 we present the results for the probability density function, $P(x)$, of the agents opinions coming from the numerical integration of the master equation [47,48] (details in the Appendix D), and from Monte Carlo simulations of the propaganda-free system. The master equation can be seen as the $N \rightarrow \infty$ limit of the Monte Carlo simulations approach: since those are done for finite N , there are some small differences in the results coming from the two methods. At $p = 0$, clusters evolve to consensus regions, whereas at $p \approx 0.30$ a distinctive pattern emerges in the distribution of opinions. Even though we can still distinguish clearly several peaks corresponding to higher concentrations of agents, the consensus inside a group is lost, and its boundaries are permeable, falling under the basin of interaction of a neighbouring one, something which turns out to be essential for optimal message reception, since it will allow the entire population to interact with an external message.

However, the exposure to the message is only a precondition for following it, a second requirement being to stabilise agents in its position. Agents cease to negotiate when they share the same opinion, regardless of whether their connection is repulsive. In case propaganda convinces agents to adopt its message, the dynamics between those agents stops.

The number of followers can only increase if propaganda convinces agents at a faster rate than the rate they disperse in its absence (insets Fig. 5.1). When the fraction of repulsive links becomes too high to stabilise a low-frequency signal, the number of followers decreases, as we see in figs. 5.2 and 5.4. If the bound of confidence ϵ is large, and the signal frequency is low, it is easier to form a consensus around the signal when there are few or none repulsive interactions (Fig. 5.2, b), and Fig. 5.4, b)). When the signal frequency is low and ϵ is small, the region of optimal reception of the message shrinks until it coincides with the order-disorder transition (Fig. 5.2, b), and Fig. 5.4, a)), where clusters are no longer consensus regions - facilitating interaction with neighbouring ones- but can still be clearly identified - agents

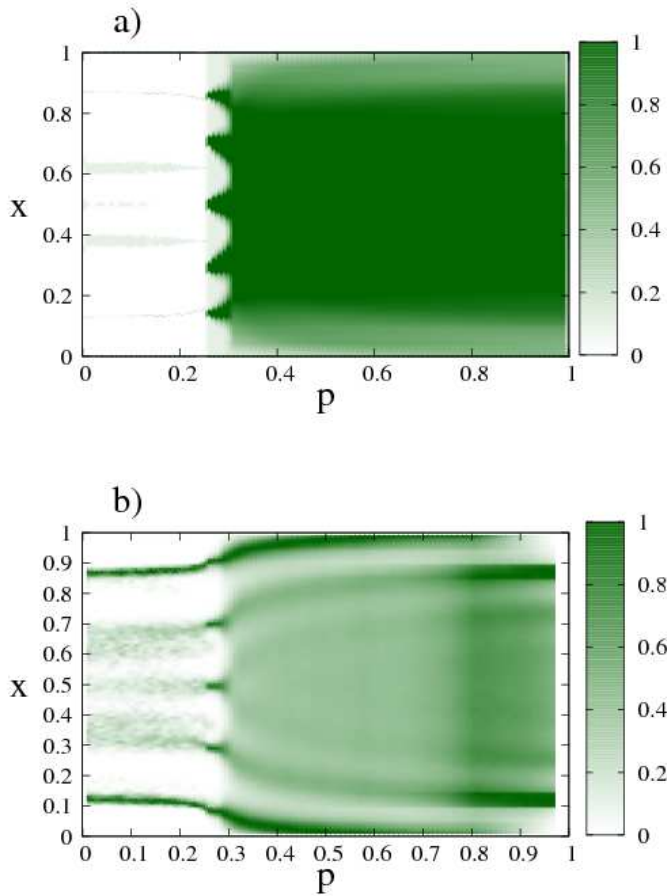


Figure 5.3. Density plot of the distribution $P(x)$ of agents as a function of p in the propaganda-free system for $\epsilon = 0.1$ revealing a order-disorder transition at $p \approx 0.30$. a) steady state results of the master equation. b) simulations with $N = 10^4$ and averaged over 100 runs, for $t = 14000$. For better viewing, in the simulation results, the image was rescaled by dividing by the highest value at each probability and, in the master equation results, we considered each value greater than 1 as 1, and each value smaller than 0.1 as 0.1.

don't spread much, which facilitates stabilisation.

Figure 5.5 shows how agents distribute themselves in the opinion space, as a function of p , when $S = 0.1$ and $T = 2$. We observe that when ϵ is small, (Fig. 5.5, a)) and the value of p is below the order-disorder transition region, the lack of followers reflects the formation of some groups that adopt an opinion outside the message's basin of attraction, and implies the permanent rejection of the message by a significant fraction of the population. As previously mentioned, when ϵ is large (Fig. 5.5, b)) and all interactions are attractive, the message is adopted by the entire population.

By contrast, when p is too high to stabilize the signal, we don't observe the appearance of a plural society with well defined groups. Instead, most agents can spend some time adopting the message, forming a cluster around the propaganda, (Fig. 5.5) that has its support base being continuously refreshed. In Fig. 5.6 we plot a typical trajectory for one agent: when the probability of repulsive links is high, the agent changes its opinion constantly, without going far from the propaganda position. This represents a situation where a new level of opinion has been reached by most members of society, and yet there is still negotiation around details. Meanwhile, the situation of the few agents that don't gather around the external message depends on the type of society, as defined by its interaction threshold: for small ϵ (Fig. 5.5, a)), they constantly change their opinion over all the opinion range, and are not beyond the possibility of still being convinced by the propaganda; while for large ϵ (Fig. 5.5, b)) agents form a cluster in the extreme opposite position, if the external message was also extreme.

5.4 Summary and Conclusions

In this work we have analysed the response to an external message, of a social system represented by the Deffuant *et al.* model with a combination of positive and repulsive interactions. We focused in more detail on the case of a low confidence bound, or close-minded society, where the presence of a given fraction of repulsive links is required for the entire population to adopt the message.

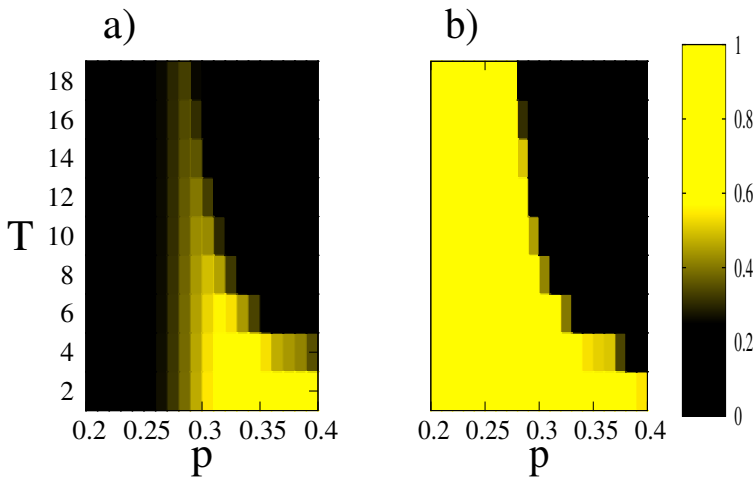


Figure 5.4. The fraction of followers as a function of p and T . As the period T increases, it becomes increasingly harder for systems with a high probability of repulsive links to follow the message. Parameters: a) $\epsilon = 0.1$ and b) $\epsilon = 0.7$. Other parameters: $S = 0.1$, $N = 10^3$. Averages over 100 runs.

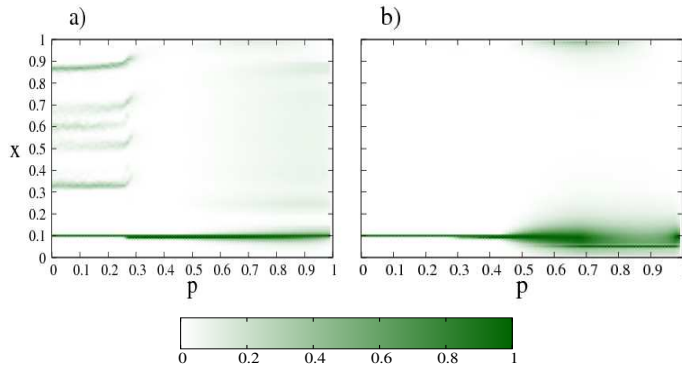


Figure 5.5. Two-dimensional plot of the distribution of agents in opinion space, as a function of p and with $S = 0.1$. Parameters: a) $\epsilon = 0.1$ and b) $\epsilon = 0.7$. For better viewing the image was rescaled by dividing by the highest value at each probability. Averages over 100 runs, $N = 10^4$, $T = 2$ and $S = 0.1$.

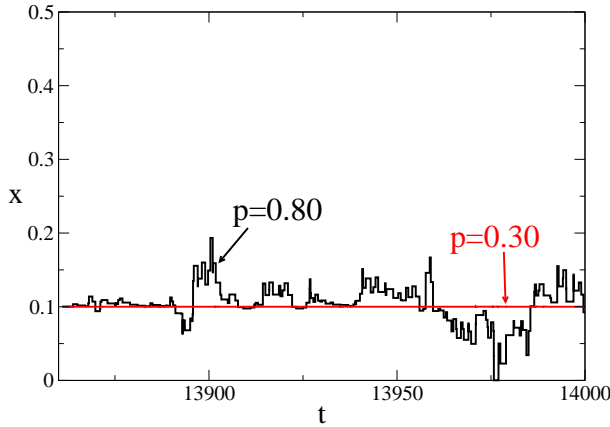


Figure 5.6. Typical trajectory for one agent under signal influence with $\epsilon = 0.1$ and other parameters as in Fig. 5.5.

In that small ϵ case, the region of optimal response to the signal starts to build around an order-disorder transition region, that we identified resorting to the master equation and simulation results of the propaganda-free system. When the signal frequency decreases, this optimal region shrinks until it coincides with the order-disorder transition point. The same coincidence was noticed in previous studies [89, 108, 115] showing an optimal response induced by diversity or competitive interactions, and we conclude that it is expected in extended systems where some of the units can be in a state that is inaccessible to the external signal, whether it is because of the existence of a potential barrier like in the previous works, or because of a threshold of interaction. We saw that the presence of repulsive links and consequent dispersion of opinions is a necessary condition for a collective adoption of the message, by increasing the number of agents within the reach of propaganda. Below the transition region, we assist to the formation of a plural society, because a substantial fraction of agents doesn't interact with propaganda.

We discussed results concerning an intermittent propaganda that has always the same value S . We also tested the case of a sinusoidal propaganda, and found the same enhancement of the response for a certain fraction of repulsive links, that, not surprisingly, was harder to stabilise in the exact signal position. Since, unlike in previous studies [89, 108, 115], agents don't

have preferred opinions between which they can oscillate, the time-varying propaganda case corresponds simply to a very low frequency intermittent message, that as we saw can only receive a significant response in the order-disorder transition region.

It is not a surprise that a close-minded society with strict agreement rules, or the paradigm of a very conservative society, is not open to outside influences. What is not so expected is to find out that the presence of repulsive links can in fact drive the population to form a consensus around an external message, regardless of whether the message is extreme or moderate. In this situation, and as a result of wanting to be apart, agents end up together sharing the same opinion.

In this work we stress the importance that repulsive links have in the dynamics the Deffuant *et al.* model. Further studies should address the effect that repulsive interactions have in the dynamics of other continuous opinion models with different interacting rules.

6

Synchronisation induced by repulsive interactions in the van der Pol oscillator

We study a system of identical van der Pol oscillators, globally coupled through their velocities, to see how the presence of competitive interactions affects its synchronisation properties. We will address the question from two points of view. Firstly, we will investigate the role of competitive interactions, on the synchronisation among identical oscillators. Then, we will show the presence of an intermediate fraction of repulsive links results in the appearance of macroscopic oscillations at that signal's rhythm, in regions where the individual oscillator is unable to synchronise with a weak external signal.

6.1 Introduction

Synchronisation, [11] or the ability of coupled oscillators to adjust their rhythms, is a property that arises in many systems, from pacemaker cells in the heart firing simultaneously as a result of their interaction, [116] to the fetal heart rate adjusting its pace to maternal breathing, as an example of

forced synchronisation. [117]

Typically, oscillators with different frequencies are able to synchronise due to a strong enough positive coupling among units. However, interactions in Nature are often repulsive and, surprisingly, it was found that under some particular circumstances repulsive interactions can actually enhance synchronisation: thus, the presence of negative links can prevent the instability of the fully synchronised state when it compensates an excessive number of positive links, [118] or its sparse presence can enhance synchronisation in small-world networks. [99] Most interestingly - since it is not always desirable to achieve a state of full synchronisation - the presence of repulsive links can give rise to new forms of synchronisation, [119] that sometimes can be described as glassy or glassy-like. [120, 121, 122, 123] Additionally, the beam-forming abilities of a system of repulsively coupled Stuart-Landau oscillators were considered in. [124]

So far, studies have mostly focused on non-identical phase oscillators, and several coupling schemes have been chosen, such as local [125] or long-range, [99] and purely repulsive [119] or assuming a competition between repulsive and attractive. [126] Like in, [126] we want to isolate the effect of different proportions of repulsive interactions by considering identical oscillators. However, rather than establishing how full synchronisation becomes unstable as the fraction p of repulsive links increases, [126] our focus will be on the characterisation of the different configurations that emerge as p grows, and its implications for signal transmission when the system is subjected to an external forcing. Also, unlike [126] we will not consider phase oscillators, but instead van der Pol oscillators, [12] which implies phase, amplitude and frequency synchronisation are taken into consideration.

The establishment of the role of the coupling structure on synchronisation, independently of the detailed specification of the nodes dynamics, can rely on the study of the Laplacian matrix. [127, 104] We will identify and characterise a transition region from synchronisation to desynchronisation by analysing the eigenmodes of the Laplacian matrix corresponding to different proportions of repulsive links, adapting the formalism developed in Chapter 3. [115, 103]

The second part of the chapter will be devoted to explore the role of

competitive interactions in the synchronisation of the system with an external periodic signal. We will choose a signal whose frequency lies outside the region of entrainment for an uncoupled oscillator, as well as for an all attractively coupled system. This problem is closely related to the theoretical framework of resonance studies that we reviewed in Chapter 2. In the latter cases [115, 108] it was found that an intermediate fraction of repulsive links was able to amplify the response to an external signal, in bistable systems where the external signal was the only source of movement. In the present case, an optimal response should correspond to an adjustment between the intrinsic frequency of the oscillators and that of the external signal; as we will see, that optimal response is achieved at an intermediate proportion of repulsive links in the case of strong fast signals, whereas weak slow signals are best responded when all the links are negative.

The outline of this chapter is as follows: in section 6.2 we will introduce the model; we show that an increase of the proportion of repulsive links leads to loss of synchronisation in section 6.3; and in section 6.4 we show how the presence of repulsive links accounts for an enhanced response to external signals; in section 6.5 we will briefly mention some extensions; and conclusions are drawn in section 6.6.

6.2 Model

We consider an ensemble of van der Pol oscillators [12] $\{x_i(t), i = 1, \dots, N\}$, globally coupled through their velocities \dot{x}_i , and subjected to an external periodic forcing of amplitude A and frequency Ω . The dynamics is described by:

$$\ddot{x}_i = -x_i + \mu(1 - x_i^2)\dot{x}_i + \frac{C}{N} \sum_{j=1}^N J_{ij} (\dot{x}_j - \dot{x}_i) + A \sin(\Omega t), \quad (6.1)$$

where the nonlinearity parameter μ is a positive constant and C is the coupling strength.

The coupling between the oscillators i and j is given by the interaction

term J_{ij} and can be attractive or repulsive, according to a given probability p .

$$J_{ij} = J_{ji} = \begin{cases} -1, & \text{with probability } p, \\ 1, & \text{with probability } 1 - p. \end{cases} \quad (6.2)$$

The single van der Pol oscillator is the paradigmatic example of a non-linear oscillator whose characteristics we have reviewed in Section 1.2. It possesses a stable limit cycle as a result of its nonlinear damping term $\mu(1 - x_i^2)$: for small oscillations, $|x_i| < 1$, the system experiences negative damping and the oscillations grow, while for $|x_i| > 1$, the positive damping causes the oscillations to decrease. Therefore, independently of the initial conditions or small perturbations, its amplitude of oscillations reaches a constant (equal to 2), while its detailed shape and period T depend on μ , approaching $T \approx (3 - 2 \ln 2)\mu$ for large μ . In this case of large $\mu \gg 1$, the oscillations are called relaxational and are characterised by the presence of discontinuous jumps intercalated by periods of slow motion.

6.3 Desynchronisation among the unforced oscillators, $A = 0$

We start by seeing how the coupling can affect synchronisation among the oscillators, in the unforced ($A = 0$) system case. Having identical natural frequencies, the oscillators would become phase-synchronised when all the interactions are attractive. The presence of repulsive interactions might desynchronise them, and the way it does so depends on the type of coupling we choose. Namely, we can distinguish between reactive and dissipative coupling, depending on whether the oscillators are coupled through their positions or velocities, respectively. To get a feeling of the difference between them, we start by giving an heuristic geometrical illustration of how the coupling between two oscillators affects their dynamics, by the observation of the phase plot in Fig. 6.1.

Two oscillators D and B (Fig. 6.1) repulsively coupled through their positions change their oscillation amplitude as a result of their interaction,

which can place them increasingly farther away from the region of fast motion, and eventually destroy the oscillatory motion. In Fig. 6.1 right panel we plot two typical examples of trajectories of two individual oscillators and their respective phase plot, for $p = 0.40$. We can observe a sometimes complete destruction of the traditional shape of the Van der Pol limit cycle that sometimes (inset of the same figure).

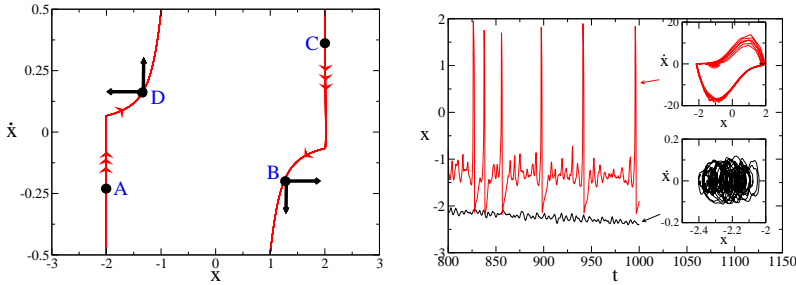


Figure 6.1. Left panel: A zoom of the limit cycle, focusing on the slow motion region. The arrowheads indicate phase flows: single arrowheads indicate slow segments of the limit cycle while triple arrowheads indicate fast jumps. The arrows on the oscillators D and B depict their interactions: a vertical arrow depicts a repulsive interaction through velocities, and a horizontal one a repulsive interaction through positions. Right panel: examples of two typical individual trajectories for $p = 0.40$ with reactive coupling, and respective phase plots, in a system with $N=100$, $C=20$. $\mu = 10$.

By contrast, the coupling through velocities preserves the essential shape of the limit cycle, even when the number of repulsive links is very high (Fig. 6.2). In case the proportion of repulsive links is not too high, the main effect of this type of coupling between oscillators D and B (Fig. 6.1) is to deform the slow motion region and sometimes drive the units closer to the region of fast motion, where a weak stimulus could be enough to enact a jumping to the other slow motion region.

Fig. 6.2 shows the trajectory (upper panels) and respective limit cycles (lower panels) of two typical individual oscillators for some probabilities p of repulsive links. In all cases, the essential characteristics of the van der Pol oscillator, such as a steady amplitude and the existence of two time scales, are preserved by this type of coupling, as it is reflected by the fact that the stable limit cycles (Fig. 6.2, lower panels) maintain its basic shape.

Having identical natural frequencies, when the coupling constant C is strong enough the position of the oscillators becomes synchronised when all the interactions are attractive. (Fig. 6.2, for $p = 0$). As the proportion of repulsive links grows, both the amplitude and the phase of the oscillators start to desynchronise (Fig. 6.2, $p = 0.4$). Finally, a further increase in the proportion of repulsive links (Fig. 6.2, $p = 0.60$ and $p = 1.0$), drives the system to a configuration where the global variable $X(t) = \frac{1}{N} \sum_i x_i(t)$ is zero, with several groups oscillating in anti-phase, with a decreased frequency and an increased amplitude of oscillations: if we consider two groups with the same size that are oscillating in anti-phase, it can be shown that their amplitude becomes rescaled as a result of their interaction by a factor of $\sqrt{1 + \frac{C}{\mu}}$ (Appendix E).

We can describe the last configuration characterised by a zero value of the average position $X(t)$ as a disordered situation at the macroscopic level. To quantify this *disordering* role of repulsive links, we define, following, [94] the complex variable $z_i = x_i + ix_i$, the average $\bar{z} = \frac{1}{N} \sum_{i=1}^N z_i$ and the variance of z_i normalised by the average value of the modulus squared, $\sigma^2[z_i]$:

$$\sigma^2[z_i] = \left\langle \frac{N^{-1} \sum_{i=1}^N |z_i - \bar{z}|^2}{N^{-1} \sum_{i=1}^N |z_i|^2} \right\rangle, \quad (6.3)$$

here and henceforth $\langle \dots \rangle$ denotes a time average.

The normalised variance can take values between $\sigma^2[z_i] = 1$ for maximum disorder, and $\sigma^2[z_i] = 0$ when all oscillators are synchronised amongst themselves. From this, we choose [94] a measure of order that reduces to the Kuramoto order parameter [128] when all units oscillate with the same amplitude:

$$\rho = \sqrt{1 - \sigma^2[z_i]}. \quad (6.4)$$

As dispersion increases, ρ decreases from $\rho = 1$ to $\rho = 0$. As we show in Fig 6.3, there is a clear synchronisation-desynchronisation transition for an intermediate fraction of repulsive links, that does not depend much on the coupling strength C .

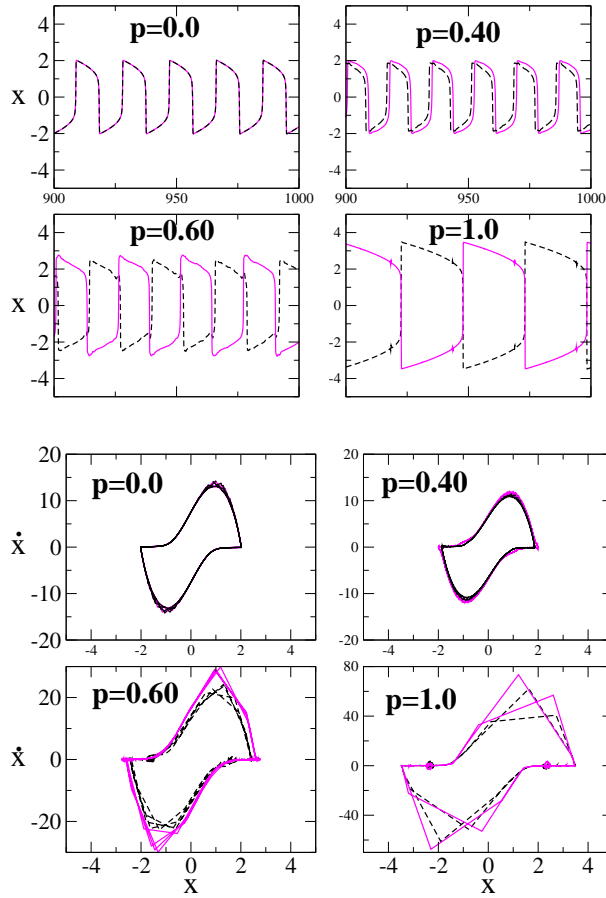


Figure 6.2. Trajectories (upper panels) and phase portraits (lower panels) of two individual oscillators, for various probabilities p of repulsive links. Regardless of initial conditions, the van der Pol oscillator reaches steady state oscillations with a constant amplitude. In the lower panels we represent the corresponding limit cycles in the phase plane of (x, \dot{x}) : as p grows the distinction between slow and fast motion becomes clearer which is manifested in the more abrupt angles in the limit cycles for $p = 0.6$ and $p = 1.0$. $N=100$, $C=20$, $\mu = 10$, $A=0$.

To characterise desynchronisation further, it is useful to look into the behaviour of the field that an oscillator feels as a result of the interaction with other units. The average number of *effective links* $F = \frac{1}{N^2} \sum_{ji} J_{ij}$, in a given run can in general be different from the particular number an oscillator has, $f_i = \frac{1}{N} \sum_{i=1}^N J_{ij}$, given that the probability of repulsive links p follows a binomial distribution with the corresponding variance. We want to know if there is a correlation between the fraction of repulsive links an oscillator has and its synchronisation with the overall majority. That is described by the following quantity G :

$$G = \left\langle \frac{1}{N} \sum_{ji} \dot{x}_j \dot{x}_i [f_i - F] \right\rangle = \left\langle \dot{X} \sum_i \dot{x}_i [f_i - F] \right\rangle, \quad (6.5)$$

being $\dot{X} = \frac{1}{N} \sum_j \dot{x}_j$ the mean velocity. We observe that the order-disorder transition region $p \sim [0.4, 0.45]$ we identify in the upper panel of Fig. 6.3, is accompanied by an increase in the influence on an oscillator of its particular coupling configuration, as signalled by the peak in G (Fig. 6.3, lower panel). The oscillators with a higher than average number of repulsive links form a loosely synchronised group in a different slow region than the one where the majority concentrates.

The partial independence of the state of the oscillator on the global configuration opens the possibility of the existence of several different global states, and thus hints at the existence of metastable states. We can relate this behaviour to the coupling structure, by the spectral analysis of the associated Laplacian matrix $J'_{ij} = J_{ij} - \delta_{ij} \sum_{k=1}^N J_{kj}$, [115] where δ_{ij} is the Kronecker's delta. We begin by rewriting Eq. (6.1) as system of two equations that highlight a fast motion for the x_i variable and a slow motion for the y_i variable:

$$\dot{x}_i = \mu \left[x_i - \frac{1}{3} x_i^3 - y_i + \frac{D}{N} \sum_{j=1}^N J'_{ij} x_j \right] \quad (6.6a)$$

$$\dot{y}_i = \frac{1}{\mu} [x_i - A \sin(\Omega t)]. \quad (6.6b)$$

where $D = \frac{C}{\mu}$.

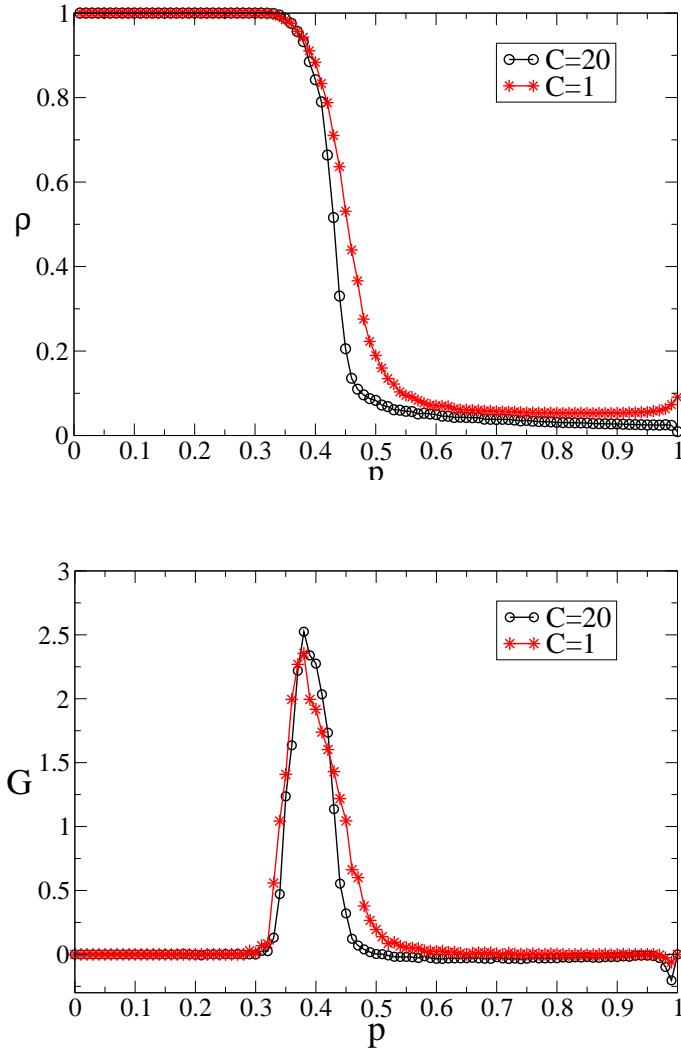


Figure 6.3. The measures of disorder ρ (upper panel) and G (lower panel). Averages over 100 runs, and N , C , μ and A as in Fig. 6.2

We focus on Eq. (6.6a), letting the slow variable y_i be a constant. The Laplacian appears naturally in the coupling term, and we can see its positive eigenvalues should help deviations from a given state along the x variable. [115, 104] We now introduce the eigenvalues Q_α and eigenvectors $e^\alpha = (e_1^\alpha, \dots, e_N^\alpha)$ of the Laplacian matrix, with the normalisation condition $\sum_i e_i^\alpha e_i^\beta = \delta_{\alpha\beta}$.

$$\sum_{j=1}^N J'_{ij} e_j^\alpha = Q_\alpha e_i^\alpha. \quad (6.7)$$

Let us assume the state of a unit i is x_i^o at a given time, where x_i^o is drawn from any symmetric random distribution. We perturb the initial states as $x_i^o + s_i$, and express s_i in terms of the eigenvalues and eigenvectors of the Laplacian, so that $s_i = \sum_{\alpha=1}^N B_\alpha e_i^\alpha$. We aim to see how the interaction with other units influences the reaction to perturbations.

We will assume for simplification that $\sum_{i=1}^N x_i^o e_i^\alpha \sim \sum_{i=1}^N x_i^o \sum_{i=1}^N e_i^\alpha = 0$, and that the modes are uncoupled. After expanding the equation in terms of the Laplacian eigenvalues and eigenvectors, we then multiply the resulting equation by e_i^α and average over all elements, to find the evolution for the amplitude of the α -th mode:

$$\frac{dB_\alpha}{dt} = -\frac{1}{3} B_\alpha^3 + \text{PR}_\alpha \left(\frac{C}{\mu} \frac{Q_\alpha}{N} - k \right) B_\alpha, \quad (6.8)$$

where $k = \frac{1}{N} \sum_{i=1}^N (x_i^o)^2 - 1$ is a quantity related to the variance of the initial conditions, and the participation ratio $\text{PR}_\alpha = 1 / \sum_{i=1}^N [e_i^\alpha]^4$ is a classical measure of localisation that estimates the number of oscillators that participate significantly in a state e^α : for a state localised on a fraction f of elements, PR_α tends to f . According to Eq. (6.8), unless $Q_\alpha > \frac{kN\mu}{C}$, the amplitude of the mode B_α tends to zero, and any deviation from the initial state vanishes. Otherwise, mode α is said to be an *open mode*.

In a precise way, we will define ‘‘localised’’ modes as the ones whose participation ratio is less than $0.1N$, and define a measure M of localisation [115] as $M = \frac{N_L^2}{N_O N}$, where N_L is the number of open localised modes, i.e. those satisfying $\text{PR}_\alpha < 0.1N$, and N_O is the total number of open modes α .

While for extreme probabilities p of repulsive links the number of possible values for Q_α is very restricted, we find that for intermediate levels of p the distribution of Q_α is broader and the eigenvalues at both tails of the spectrum are localised: the upper panel of Fig. 6.4 illustrates this fact for some examples of p .

In our regime of strong non-linearity, or $\mu \gg 1$, the time an oscillator spends on a fast motion is very close to zero; in such case we should have $k \approx 0$ and the condition for open modes can be fulfilled at low enough probabilities of repulsive links. Of the open modes, those that correspond to positive Laplacian eigenvalues facilitate the growth of perturbations, while those that are negative inhibit it. We wish to identify a probability of repulsive links that makes the system flexible enough to sustain deviations from the initial symmetric configuration, yet stable enough so that perturbations don't spread immediately throughout the entire system, as that is what we observe at the transition region (Fig. 6.3 lower panel), where some oscillators are more loosely synchronised than others. We can anticipate [115] that such situation corresponds to a localisation [109, 110] of positive Laplacian modes.

As we see in Fig. 6.4, the peak in G , that signals the range of p where there is an heightened dependence of the state of an oscillator on its coupling structure (Fig. 6.3), coincides with a localisation of the positive eigenvalues of the Laplacian. Those localised positive open modes are responsible for keeping the loss of synchronisation within controllable limits.

6.4 Synchronisation with the external signal, $A \neq 0$

In this section, we will see how competitive interactions affect the response to an external periodic signal. Since in general there can be several frequencies present in the output of the global variable $X(t) = \frac{1}{N} \sum_i x_i(t)$, we say the system is synchronised with the external signal when the highest peak in the Fourier spectrum corresponds to that frequency.

When the natural frequency of oscillations coincides with the external

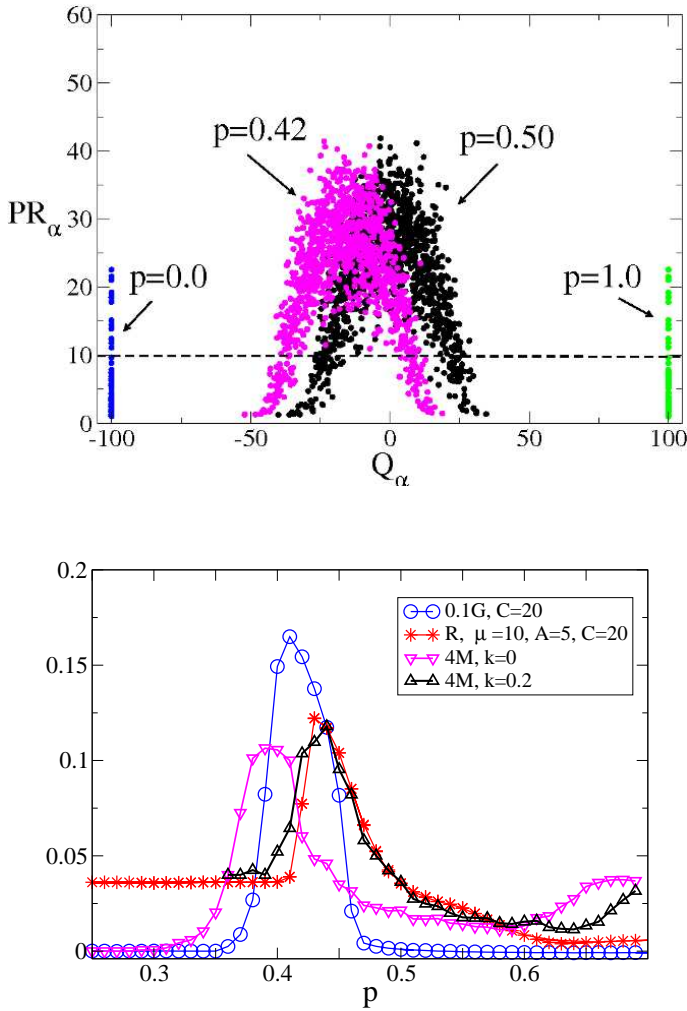


Figure 6.4. Upper panel: we plot the participation ratio PR_α for the Q_α eigenvalues. As the probability of repulsive links p grows the eigenvalues become dislocated towards higher values. The eigenvalues whose participation ratio is below the dashed line are localised. Lower panel: the measures of localisation M , the measure of disorder G , and the spectral power amplification R , all have the maximum value at roughly the same p . For better viewing, we multiplied M by 4, and G by 0.1 $N=100$. In the case of M and $k=0.2$ we have $C=20$ and $\mu = 10$.

forcing frequency, synchronisation is achieved for vanishing A , and as the two frequencies diverge, stronger forcings are needed to entrain the system. We will call a signal *strong* when its amplitude is greater than the amplitude of oscillation of the unforced van der Pol unit, and we will call it *fast* when its frequency is higher than the natural frequency of the individual van der Pol oscillator.

We will distinguish between strong fast and weak slow signals, because the mechanism of synchronisation differs in the two cases, although, in both cases, competitive interactions are required for an enhanced response.

6.4.1 Strong fast signals benefit from intermediate p

In Fig. 6.5 we plot the synchronisation regions and their relative strength, as measured by the spectral power amplification factor [84] R , given by:

$$R = 4A^{-2} |\langle e^{-i\Omega t} X(t) \rangle|^2 \quad (6.9)$$

R is roughly proportional to the square of the normalised amplitude of the oscillations of $X(t)$ at the frequency Ω , being $R < 1$ when the amplitude of oscillations of the forced system is smaller than the amplitude of the external signal.

When $p = 0$, (Fig. 6.5, upper panel) the synchronisation region with respect to the frequency Ω and amplitude A of the external signal has the typical triangular-like shape seen on Arnold tongues. [11] An intermediate fraction of repulsive links ($p = 0.43$, Fig. 6.5, lower panel) pushes the synchronisation borders beyond the $p = 0$ values, allowing for synchronisation of faster signals at weaker forcing.

Fig. 6.6 shows the steady-state trajectory of the macroscopic variable $X(t)$, for different probabilities p of repulsive links, and illustrates the fact a certain proportion of repulsive links is required for the system to adjust its rhythm to that of the external signal (Fig. 6.6, $p = 0.40$), whereas Fig. 6.7 confirms that this optimal response only occurs for an intermediate range of the probability of repulsive links. It should be noted that when entrained, the oscillators adjust their frequency while keeping their natural amplitude

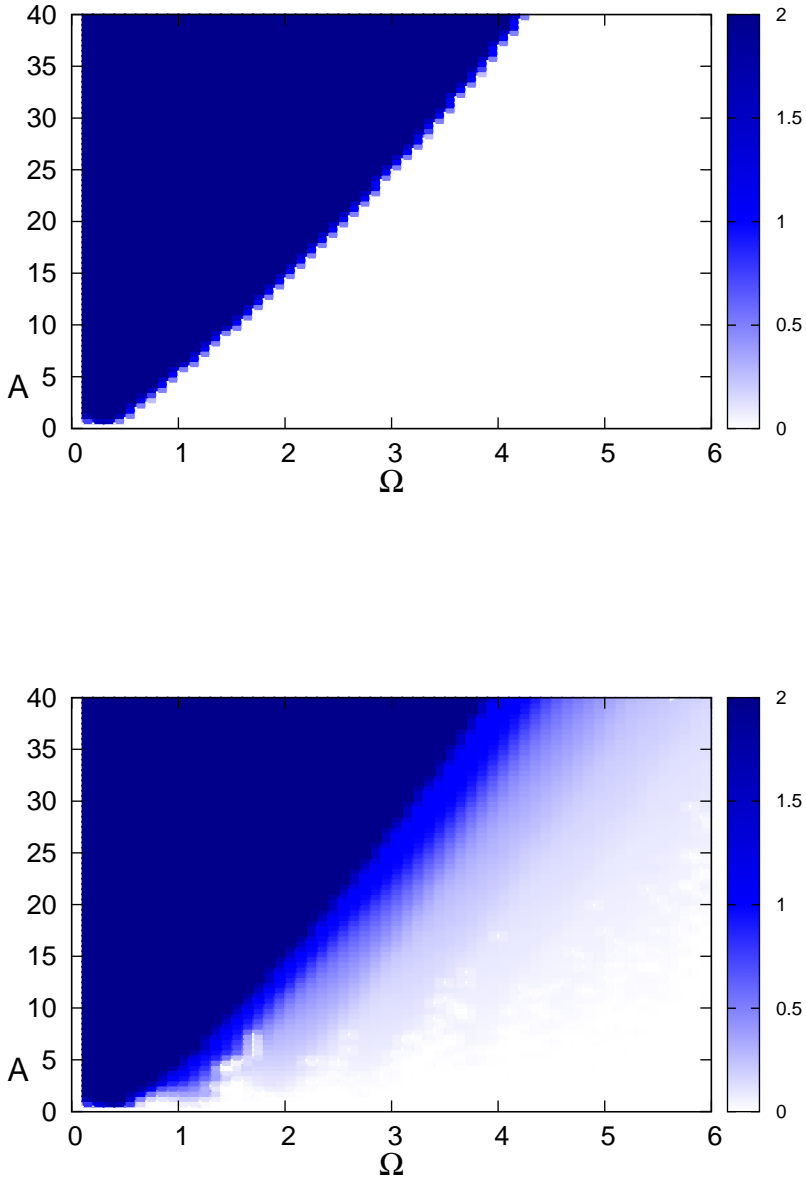


Figure 6.5. We plot the spectral power amplification R in the synchronisation regions for $p = 0$ (upper panel) and $p = 0.43$ (lower panel). For better viewing, we use a color code that saturates for $R \geq 2$. N , C and μ as in Fig. 6.2.

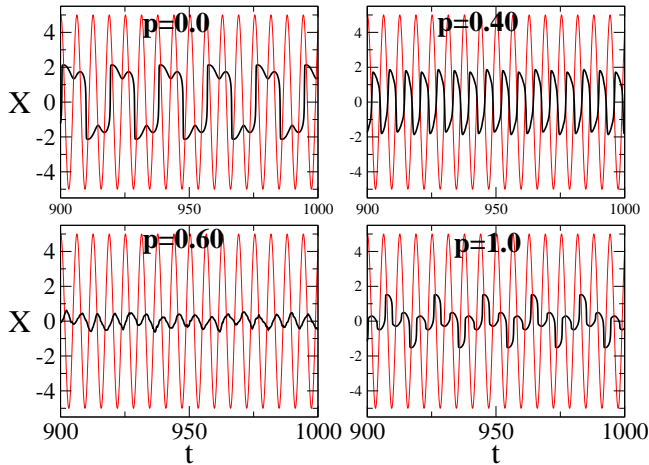


Figure 6.6. Time evolution of the macroscopic variable $X(t)$ when the system is forced by an external sinusoidal fast signal (lighter color) of amplitude $A = 5$ and frequency $\Omega = 1.0$, for several probabilities of repulsive links p . N , C and μ as in Fig. 6.2.

(Fig. 6.6), therefore, the spectral amplification factor R is smaller than 1, when $A > 2$. As expected, the more the natural frequency deviates from the forcing frequency, the stronger the signal needs to be in order to entrain the system: namely (Fig. 6.7), for a forcing frequency $\Omega = 1$, the signal strength needs to be $A = 12$ instead of $A = 5$, when the natural frequency $\omega = 2\pi/T$ is ≈ 0.19 ($\mu = 20$) instead of ≈ 0.39 ($\mu = 10$).

To understand the significance of competitive interactions we recall the results of the last section. The probability region where weak fast signals can be entrained is signalled by the peak in the spectral power amplification R , and coincides with the localisation region, as given by the peak in M (Fig. 6.4).

This localisation, or controlled disorder, is crucial for an enhanced response to fast signals, for it allows the amplitude of oscillations to be deformed, varying slightly enough to place some oscillators closer to the fast motion region, thus allowing a jump to another slow region under an external forcing; but not so much that there is a risk they would trigger a

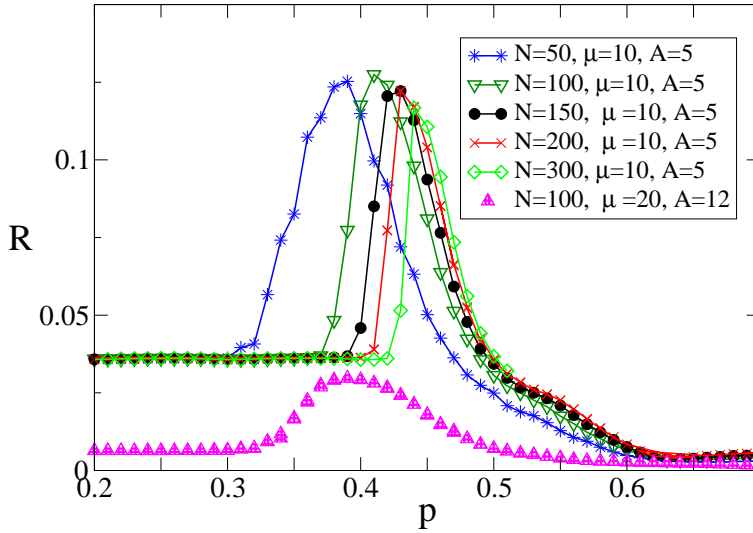


Figure 6.7. Spectral power amplification, for $C = 20$, $\Omega = 1$ and several system sizes N , averages over 100 runs. We note that smaller systems become synchronised at lower fractions of repulsive links, and are not so dependent on the precise fraction of repulsive links. Additionally, we also observed (figures not shown) a resonance with system size for different probabilities of repulsive links. This kind of dependence has been explained elsewhere. [115]

chain reaction, unless there is a permanent pulling into some direction - that is, unless the signal is acting.

6.4.2 Weak slow signals benefit from very high p

In the previous section, we chose to measure the enhancement at the collective level, using the macroscopic variable $X(t)$ in our measure of response R , Eq. (6.9); that corresponded to a synchronisation with the external forcing at the individual level: the greater the number of entrained oscillators, the greater the response was.

We find a different situation when we subject our system to a very weak slow signal with an amplitude that is smaller than 1, say $A = 0.9$. A complete amplitude and frequency synchronisation with this forcing would imply a fast motion, in the interval $[-1, 1]$, without any intercalating period of slow motion, thus basically destroying the defining feature of a relaxational oscillator (Section 6.2). We find it impossible for such a weak signal to entrain an individual oscillator. And yet, we observe that for a high enough fraction of repulsive links (insets Fig. 6.8 and Fig. 6.9), there is a nearly coincidence between the trajectory of the global variable $X(t)$ and the forcing $A \sin(\Omega t)$, with an almost imperceptible phase delay. Therefore, the simplest measure of entrainment, that falls to zero if there is a perfect synchronisation, is:

$$D = \frac{\langle [X(t) - A \sin(\Omega t)]^2 \rangle}{\langle X(t)^2 \rangle}, \quad (6.10)$$

The results plotted in Fig. 6.8 show how the synchronisation with the external signal as the fraction p of repulsive links mirrors the loss of synchronisation seen in Fig. 6.3 for the unforced system.

Again, the mechanism has its roots on the disorder induced by the presence of repulsive links. As we saw, after the transition region (Fig. 6.3, $p \approx 0.45$), the unforced system tends to adopt a configuration corresponding to a zero value of the macroscopic variable X (Fig. 6.6, $p = 0.6$ and $p = 1.0$). On the other hand, the forcing induces an asymmetry in the oscillations favouring the time spent on the side of the signal's extremum, as seen in

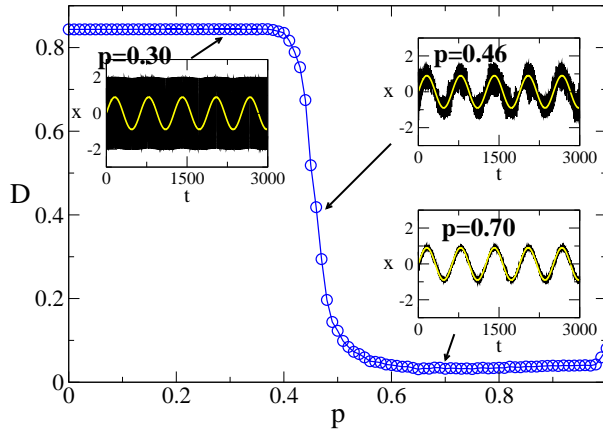


Figure 6.8. Illustration of representative macroscopic trajectories: very weak slow signal is best followed the more repulsive connections it has. Other parameters: $A = 0.9$, $\Omega = 0.01$. N , C and μ as in Fig. 6.2.

the lower panel of Fig. 6.9. Slight as this asymmetry may be, it is enough to cause the superposition of the individual waves on the same side as the signal's extremum, while on the other side, the oscillations cancel each other (see lower panel of Fig. 6.9 for $p = 1.0$). The total synchronisation of the system in case p is zero or small, naturally prevents this phenomenon to happen (see lower panel of Fig. 6.9 for $p = 0.0$).

6.5 Further applications: FitzHugh-Nagumo

The single uncoupled van der Pol oscillator can be transformed either into a linear oscillator by taking $\mu = 0$ or by replacing the nonlinear damping term $\mu(1 - x_i^2)$, Eq. (6.1) by a constant; or into an excitable system - a simplified FitzHugh-Nagumo - by adding a constant a such that $|a| > 1$ to Eq. (6.6b). So, a first direct extension consists in a brief exploration of how those transformations affect our results.

Not surprisingly, we didn't find an enhanced response for linear os-

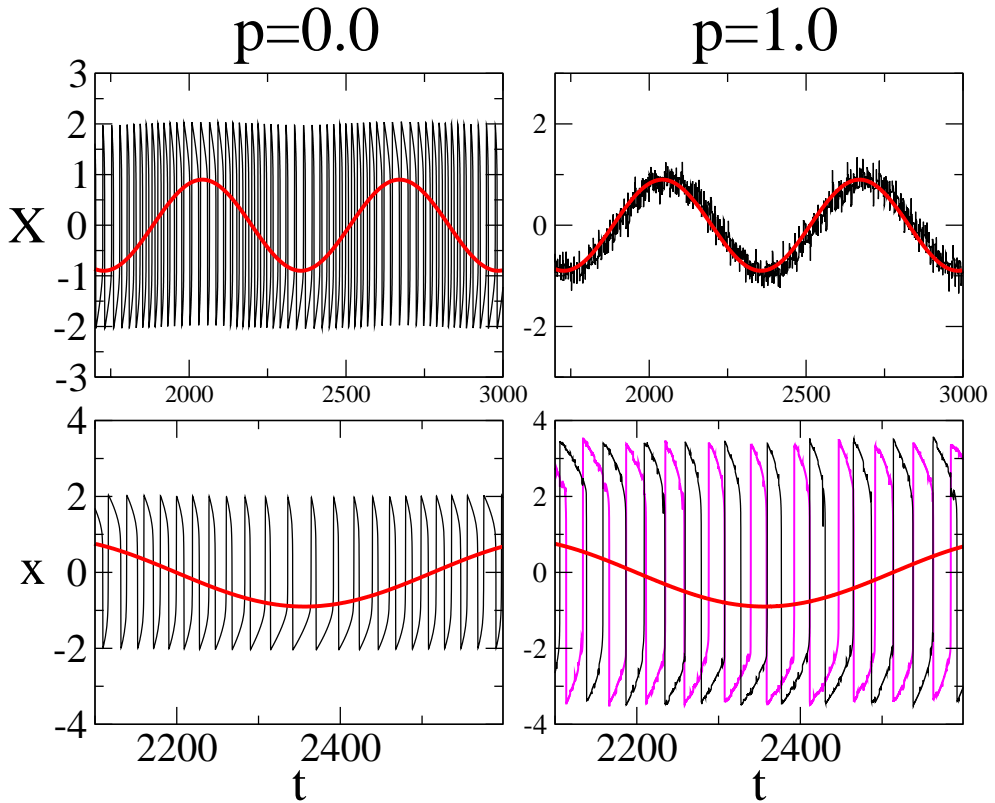


Figure 6.9. The slower oscillation corresponds to the external signal while the higher frequency oscillations correspond to either the trajectory of the macroscopic variable $X(t)$ or two typical individual trajectories. Upper panels: When $p = 1.0$ we observe the synchronisation of the macroscopic variable with a signal that is very weak and slow. Lower panels: we zoom, and plot two representative individual trajectories. $A = 0.9$, $\Omega = 0.01$. N , C and μ as in Fig. 6.2.

oscillators: both mechanisms of enhancement for slow and fast signals rely on the existence of a slow motion region. This situation contrasts with the case studied in [94]. In that paper, the authors studied a system of linear oscillators with a distribution of natural frequencies. Defining as a measure of diversity the variance of the natural frequencies, they found an optimal response to an external signal for an intermediate level of diversity. Interestingly enough, the enhancement of response also had its origins in an intermediate level of disorder. However, the microscopic mechanism was rather different: some oscillators had a natural frequency that resonated with the signal's frequency, and were able to pull the others due to the positive coupling. In our case, there isn't any single oscillator whose frequency can be entrained by the external signal.

On the other hand, the mechanisms we proposed should be applicable to the FitzHugh-Nagumo model. Adding a constant a to Eq. (6.6b) the system becomes:

$$\dot{x}_i = \mu \left[x_i - \frac{1}{3}x_i^3 - y_i + \frac{D}{N} \sum_{j=1}^N J'_{ij}x_j \right] \quad (6.11a)$$

$$\dot{y}_i = \frac{1}{\mu} [x_i - A \sin(\Omega t) + a]. \quad (6.11b)$$

The interaction via competitive interactions can play the same role of noise or diversity, thus enabling rhythmic excursions away from the fixed point. The result shown in Fig. 6.10 bears some similarity with the phenomenon by which we observe that the periodicity of oscillations becomes maximally ordered for an intermediate level of noise, [129, 130, 131] diversity, [132] or competitive interactions. [99, 133] In our case, however, and like it was observed in [100] for the case of active rotators, we don't observe any oscillations at all unless some interactions are repulsive.

When we force the excitable system by a strong enough fast signal (Fig. 6.5), it starts to oscillate even for $p = 0$, and for an intermediate amount of repulsive interactions the main frequency of oscillations coincides with the external signal (Fig. 6.5, $p = 0.40$).

On the other hand, when we force a system of FitzHugh-Nagumo ele-

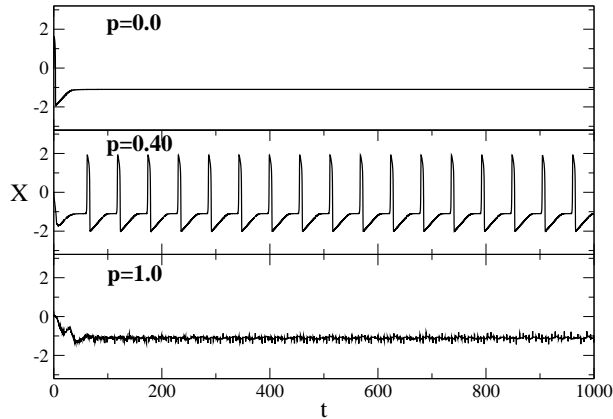


Figure 6.10. The trajectory of the global variable X for different fractions of repulsive links p in the unforced FitzHugh-Nagumo system showing a similar phenomenon to coherence resonance. Other parameters: $a = 1.1$, N , C and μ as in Fig. 6.2.

ments by slow weak signals (Fig. 6.5) we observe bursts with the periodicity of the signal for $p = 0$, while for $p = 1$ the global variable roughly oscillates along with the external forcing. Even though the periodicity of the external signal is detected for all fractions of repulsive links, we can imagine situations where we actually want to replicate the behaviour of the external signal, and that is only possible when the fraction of repulsive links is large enough.

Both of these results are expected taking into account the arguments we gave for the van der Pol oscillator case.

6.6 Conclusions

We have shown that the presence of repulsive links in a system of globally coupled van der Pol oscillators can enhance the response to an external signal. This phenomenon is verified regardless of whether the signal is strong and fast, or weak and slow, and it is in every case directly related to a loss of synchronisation and the existence of a slow motion region, but the

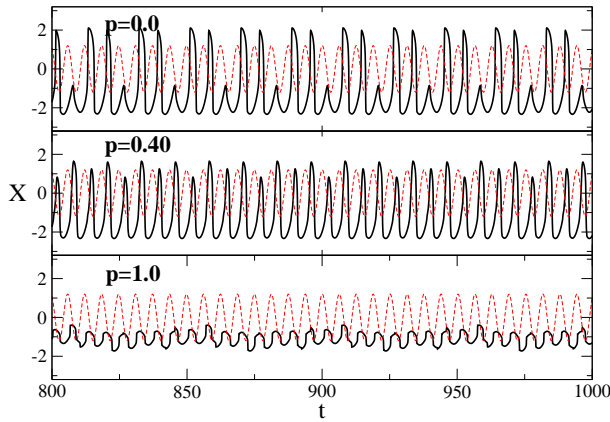


Figure 6.11. Trajectories of the global variable X for a system of FitzHugh-Nagumo units in the excitable regime forced by a fast signal, for increasing fractions of repulsive links p . Other parameters: $a = 1.1$, $A=12$, $\Omega = 1$, N , C and μ as in Fig. 6.2. The pointed line shows the external signal multiplied by 0.1, for better viewing.

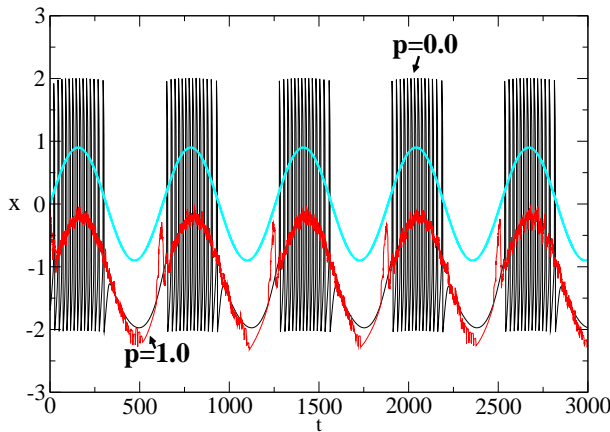


Figure 6.12. Representative trajectories of the global variable for a system of FitzHugh-Nagumo units in the excitable regime, $a = 1.1$, for some probabilities p of repulsive links. Other parameters: $\Omega = 0.01$, $A=0.9$, and N , C and μ as in Fig. 6.2. The signal is represented in a lighter color.

microscopic mechanism of enhancement is different in each case.

From the point of view of a strong fast signal, the van der Pol oscillator can be approximated by a bistable system, implying a threshold that is regularly overcome with the help of an intermediate proportion of repulsive links, by means of the deformation of the slow motion region. In the case of very slow signals, the mechanism is associated with the tendentious anti-phase oscillations that occur when there is a majority of repulsive links.

In both cases, enhancement is directly related to a loss of full synchronisation when the fraction of repulsive links increases. One can imagine that a different coupling scheme might enhance or hinder the results we found, since it is known that the network topology plays a role in synchronisation properties. [134]

Part III

Conclusions

7

Conclusions and Outlook

We have shown that the presence of competitive interactions can optimise the response to weak signals, and gave as specific examples four different models where the effect was verified.

Chapters 3 and 4 considered systems that were bistable in the absence of repulsive links. The presence of an intermediate fraction of repulsive links leads to the appearance of many multistable states separated by small barriers for whom the signal becomes suprathreshold raising the possibility of amplifying even very weak or very fast signals, with an amplification proportional to the strength of the signal. Specifically, the conclusions of each model are:

Chapter 3: The ϕ^4 model

In this chapter we related the enhancement of response to the coupling structure of the network, independently of the very detailed specification of the model. We have shown that the optimal probability of repulsive links is associated with a localisation of positive modes of the Laplacian matrix, which enables a sustained reaction to perturbations. Additionally, we verified and explained a resonance induced by the system-size or the coupling strength.

Chapter 4: A discrete bistable model

In this chapter, we studied a discrete model constituted by units that can only take one of two values. Using Monte Carlo simulations, we verified that when the system has the optimal fraction of repulsive links, the response to external perturbations acquires a step-by-step characteristic. We also investigated the role of the underlying network of interactions, showing how the probability of repulsive links that enhances the response grows with the number of units, and it is higher when the coupling is global.

We isolated the effects of competitive interactions, by considering diversity-free networks. Additionally, we considered the cooperation between noise, diversity and repulsive links, concluding that the presence of noise renders the system more sensitive to perturbations, but also decreases the coherence of the collective response, while the presence of diversity broadens the amplification region.

The research then proceeded to two non-bistable models with a different implementation of a threshold. Those two systems are intrinsically different from the ones discussed before, and as such both the mechanism of response, as well as the results, are rather different. In the modified version of the Deffuant *et al.* model, as well as in the system of van der Pol oscillators, there isn't a potential barrier to be crossed, and therefore the distinction between sub- and suprathreshold signals can not be interpreted in the same sense.

Chapter 5: Mass media reception in a continuous opinion model

We interpreted the discrete model described in Chapter 4 as an opinion formation model, which suggests that in a society where individuals choices are conditioned by the majority opinion of their neighbours, it is helpful to include some fraction of repulsive interactions, in order for that society to be receptive to external influences. That discrete model was very general, and we wanted to confirm further that in a society the presence of repulsive interactions can in fact help the transmission of a message. To that end, we started from a more established model of opinion formation - the Deffuant *et al.* model and modified it to include repulsive interactions.

This study allowed us to confirm and put on a firmer ground the idea that in order for a close-minded society to build a consensus around an exter-

nal message, its members should interact via a combination between positive and repulsive connections. We clarified that an intermediate level of repulsive links is best suited to respond to several types of messages. However, we also found that when the time intervals between the transmission of an external message are sufficiently short, society can build a consensus around it, provided the fraction of repulsive links is larger than a given number. This means that even when all its members have a tendency to reject each other's opinion they can build a consensus around the external message. In this case, at variance with the previous cases, it is not appropriate to talk about *resonance*.

Another difference with previous models is that the order-disorder transition that is found to coincide with the region of amplification for low-frequency signals, is of a different nature than the one found in the previous cases. There, order was equated with consensus. Here, order is equated with a fragmented society with very well defined clusters, where there is consensus inside a cluster.

Chapter 6: Synchronisation induced by repulsive interactions in the van der Pol oscillator

The system of van der Pol oscillators is a paradigmatic example of a model that exhibits synchronisation. This study further unveiled the coincidence between the fraction of repulsive links that induced a particular loss of synchronisation and the one that enhances the response to a weak signal. Further, we have shown that in the case of fast signals the formulation developed in Chapter 4 could indeed be applied to this system with significantly different characteristics but the same coupling matrix.

Besides a *spatial* threshold, this model has additionally a temporal threshold which led us to propose a different mechanism in the case of fast and slow signals. In the situation of very weak and slow signals, the collective response is best enhanced the higher the proportion of repulsive links is, by means of a mechanism that exploits a tendentious anti-phase configuration. Like in the previous Chapter 5 it is not always appropriate to talk about *resonance* - only in case of fast signals.

To summarise, we found the same general effect - an enhancement of

the response to weak signals by the presence of competitive interactions - in different types of systems. In general, in all the studied systems, we found a coincidence between a loss of order and an amplification of response. This is a requirement that enables the crossing of different types of thresholds. However, once this first requirement is satisfied, the different systems employ different mechanisms of amplification, and accordingly can show different optimal probabilities of repulsive links.

7.1 Future work

Future research should proceed along the two directions that we outline below.

To establish the role of the Laplacian

We have shown that in the global coupled systems it is easy to predict the location of the resonance peaks, just by identifying the proportion of repulsive links that induces a localisation of positive eigenmodes. Exploring this idea leads us to the consideration of the effect of the underlying network in non-global coupling cases. Indeed, different topologies exhibit different localisation properties and, as expected, the optimal probability depends on the network, being lower when the coupling is not global.

The localisation measure we chose assumes implicitly that averaged global quantities are enough to classify localisation properties. However, in the case of networks with high clustering this kind of mean-field analysis doesn't hold. Also, in networks where the localisation properties vary according to the units position in the graph, the situation is more complex: that can be the case of scale-free networks, for instance. There arises the need to try and find out if there is a more general measure of localisation that applies to all networks, or even if the sole combination of localisation and the presence of positive Laplacian modes doesn't result in all cases in an amplified response.

Practical applications

A second challenge is to find out whether the concepts developed in this thesis in an idealised manner would work in more realistic and complex

circumstances. For instance, it would be good to extract from the models of opinion formation we proposed what is specifically new, and to devise a way to test it. This is a project underway, that is being done in collaboration with sociologists.

These two directions outlined above - the definition of a precise measure that enables us to predict the location of the resonance peaks according to the topology of the network, and the implementation of a project to test the consequences of the modified version of the Deffuant *et al.* model - are already being followed by us.

Besides that, our work opens up wider perspectives about the role of repulsive links in information processing in various systems, like the brain, where a combination of positive and negative links is known to exist, but its function hasn't yet been fully established.

Part IV

Appendices

A

Spectral Analysis

In this appendix I will give some details about the spectral analysis calculations used in Chapter 3.

Let us assume the state of a unit i is s_i^o at a given time. Our goal is to see how the interaction with the other units modifies this state.

We define the eigenvalues Q_α and (normalized) eigenvectors $e^\alpha = (e_1^\alpha, \dots, e_N^\alpha)$ of the Laplacian coupling matrix J'_{ij}

$$J'_{ij} = J_{ij} - \delta_{ij} \sum_{k=1}^N J_{kj}, \quad (\text{A.1})$$

$$\sum_{j=1}^N J'_{ij} e_j^\alpha = Q_\alpha e_i^\alpha. \quad (\text{A.2})$$

with the normalization condition:

$$\sum_i e_i^\alpha e_i^\beta = \delta_{\alpha\beta} \quad (\text{A.3})$$

The translation invariance of the system requires that:

$$\sum_{j=1}^N J'_{ij} = 0 \quad (\text{A.4})$$

We write the perturbations in terms of the eigenvalues and eigenvectors of the Laplacian.

$$x_i = \sum_{\alpha=1}^N B_{\alpha} e_i^{\alpha}, \quad (\text{A.5})$$

Now let's replace some terms in the equation 3.1 as:

$$\sum_{j=1}^N J_{ij}(s_j - s_i) = \sum_{j=1}^N J'_{ij} s_j \quad (\text{A.6})$$

$$= \sum_{j=1}^N J'_{ij} (s_j^o + x_j) \quad (\text{A.7})$$

$$= \sum_{j=1}^N J'_{ij} s_j^o + \sum_{j=1}^N J'_{ij} \sum_{\alpha=1}^N B_{\alpha} e_j^{\alpha} \quad (\text{A.8})$$

$$= \sum_{j=1}^N J'_{ij} s_j^o + \sum_{\alpha=1}^N B_{\alpha} Q_{\alpha} e_i^{\alpha} \quad (\text{A.9})$$

$$s_i = s_i^o + x_i \quad (\text{A.10})$$

$$= s_i^o + \sum_{\alpha=1}^N B_{\alpha} e_i^{\alpha} \quad (\text{A.11})$$

$$(\text{A.12})$$

$$s_i^3 = (s_i^o + x_i)^3 \quad (\text{A.13})$$

$$= ((s_i^o)^2 + x_i^2 + 2s_i^o x_i)(s_i^o + x_i) \quad (\text{A.14})$$

$$= (s_i^o)^3 + (s_i^o)^2 x_i + s_i^o x_i^2 + x_i^3 + 2(s_i^o)^2 x_i + 2s_i^o x_i^2 \quad (\text{A.15})$$

$$= (s_i^o)^3 + 3(s_i^o)^2 x_i + 3s_i^o x_i^2 + x_i^3 \quad (\text{A.16})$$

$$s_i - s_i^3 = s_i^o + x_i - (s_i^o)^3 - 3(s_i^o)^2 x_i - 3s_i^o x_i^2 - x_i^3 \quad (\text{A.17})$$

Expanding the right side of Eq.(3.1) for $A = 0$, multiplying the resulting equation by e_i^α , and considering the normalization condition A.3, we get:

$$\begin{aligned} & (s_i^o)e_i^\alpha + x_i e_i^\alpha - (s_i^o)^3 e_i^\alpha - 3(s_i^o)^2 x_i e_i^\alpha - 3s_i^o x_i^2 e_i^\alpha - x_i^3 e_i^\alpha = \\ & = (s_i^o)e_i^\alpha + \sum_{\beta=1}^N B_\beta e_i^\beta e_i^\alpha - (s_i^o)^3 e_i^\alpha - \\ & - 3(s_i^o)^2 \sum_{\beta=1}^N B_\beta e_i^\beta e_i^\alpha - 3s_i^o \left[\sum_{\beta=1}^N B_\beta e_i^\beta \right]^2 e_i^\alpha - \left[\sum_{\beta=1}^N B_\beta e_i^\beta \right]^3 e_i^\alpha = \\ = & (s_i^o)e_i^\alpha + \sum_{\beta=1}^N B_\beta e_i^\beta e_i^\alpha - (s_i^o)^3 e_i^\alpha - 3(s_i^o)^2 \sum_{\beta=1}^N B_\beta e_i^\beta e_i^\alpha - 3s_i^o \sum_{\beta,\gamma=1}^N B_\beta B_\gamma e_i^\beta e_i^\gamma e_i^\alpha - \\ & - \sum_{\beta,\gamma,\eta=1}^N B_\beta B_\gamma B_\eta e_i^\beta e_i^\gamma e_i^\eta e_i^\alpha \end{aligned}$$

We will assume that:

$$\frac{1}{N} \sum_{i=1}^N s_i^o e_i^\alpha \approx \frac{1}{N^2} \sum_{i=1}^N s_i^o \sum_{i=1}^N e_i^\alpha \quad (\text{A.18})$$

Which is true in the limit of $N \rightarrow \infty$

Also:

$$\sum_{i=1}^N e_i^\alpha = 0 \quad (\text{A.19})$$

unless $Q_\alpha = 0$

Now let's average over all elements, to find the evolution of a given mode.

$$\frac{dB_\alpha}{dt} = - \sum_{\beta, \gamma, \eta} F^{\beta\gamma\eta\alpha} B_\beta B_\gamma B_\eta + \left(C \frac{Q_\alpha}{N} - K \right) B_\alpha, \quad (\text{A.20})$$

where

$$F^{\beta\gamma\eta\alpha} = \sum_{i=1}^N e_i^\beta e_i^\gamma e_i^\eta e_i^\alpha, \quad (\text{A.21})$$

$$K = \frac{3}{N} \sum_{i=1}^N (s_i^o)^2 - 1. \quad (\text{A.22})$$

If we neglect the coupling between modes, this approximation leads to $F^{\beta\gamma\eta\alpha} = 1/\text{PR}_\alpha$ if $\alpha = \beta = \gamma = \eta$ and 0 otherwise. We then obtain the following equation for the amplitude of the α -th mode:

$$\frac{dB_\alpha}{dt} = -B_\alpha^3 + \text{PR}_\alpha \left(C \frac{Q_\alpha}{N} - K \right) B_\alpha. \quad (\text{A.23})$$

According to this approximation, unless $Q_\alpha > \frac{KN}{C}$, the amplitude of the mode B_α tends to zero, and any small perturbation vanishes. Otherwise, the amplitude of the mode α tends to a steady state value:

$$B_\alpha = \pm \left[\sqrt{\text{PR}_\alpha \left(C \frac{Q_\alpha}{N} - K \right)} \right]. \quad (\text{A.24})$$

In this case, mode α is said to be an *open mode*.

B

A method to detect potential wells

In this appendix, I explain how we detected the number of states in Chapter 3, by adapting the method proposed in V. N. Livina, F. Kwasniok, and T. M. Lenton, *Clim. Past*, 6, 77-82, (2010)

The method was developed to detect the number of states in geophysical time series, which have observational noise and often nonstationarities. Therefore, the method [107] starts considering a stochastic Langevin equation:

$$\dot{z} = -U'(z) + \sigma\eta, \quad (\text{B.1})$$

where $U(z)$ is a potential function, σ is the noise level and η is a Gaussian white noise with zero mean and unit variance. In the context of the original work, the state variable z represents some large-scale climate variable like temperature.

We assume a general polynomial potential:

$$U(z) = \sum_{i=1}^L a_i z^i, \quad (\text{B.2})$$

where the order L is even and the leading coefficient a_L is positive for eq. (B.1) to possess a stationary solution. The order of the polynomial

controls the complexity of the potential (the number of potential wells), with increasing values of L allowing more states to be accommodated: a fourth-order polynomial can capture a system with two states (double-well potential).

The number of system states is estimated by means of a polynomial fit of the probability density function of the data. Suppose the system is governed by eq. (B.1). The corresponding Fokker-Planck equation for the probability density function $p(z, t)$

$$\partial_t p(z, t) = \partial_z [U'(z)p(z, t)] + \frac{1}{2}\sigma^2 \partial_z^2 p(z, t) \quad (\text{B.3})$$

has a stationary solution given by (see [73])

$$p(z) \sim \exp[-2U(z)/\sigma^2]. \quad (\text{B.4})$$

Given this one-to-one correspondence between the potential and the stationary probability density of the system, the potential can be reconstructed from time series data of the system as

$$U = -\frac{\sigma^2}{2} \log p_d, \quad (\text{B.5})$$

where p_d is the empirical probability density of the data. This is estimated using a standard Gaussian kernel estimator [135]. Then least-square fits of $-\log p_d$ (weighted with the probability density of the data with polynomials of increasing even order L are calculated, starting with $L = 2$, until a negative leading coefficient a_L is encountered. The polynomial of highest degree before first obtaining a negative leading coefficient is considered the most appropriate representation of the probability density of the time series, both locally and globally, avoiding overfitting of sampling fluctuations in the probability density.

The number of states S in the system is then determined as

$$S = 1 + \frac{I}{2}, \quad (\text{B.6})$$

where I is the number of inflection points of the fitted polynomial potential of appropriate degree L as described above. This definition takes into account not only the degree of the polynomial but its actual shape. We only

look at even-order potentials with positive leading coefficient. These have positive curvature both at minus and plus infinity. Thus, inflection points can only occur in pairs (if any). Any potential has at least one state (with no inflection points). Then we count one further state for each pair of inflection points. This can be either a real minimum (well) or just a flattening in the potential (corresponding to degeneracies in the potential; definition (B.6) accommodates both possibilities). The number of inflection points is numerically given as the number of sign changes in the second derivative on a fine enough mesh.

If necessary, the coefficients that determine the shape of the potential are then estimated using the unscented Kalman filter (UKF). The method was developed for the stochastic model with noise component and performs polynomial fit of the histogram which is expected to be smooth (i.e. no discrete peak). To detect the number of states in the ϕ^4 model with competitive interactions, we had to add a noise component to the model trajectories to make the method applicable. Yet, to minimise the effect of noise, we considered white Gaussian noise of small amplitude (0.01 of the trajectory amplitude), which allowed us to "fill" the histogram and make it suitable for smooth polynomial fit. Note that adding noise can only hide a certain shallow well in the potential, but never lead to a false detection of non-existent states, and therefore adding noise cannot lead to false detection of additional states.

C

The rewiring algorithm mentioned in the Divide and Conquer chapter 4

To settle the issue of whether the resonance phenomenon was induced by variability in the number of repulsive links or not, we decided to construct a network in which every agent had exactly the same number of positive and of repulsive links. We did so, adapting the “local rewiring algorithm” (S. Maslov, K. Sneppen, *Science* **296**, 910 (2002)) to construct a random network where every node has exactly the same number of links k and the same proportion p of repulsive links – the “no dispersion” network.

In a network with N nodes each with $2k$ neighbours, there will be $2pk$ repulsive links.

The network is constructed as follows: we start with a ring where each of the N nodes has $2k$ nearest neighbours. Then we randomize the network by repeating the elementary rewiring step: we select two links at random, and rewire them by switching partners, excluding the appearance of multiple edges. If we want a global coupled network, the randomised links will be all repulsive, and we later add attractive links until everyone is coupled. Otherwise, the first $2pk$ links in the ring to be randomised are repulsive, and the rest $(1-p)2k$ are attractive.

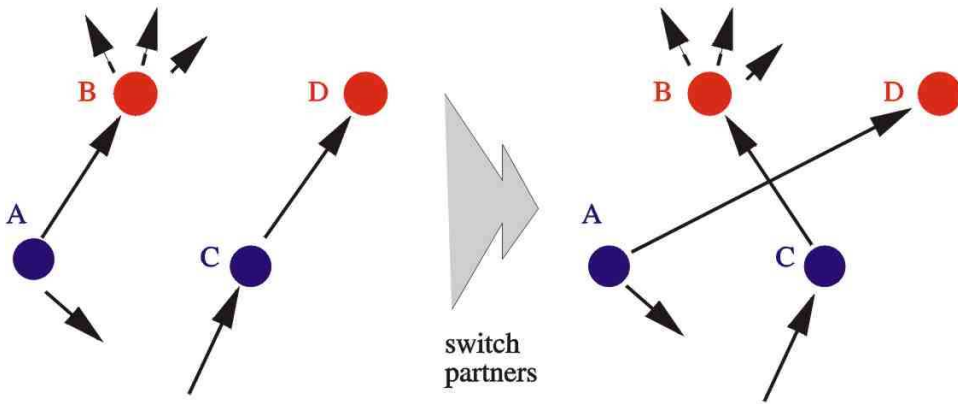


Figure C.1. An illustration of the rewiring algorithm. A pair of directed edges $A \rightarrow B$ and $C \rightarrow D$ is randomly selected. These edges are then rewired in such a way that A becomes connected to D , while C to B , provided that none of these edges already exist in the network, in which case the rewiring step is aborted and a new pair of edges is selected. The rewiring algorithm conserves both the in- and out-connectivity of each individual node. Source: <http://www.cmth.bnl.gov/maslov/>

D

Master Equation for the Deffuant model with repulsive links

In this Appendix we present the derivation of the master equation whose results were used in Chapter 5.

D.1 Model

Let's remember the model in Chapter 5 for the case without propaganda. We consider a set of N agents which, at a given time n , can adopt the opinion x_n^i , in the interval $[0, 1]$. We assign a weight ω_{ij} to the link connecting nodes i and j and consider the symmetric case $\omega_{ij} = \omega_{ji}$ (or an undirected network). The weights take positive or negative values: $\omega_{ij} = 1$ or $\omega_{ij} = -1$, depending on a given probability p .

At time t two individuals, say i and j , are randomly chosen. If their opinions satisfy $|x_t^i - x_t^j| < \epsilon$, they are updated according to:

- If $\omega_{ij} = 1$

$$\begin{aligned}x_{n+1}^i &= x_n^i + 0.5(x_n^j - x_n^i), \\x_{n+1}^j &= x_n^j + 0.5(x_n^i - x_n^j),\end{aligned}\tag{D.1}$$

- If $\omega_{ij} = -1$,

$$\begin{aligned} x_{n+1}^i &= x_n^i - 0.5(x_n^j - x_n^i), \\ x_{n+1}^j &= x_n^j - 0.5(x_n^i - x_n^j), \end{aligned} \quad (\text{D.2})$$

We impose the condition that x_n^i must remain in the interval $[0, 1]$: if $x_n^i < 0$, $x_n^i = 0$, and if $x_n^i > 1$, $x_n^i = 1$.

D.2 The Master equation

The pdf $P_{n+1}(x)$ reflects the contributions:

- (i) With probability $1 - p$ two individuals, say i, j , are chosen for updating according to the basic evolution rule Eq. (D.1) and $N - 2$ variables remain unchanged.
- (ii) With probability p two individuals, say i, j , are chosen for updating according to the evolution rule Eq. (D.2) and $N - 2$ variables remain unchanged.

$$\begin{aligned} P_{n+1}(x) &= (1 - p) \left[\frac{N-2}{N} P_n(x) + \frac{1}{N} A_{n+1}^i(x) + \frac{1}{N} A_{n+1}^j(x) \right] \\ &\quad + p \left[\frac{N-2}{N} P_n(x) + \frac{1}{N} R_{n+1}^i(x) + \frac{1}{N} R_{n+1}^j(x) \right]. \end{aligned} \quad (\text{D.3})$$

D.2.1 Attractive part

We call $A_{n+1}^i(x)$ the probability that x_{n+1}^i adopts the value x at the step $n + 1$. According to that rule, the evolution equation is:

$$\begin{aligned} A_{n+1}^i(x) &= \int_{|x_n^i - x_n^j| < \epsilon} dx_n^i dx_n^j P_n(x_n^i) P_n(x_n^j) \delta \left(x - \frac{x_n^i + x_n^j}{2} \right) \\ &\quad + \int_{|x_n^i - x_n^j| > \epsilon} dx_n^i dx_n^j P_n(x_n^i) P_n(x_n^j) \delta(x - x_n^i), \end{aligned} \quad (\text{D.4})$$

And a similar expression for j .

Using $\delta(ax) = \frac{1}{|a|}\delta(x)$, we have

$$\delta\left(x - \frac{x_n^i + x_n^j}{2}\right) = \delta\left(\frac{x_n^i - (2x - x_n^j)}{-2}\right) \quad (\text{D.5})$$

$$= \delta\left(-\frac{1}{2}(x_n^i - (2x - x_n^j))\right) \quad (\text{D.6})$$

$$= 2\delta(x_n^i - (2x - x_n^j)) \quad (\text{D.7})$$

$$\begin{aligned} & \int_{|x_n^i - x_n^j| < \epsilon} dx_n^i dx_n^j P_n(x_n^i) P_n(x_n^j) \delta\left(x - \frac{x_n^i + x_n^j}{2}\right) = \\ 2 & \int_{|x_n^i - x_n^j| < \epsilon} dx_n^i dx_n^j P_n(x_n^i) P_n(x_n^j) \delta(x_n^i - (2x - x_n^j)) = \\ & 2 \int_{|x - x_n^j| < \frac{\epsilon}{2}} dx_n^j P_n(2x - x_n^j) P_n(x_n^j) \end{aligned} \quad (\text{D.8})$$

Then:

$$\begin{aligned} & \frac{N-2}{N} P_n(x) + \frac{1}{N} A_{n+1}^i(x) + \\ & \frac{1}{N} A_{n+1}^j(x) = \\ & \frac{N-2}{N} P_n(x) + \frac{4}{N} \int_{|x-x'| < \epsilon/2} dx' P_n(2x-x') P_n(x') + \\ & \frac{2}{N} \int_{|x_n^i - x_n^j| > \epsilon} dx_n^i dx_n^j P_n(x_n^i) P_n(x_n^j) \delta(x - x_n^i) \end{aligned} \quad (\text{D.9})$$

Note also that:

$$\int_0^1 dx_n^i dx_n^j = \int_{|x_n^i - x_n^j| < \epsilon} dx_n^i dx_n^j + \int_{|x_n^i - x_n^j| > \epsilon} dx_n^i dx_n^j \quad (\text{D.10})$$

or:

$$\begin{aligned}
& \int_{|x_n^i - x_n^j| < \epsilon} dx_n^i dx_n^j P_n(x_n^i) P_n(x_n^j) \delta(x - x_n^i) + \\
& \int_{|x_n^i - x_n^j| > \epsilon} dx_n^i dx_n^j P_n(x_n^i) P_n(x_n^j) \delta(x - x_n^i) = \\
& \int_0^1 dx_n^i \int_0^1 dx_n^j P_n(x_n^i) P_n(x_n^j) \delta(x - x_n^i) = \\
& P_n(x)
\end{aligned} \tag{D.11}$$

or:

$$\begin{aligned}
& \int_{|x_n^i - x_n^j| > \epsilon} dx_n^i dx_n^j P_n(x_n^i) P_n(x_n^j) \delta(x - x_n^i) = \\
P_n(x) - & \int_{|x_n^i - x_n^j| < \epsilon} dx_n^i dx_n^j P_n(x_n^i) P_n(x_n^j) \delta(x - x_n^i)
\end{aligned} \tag{D.12}$$

We now have the contribution of the attractive interaction to the Master Equation:

$$\begin{aligned}
& \frac{N-2}{N} P_n(x) + 4 \int_{|x-x'| < \epsilon/2} dx' P_n(2x-x') P_n(x') + \\
\frac{2}{N} \left[P_n(x) - \int_{|x_n^i - x_n^j| < \epsilon} dx_n^i dx_n^j P_n(x_n^i) P_n(x_n^j) \delta(x - x_n^i) \right] = \\
& P_n(x) + 4 \int_{|x-x'| < \epsilon/2} dx' P_n(2x-x') P_n(x') - \\
& \frac{2}{N} \left[P_n \int_{|x_n^i - x_n^j| < \epsilon} dx_n^j P_n(x_n^j) \right]
\end{aligned} \tag{D.13}$$

D.2.2 Repulsive part

$$\left[\frac{N-2}{N} P_n(x) + \frac{1}{N} R_{n+1}^i(x) + \frac{1}{N} R_{n+1}^j(x) \right]. \tag{D.14}$$

Note that:

$$\begin{aligned}
& R_{n+1}^i(x) = \\
& \int_{\substack{|x_n^i - x_n^j| < \epsilon \\ 0 \leq \frac{3x_n^i - x_n^j}{2} \leq 1}} dx_n^i dx_n^j P_n(x_n^i) P_n(x_n^j) \delta\left(x - \frac{3x_n^i - x_n^j}{2}\right) + \\
& \int_{\substack{|x_n^i - x_n^j| < \epsilon \\ \frac{3x_n^i - x_n^j}{2} < 0}} dx_n^i dx_n^j P_n(x_n^i) P_n(x_n^j) \delta(x) + \\
& \int_{\substack{|x_n^i - x_n^j| < \epsilon \\ \frac{3x_n^i - x_n^j}{2} > 1}} dx_n^i dx_n^j P_n(x_n^i) P_n(x_n^j) \delta(x - 1) \quad (D.15)
\end{aligned}$$

And a similar expression for j .

Using $\delta(ax) = \frac{1}{|a|} \delta(x)$, we obtain:

$$\begin{aligned}
& \int_{|x_n^i - x_n^j| < \epsilon} dx_n^i dx_n^j P_n(x_n^i) P_n(x_n^j) \delta\left(x - \frac{3x_n^i - x_n^j}{2}\right) = \\
& 2 \int_{|x - x_n^j| < \frac{\epsilon}{2}} dx_n^i P_n(3x_n^i - 2x) P_n(x_n^i) \quad (D.16)
\end{aligned}$$

And the same for j .

Then we get:

$$\begin{aligned}
& \left[\frac{N-2}{N} P_n(x) + \frac{1}{N} R_{t+1}^i(x) + \frac{1}{N} R_{t+1}^j(x) \right] = \\
& \frac{N-2}{N} P_n(x) + \frac{4}{N} \int_{|x-x_n^j| < \frac{\epsilon}{2}} dx_n^i P_n(3x_n^i - 2x) P_n(x_n^i) + \\
& \quad \frac{2}{N} \int_{|x_n^i - x_n^j| < \epsilon} dx_n^i dx_n^j P_n(x_n^i) P_n(x_n^j) \delta(x) + \\
& \quad \frac{2}{N} \int_{\substack{|x_n^i - x_n^j| < \epsilon \\ \frac{3x_n^i - x_n^j}{2} \geq 1}} dx_n^i dx_n^j P_n(x_n^i) P_n(x_n^j) \delta(x-1) + \\
& \quad \frac{2}{N} \int_{|x_n^i - x_n^j| > \epsilon} dx_n^i dx_n^j P_n(x_n^i) P_n(x_n^j) \delta(x - x_n^i) \quad (D.17)
\end{aligned}$$

Using again:

$$\begin{aligned}
& \int_{|x_n^i - x_n^j| > \epsilon} dx_n^i dx_n^j P_n(x_n^i) P_n(x_n^j) \delta(x - x_n^i) = \\
& P_n(x) - \int_{|x_n^i - x_n^j| < \epsilon} dx_n^i dx_n^j P_n(x_n^i) P_n(x_n^j) \delta(x - x_n^i) \quad (D.18)
\end{aligned}$$

We get:

$$\begin{aligned}
& \left[\frac{N-2}{N} P_n(x) + \frac{1}{N} R_{n+1}^i(x) + \frac{1}{N} R_{n+1}^j(x) \right] = \\
& \frac{N-2}{N} P_n(x) + \frac{4}{N} \int_{|x-x_n^j| < \frac{\epsilon}{2}} dx_n^i P_n(3x_n^i - 2x) P_n(x_n^i) + \\
& \quad \frac{2}{N} \int_{\substack{|x_n^i - x_n^j| < \epsilon \\ \frac{3x_n^i - x_n^j}{2} \leq 0}} dx_n^i dx_n^j P_n(x_n^i) P_n(x_n^j) \delta(x) + \\
& \quad \frac{2}{N} \int_{\substack{|x_n^i - x_n^j| < \epsilon \\ \frac{3x_n^i - x_n^j}{2} \geq 1}} dx_n^i dx_n^j P_n(x_n^i) P_n(x_n^j) \delta(x-1) + \\
& \quad \frac{2}{N} \left[P_n(x) - \int_{|x_n^i - x_n^j| < \epsilon} dx_n^i dx_n^j P_n(x_n^i) P_n(x_n^j) \delta(x - x_n^i) \right] \quad (D.19)
\end{aligned}$$

And using:

$$\int_{|x_n^i - x_n^j| < \epsilon} dx_n^i dx_n^j P_n(x_n^i) P_n(x_n^j) \delta(x - x_n^i) = \int_{|x - x_n^j| < \epsilon} dx_n^j P_n(x) P_n(x_n^j) \quad (\text{D.20})$$

One obtains the contribution of the repulsive part:

$$\begin{aligned} P_n(x) + \frac{4}{N} \int_{|x - x_n^j| < \frac{\epsilon}{2}} dx_n^i P_n(3x_n^i - 2x) P_n(x_n^i) + \\ \frac{2}{N} \int_{\substack{|x_n^i - x_n^j| < \epsilon \\ \frac{3x_n^i - x_n^j}{2} \leq 0}} dx_n^i dx_n^j P_n(x_n^i) P_n(x_n^j) \delta(x) + \\ \frac{2}{N} \int_{\substack{|x_n^i - x_n^j| < \epsilon \\ \frac{3x_n^i - x_n^j}{2} \geq 1}} dx_n^i dx_n^j P_n(x_n^i) P_n(x_n^j) \delta(x - 1) - \\ \frac{2}{N} \int_{|x - x_n^j| < \epsilon} dx_n^j P_n(x) P_n(x_n^j) \end{aligned} \quad (\text{D.21})$$

D.2.3 The Master Equation

Finally the master equation becomes:

$$\begin{aligned}
& P_{n+1}(x) = \\
(1-p)[P_n(x) &+ \frac{4}{N} \int_{|x-x_n^i| < \epsilon/2} dx_n^i P_n(2x-x_n^i) P_n(x_n^i) - \\
& \frac{2}{N} P_n \int_{|x-x_n^i| < \epsilon} dx_n^i P_n(x_n^i)] + \\
p[P_n(x) &+ \frac{4}{N} \int_{|x-x_n^i| < \frac{\epsilon}{2}} dx_n^i P_n(3x_n^i-2x) P_n(x_n^i) + \\
& \frac{2}{N} \int_{\substack{|x_n^i-x_n^j| < \epsilon \\ \frac{3x_n^i-x_n^j}{2} \leq 0}} dx_n^i dx_n^j P_n(x_n^i) P_n(x_n^j) \delta(x) + \\
& \frac{2}{N} \int_{\substack{|x_n^i-x_n^j| < \epsilon \\ \frac{3x_n^i-x_n^j}{2} \geq 1}} dx_n^i dx_n^j P_n(x_n^i) P_n(x_n^j) \delta(x-1) - \\
& \frac{2}{N} \int_{|x-x_n^j| < \epsilon} dx_n^j P_n(x) P_n(x_n^j)] \tag{D.22}
\end{aligned}$$

or

$$\begin{aligned}
P_{n+1}(x) = & \\
P_n(x) + (1-p) & \left[\frac{4}{N} \int_{|x-x_n^i| < \epsilon/2} dx_n^i P_n(2x-x_n^i) P_n(x_n^i) - \right. \\
& \left. \frac{2}{N} P_n \int_{|x-x_n^i| < \epsilon} dx_n^i P_n(x_n^i) \right] + \\
p & \left[\frac{4}{N} \int_{|x-x_n^i| < \frac{\epsilon}{2}} dx_n^i P_n(3x_n^i-2x) P_n(x_n^i) + \right. \\
& \frac{2}{N} \int_{\substack{|x_n^i-x_n^j| < \epsilon \\ \frac{3x_n^i-x_n^j}{2} \leq 0}} dx_n^i dx_n^j P_n(x_n^i) P_n(x_n^j) \delta(x) + \\
& \frac{2}{N} \int_{\substack{|x_n^i-x_n^j| < \epsilon \\ \frac{3x_n^i-x_n^j}{2} \geq 1}} dx_n^i dx_n^j P_n(x_n^i) P_n(x_n^j) \delta(x-1) - \\
& \left. \frac{2}{N} \int_{|x-x_n^j| < \epsilon} dx_n^j P_n(x) P_n(x_n^j) \right] \tag{D.23}
\end{aligned}$$

Considering that $\Delta t = 1/N$, and $N \rightarrow \infty$, we replace:

$$(P_{n+1}(x) - P_n(x)) N = \frac{\partial P}{\partial t} \tag{D.24}$$

and

$$\begin{aligned}
& \frac{\partial P}{\partial t}(x) = \\
(1-p) & \left[4 \int_{|x-x_n^i| < \epsilon/2} dx_n^i P_t(2x-x_n^i) P_t(x_n^i) - 2P_t \int_{|x-x_t^i| < \epsilon} dx_t^i P_t(x_t^i) \right] + \\
& p \left[4 \int_{|x-x_t^i| < \frac{\epsilon}{2}} dx_t^i P_t(3x_t^i - 2x) P_t(x_t^i) + \right. \\
& 2 \int_{\substack{|x_t^i-x_t^j| < \epsilon \\ \frac{3x_t^i-x_t^j}{2} \leq 0}} dx_t^i dx_t^j P_t(x_t^i) P_t(x_t^j) \delta(x) + \\
& 2 \int_{\substack{|x_t^i-x_t^j| < \epsilon \\ \frac{3x_t^i-x_t^j}{2} \geq 1}} dx_t^i dx_t^j P_t(x_t^i) P_t(x_t^j) \delta(x-1) - \\
& \left. 2 \int_{|x-x_t^j| < \epsilon} dx_t^j P_t(x) P_t(x_t^j) \right]
\end{aligned} \tag{D.25}$$

D.2.4 Integration limits at the boundaries

- to prevent the final opinion to be smaller than 0

$$\int_{\substack{|x_t^i-x_t^j| < \epsilon \\ \frac{3x_t^j-x_t^i}{2} \leq 0}} dx_t^i dx_t^j P_t(x_t^i) P_t(x_t^j) \delta(x) = \int_0^{\frac{\epsilon}{2}} dx_t^j \left[\int_{3x_t^j}^{x_t^j+\epsilon} dx_t^i P_t(x_t^i) \right] P_t(x_t^j) \delta(x)
\end{aligned} \tag{D.26}$$

because (see also Fig. D.1),

$$3x^j = x^i + \epsilon \implies x^j = \frac{\epsilon}{2} \implies x^j \in [0, \frac{\epsilon}{2}] \tag{D.27}$$

From this, we see that ϵ cannot be greater than $\frac{2}{3}$. Yet, the results coming from the numerical integration of the Master Equation don't coincide with results from simulations, for large ϵ and $p \neq 0$, even if they are smaller than $\frac{2}{3}$.

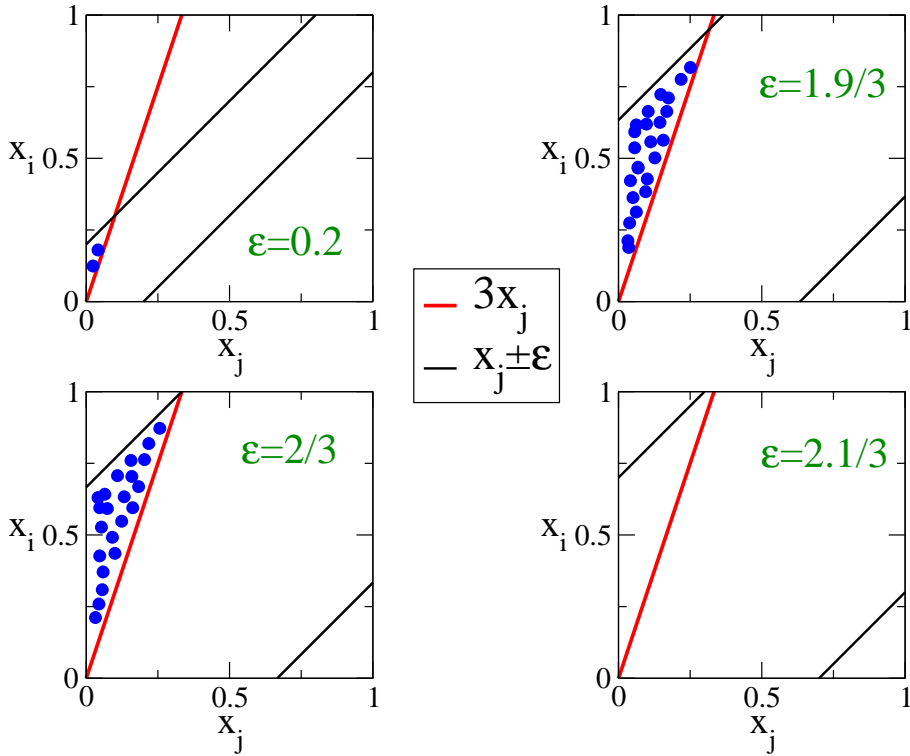


Figure D.1. The case to prevent the final opinion to be smaller than 0. We give several examples of the integration region, shown in blue dots, for different ϵ

- to prevent the final opinion to be greater than 1

See Fig. D.2:

$$\int_{\substack{|x_t^i - x_t^j| < \epsilon \\ \frac{3x_t^j - x_t^i}{2} \geq 1}} dx_t^i dx_t^j P_t(x_t^i) P_t(x_t^j) \delta(x - 1) = \\
 \int_{\frac{2-\epsilon}{2}}^1 dx_t^j \left[\int_{x_t^j - \epsilon}^{3x_t^j - 2} dx_t^i P_t(x_t^i) \right] P_t(x_t^j) \delta(x - 1) \tag{D.28}$$

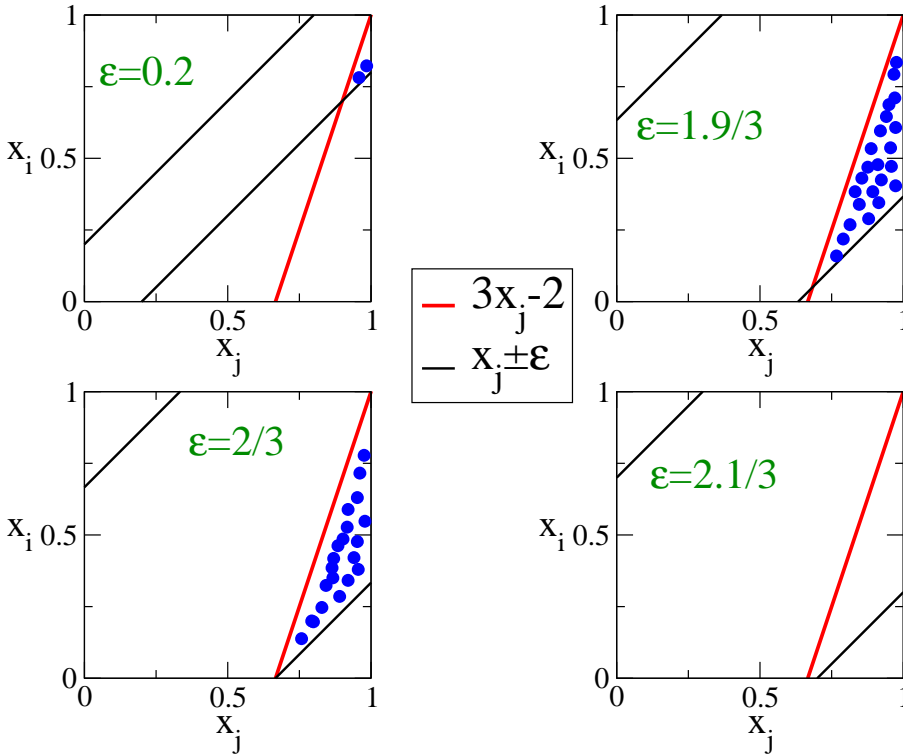


Figure D.2. The case to prevent the final opinion to be greater than 1. We give several examples of the integration region, shown in blue dots, for different ϵ

D.2.5 The normalization condition

Defining the moments as $M_k(t) = \int dx x^k P(x, t)$ the normalization condition is $\frac{dM_0}{dt} = 0$, $\int_0^1 \frac{dP(x, t)}{dt} dx = 0$.

Moments of the Master Equation for the attractive part

The Master Equation with deltas for the attractive part is:

$$\frac{\partial P}{\partial t}(x) = \int_{|x_n^i - x_n^j| < \epsilon} dx_n^i dx_n^j P_n(x_n^i) P_n(x_n^j) \left[2\delta\left(x - \frac{x_n^i + x_n^j}{2}\right) - \delta(x - x_n^i) - \delta(x - x_n^j) \right] \quad (\text{D.29})$$

We multiply both terms by x^k and integrate, noting that $\int x^k \delta(x-a) = a^k$. We obtain:

$$\frac{\partial M_k}{\partial t}(x) = \int_{|x_n^i - x_n^j| < \epsilon} dx_n^i dx_n^j P_n(x_n^i) P_n(x_n^j) \left[2\left(\frac{x_n^i + x_n^j}{2}\right)^k - (x_n^i)^k - (x_n^j)^k \right] \quad (\text{D.30})$$

So, if $k = 0$, then $\frac{\partial M_0}{\partial t}(x) = 0$.

Moments of the Master Equation for the repulsive part

The Master Equation with deltas for the repulsive part has several terms:

This following term covers the entire region in Fig. D.3. If we integrate to calculate the first moment, and consider that $P_t(x_t^i)P_t(x_t^j) = AB$ (any constant) and $x \in [0, 1]$ we get:

$$\begin{aligned} & -2 \int_{|x_t^i - x_t^j| < \epsilon} dx_t^j P_t(x_t^i) P_t(x_t^j) \delta(x - x_t^i) \rightarrow \\ & -2 \int_{-\infty}^{\infty} dx \int_{|x_t^i - x_t^j| < \epsilon} dx_t^j P_t(x_t^i) P_t(x_t^j) \delta(x - x_t^i) \rightarrow \\ & -2AB \int_{|x_t^i - x_t^j| < \epsilon} dx_t^j \int_{-\infty}^{\infty} dx \delta(x - x_t^i) \rightarrow \\ & -2AB(2\epsilon - \epsilon^2) = -AB(4\epsilon - 2\epsilon^2) \quad (\text{D.31}) \end{aligned}$$

Next we have the two terms coming from the boundary contributions:

$$\begin{aligned}
& \int_{\substack{|x_t^i - x_t^j| < \epsilon \\ \frac{3x_t^j - x_t^i}{2} \leq 0}} dx_t^i dx_t^j P_t(x_t^i) P_t(x_t^j) \delta(x) \rightarrow \\
& \int_{-\infty}^{\infty} dx \int_{\substack{|x_t^i - x_t^j| < \epsilon \\ \frac{3x_t^j - x_t^i}{2} \leq 0}} dx_t^i dx_t^j P_t(x_t^i) P_t(x_t^j) \delta(x) \rightarrow \\
& AB \int_{\substack{|x_t^i - x_t^j| < \epsilon \\ \frac{3x_t^j - x_t^i}{2} \leq 0}} dx_t^i dx_t^j \int_{-\infty}^{\infty} dx \delta(x) \rightarrow \\
& AB(0.25\epsilon^2) \tag{D.32}
\end{aligned}$$

$$\begin{aligned}
& \int_{\substack{|x_t^i - x_t^j| < \epsilon \\ \frac{3x_t^j - x_t^i}{2} \geq 1}} dx_t^i dx_t^j P_t(x_t^i) P_t(x_t^j) \delta(x - 1) \rightarrow \\
& \int_{-\infty}^{\infty} dx \int_{\substack{|x_t^i - x_t^j| < \epsilon \\ \frac{3x_t^j - x_t^i}{2} \geq 1}} dx_t^i dx_t^j P_t(x_t^i) P_t(x_t^j) \delta(x - 1) \rightarrow \\
& AB \int_{\substack{|x_t^i - x_t^j| < \epsilon \\ \frac{3x_t^j - x_t^i}{2} \geq 1}} dx_t^i dx_t^j \int_{-\infty}^{\infty} dx \delta(x - 1) \rightarrow \\
& AB(0.25\epsilon^2) \tag{D.33}
\end{aligned}$$

Finally, the last term covers the entire region (Fig. D.3), excluding the boundaries:

$$\begin{aligned}
& \int_{\substack{|x_t^i - x_t^j| < \epsilon \\ 0 \leq \frac{3x_t^i - x_t^j}{2} \leq 1}} dx_t^j P_t(x_t^i) P_t(x_t^j) 2\delta \left(x - \frac{3x_t^i - x_t^j}{2} \right) \rightarrow \\
& \int_{-\infty}^{\infty} dx \int_{\substack{|x_t^i - x_t^j| < \epsilon \\ 0 \leq \frac{3x_t^i - x_t^j}{2} \leq 1}} dx_t^j P_t(x_t^i) P_t(x_t^j) 2\delta \left(x - \frac{3x_t^i - x_t^j}{2} \right) \rightarrow \\
& 2AB \int_{\substack{|x_t^i - x_t^j| < \epsilon \\ 0 \leq \frac{3x_t^i - x_t^j}{2} \leq 1}} dx_t^j \int_{-\infty}^{\infty} dx \delta \left(x - \frac{3x_t^i - x_t^j}{2} \right) \rightarrow \\
& AB(4\epsilon - 2\epsilon^2) - AB0.5\epsilon^2 \tag{D.34}
\end{aligned}$$

Summing the contribution from all the terms, we see the normalization condition is verified:

$$- AB(4\epsilon - 2\epsilon^2) + AB0.5\epsilon^2 + AB(4\epsilon - 2\epsilon^2) - AB0.5\epsilon^2 = 0 \tag{D.35}$$

D.2.6 Numerical integration of the Master Equation - practical issues

We discretize the opinion range into $M = 2000$ boxes.

We implement $\delta(x)$ as a M , since it is the maximum allowed value.

We used a fourth-order Runge-Kutta method.

D.2.7 Strange Master Equation results

- Undetected clusters

The Master Equation approach has a known problem: when a δ function is reached, it loses accuracy, not detecting some clusters. The position of those clusters, in simulations, is not precisely located.

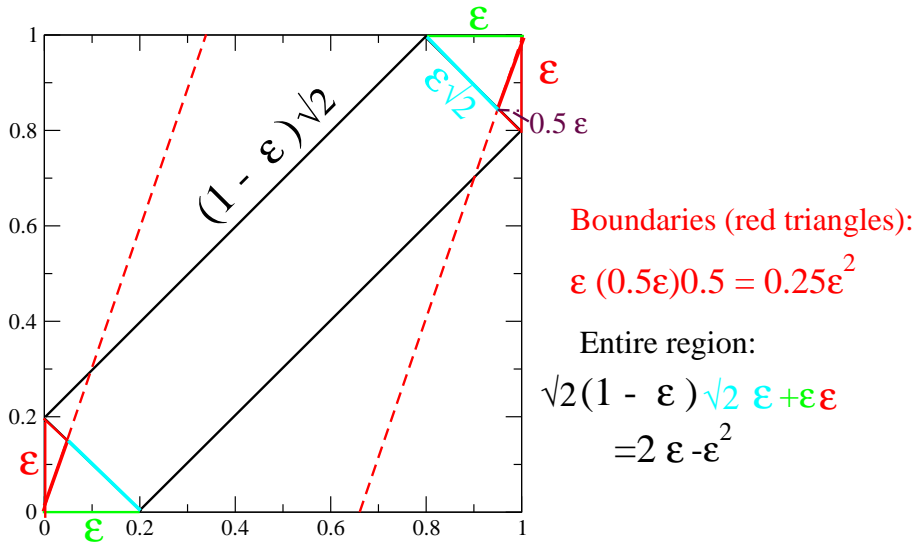


Figure D.3. Auxiliary figure to understand the areas of integration of the several terms of the repulsive part

Shall we let the numerical integration evolve until it reaches a steady state (with δ), or shall we control its running time by comparing results with simulations?

- inaccurate for big ϵ

We saw the Master Equation is valid when $\epsilon < \frac{2}{3}$. However, even for lower ϵ (e.g.: $\epsilon = 0.5$) the results become inaccurate when $p \neq 0$. This is a consequence of the increasing influence of the boundary conditions.

E

Some calculus concerning The Van der Pol system

This appendix concerns some results of Chapter 6, so let's begin by recalling the model. We consider an ensemble of N van der Pol oscillators globally coupled through their velocities, and subjected to an external periodic forcing.

$$\ddot{x}_i = -x_i + \mu(1 - x_i^2)\dot{x}_i + \frac{C}{N} \sum_{j=1}^N J_{ij} (\dot{x}_j - \dot{x}_i) + A \sin(\Omega t). \quad (\text{E.1})$$

The interaction matrix J_{ij} reflects the presence of attractive and repulsive interactions between the units. More specifically, we adopt the following values at random:

$$J_{ij} = J_{ji} = \begin{cases} -1, & \text{with probability } p, \\ 1, & \text{with probability } 1 - p. \end{cases} \quad (\text{E.2})$$

E.0.8 The system

Let's transform it into a two-dimensional form that highlights a fast and a slow motion:

$$\begin{cases} \dot{x}_i = \mu(x_i - \frac{1}{3}x_i^3 - y_i) + \frac{C}{N} \sum_{j=1}^N J_{ij} (x_j - x_i) \\ \dot{y}_i = \frac{1}{\mu} [x_i - A \sin(\Omega t)]. \end{cases} \quad (\text{E.3})$$

Indeed, by differentiating the first equation of the system E.3 we arrive at Eq E.1,

$$\begin{aligned} \ddot{x}_i &= \frac{d}{dt} \left[\mu(x_i - \frac{1}{3}x_i^3 - y_i) + \frac{C}{N} \sum_{j=1}^N J_{ij} (x_j - x_i) \right] \\ &= \mu(\dot{x}_i - \dot{x}_i x_i^2 - \dot{y}_i) + \frac{C}{N} \sum_{j=1}^N J_{ij} (\dot{x}_j - \dot{x}_i) \\ &= \mu \left[\dot{x}_i - \dot{x}_i x_i^2 - \frac{1}{\mu} x_i + \frac{A}{\mu} \sin(\Omega t) \right] + \frac{C}{N} \sum_{j=1}^N J_{ij} (\dot{x}_j - \dot{x}_i) \\ &= \mu(1 - x_i^2)\dot{x}_i - x_i + A \sin(\Omega t) + \frac{C}{N} \sum_{j=1}^N J_{ij} (\dot{x}_j - \dot{x}_i) \end{aligned} \quad (\text{E.4})$$

E.0.9 The anti-phase solution

Our simulation results show that when the probability of repulsive links p is greater than the probability associated with the transition region (Chapter 6) several groups oscillating in anti-phase are formed. We want to know how the proportion of oscillators in phase and anti-phase is divided in a given group.

In case there are two groups, a group 1 with $x_i = a_i$ and group 2 with $x_i = -a_i$ how many oscillators will be part of each group?

Let's say n oscillators share the position of group 1. The interaction of the oscillator i with this groups is given by $x_j - x_i = a_i - a_i$ so it is zero. Concerning the $N - n$ oscillator that are in the opposite position, the interaction of i with them is $-2\dot{a}_i$. The equation for the group 1 is:

$$\begin{aligned}
 \ddot{a}_i &= \\
 &= -a_i + \mu(1 - a_i^2)\dot{a}_i + \frac{C}{N} [-p(N - n)(-2\dot{a}_i) + (1 - p)(M - n)(-2\dot{a}_i)] = \\
 &= -a_i + \mu(1 - a_i^2)\dot{a}_i + \frac{C}{N}(-2\dot{a}_i)(N - n - 2pN + 2pn) = \\
 &= -a_i + \mu(1 - a_i^2)\dot{a}_i + C(1 - \frac{n}{N})(-2\dot{a}_i)(1 - 2p) = \\
 &= -a_i + \mu(1 - a_i^2)\dot{a}_i + C(1 - \frac{n}{N})(2\dot{a}_i)(2p - 1) =
 \end{aligned} \tag{E.5}$$

And the second group is

$$-\ddot{a}_i = a_i + \mu(1 - a_i^2)\dot{a}_i + \frac{C}{N} [-p(n)(2\dot{a}_i) + (1 - p)(n)(2\dot{a}_i)] \tag{E.6}$$

$$= a_i - \mu(1 - a_i^2)\dot{a}_i + \frac{C}{N}(2\dot{a}_i)(n - 2pn) \tag{E.7}$$

$$= a_i - \mu(1 - a_i^2)\dot{a}_i + C\frac{n}{N}(2\dot{a}_i)(1 - 2p) \tag{E.8}$$

$$\tag{E.9}$$

Considering the two groups:

$$\begin{cases} \ddot{a}_i = -a_i + \mu(1 - a_i^2)\dot{a}_i + C(1 - \frac{n}{N})(2\dot{a}_i)(2p - 1) \\ -\ddot{a}_i = a_i - \mu(1 - a_i^2)\dot{a}_i + C\frac{n}{N}(2\dot{a}_i)(1 - 2p). \end{cases} \tag{E.10}$$

If this is true, then:

$$\frac{n}{N} = (1 - \frac{n}{N}) \implies n = \frac{N}{2} \tag{E.11}$$

E.0.10 How repulsive links modify the amplitude of oscillations

Again, let's consider two groups. The presence of repulsive links leads to the formation of several groups oscillating in anti-phase.

$$\begin{cases} \ddot{a}_i &= -a_i + \mu(1 - a_i^2)\dot{a}_i + C(1 - \frac{n}{N})(2\dot{a}_i)(2p - 1) \\ -\ddot{a}_i &= a_i - \mu(1 - a_i^2)\dot{a}_i + C\frac{n}{N}(2\dot{a}_i)(1 - 2p). \end{cases} \quad (\text{E.12})$$

Making $b_i = \frac{a_i}{A}$

$$A\ddot{b}_i = -Ab_i + \mu A^2(1 - b_i^2)A\dot{b}_i \quad (\text{E.13})$$

$$\ddot{b}_i = -b_i + \mu A^2(1 - b_i^2)\dot{b}_i \quad (\text{E.14})$$

By this formula we recover the familiar van der Pol equation with an amplitude of oscillations $|b_i| = 2$, and

$$\mu A^2 = \mu + 2C(1 - \frac{n}{N}) \quad (\text{E.15})$$

Therefore, the amplitude of oscillations is $|a_i| = A|b_i|$, and when $\mu = 10$ and $C = 20$, $a_i = 3.4$.

In this derivation we assumed the oscillators were divided in two groups with an equal number of elements in each group.

E.0.11 The measure G

We define a measure G to quantify the influence of the fraction of repulsive links a particular oscillator has on its overall synchronisation with the other elements.

The strongest it is the synchronisation among oscillators, the higher it is the value $\sum_{j,i} x_j \dot{x}_i$. The average number of repulsive links in a given run

is given by $F = \frac{1}{N^2} \sum_{ji} J_{ij}$, while the particular fraction of repulsive links an oscillator has, $f_i = \frac{1}{N} \sum_{i=1}^N J_{ij}$, can be different from the mean given that the probability of repulsive links p follows a binomial distribution.

Therefore we arrive at:

$$\begin{aligned}
 & G = \\
 & = N \left[\frac{1}{N} \sum_{i=1}^N \left[\frac{1}{N} \sum_{j=1}^N J_{ij} \frac{1}{N} \sum_{j=1}^N \dot{x}_j \dot{x}_i \right] - \frac{1}{N^2} \sum_{ji} J_{ij} \frac{1}{N^2} \sum_{ji} \dot{x}_j \dot{x}_i \right] = \\
 & = \frac{1}{N} \sum_{i=1}^N \left[f_i \sum_{j=1}^N \dot{x}_j \dot{x}_i \right] - \frac{1}{N} F \sum_{ji} \dot{x}_j \dot{x}_i = \\
 & = \frac{1}{N} \sum_{i=1}^N \left[f_i \sum_{j=1}^N \dot{x}_j \dot{x}_i \right] - \frac{1}{N} F \sum_{ji} \dot{x}_j \dot{x}_i = \\
 & = \frac{1}{N} \sum_{ji} \dot{x}_j \dot{x}_i [f_i - F]
 \end{aligned} \tag{E.16}$$

When is this measure zero? When f_i is uncorrelated with $\sum_{ji} \dot{x}_j \dot{x}_i$, that is, when the synchronisation of an element with the other oscillators doesn't depend on its fraction of repulsive links. This quantity is also zero when diversity in the form of a variance in the probability of repulsive links doesn't exist. This suggests that diversity is required to achieve this new form of synchronisation.

Bibliography

- [1] T. Wilhelm, The smallest chemical reaction system with bistability, *BMC Systems Biology* 3 (2009) 90.
- [2] R. Malka, E. Shochat, V. Rom-Kedar, Bistability and bacterial infections, *PLoS ONE* 5-5 (2010) e10010.
- [3] M. Laurent, G. Charvin, J. Guespin-Michel, Bistability and hysteresis in epigenetic regulation of the lactose operon., *Cellular and Molecular Biology* 51 (2005) 583–594.
- [4] T. S. Gardner, C. R. Cantor, J. J. Collins, Construction of a genetic toggle switch in *escherichia coli*, *Nature* 403 (2000) 339–342.
- [5] T. M. Lenton, H. Held, E. Kriegler, J. W. Hall, W. Lucht, S. Rahmstorf, H. J. Schellnhuber, Tipping elements in the earth’s climate system, *PNAS* 105 (2008) 1786–1793.
- [6] M. Scheffer, J. Bascompte, W. A. Brock, V. Brovkin, S. R. Carpenter, V. Dakos, H. Held, E. H. van Nes, M. Rietkerk, G. Sugihara, Early-warning signals for critical transitions., *Nature* 461 (2009) 53–59.
- [7] S. authors, Special report: Sustainability, *Scientific American* 302 - N 4 (2010) 53–67.
- [8] F. Mormann, R. G. Andrzejak, C. E. Elger, K. Lehnertz, Seizure prediction: the long and winding road., *Brain* 130 (2007) 314 – 333.
- [9] E. T. Hens, K. R. Schenk-Hoppe, *Handbook of Financial Markets: Dynamics and Evolution*, North-Holland, 2009.
- [10] M. S. Miguel, R. Toral, *Stochastic effects in physical systems, Instabilities and Nonequilibrium Structures VI* - eds. E. Tirapegui and J. Martínez and

- R. Tiemann, Kluwer Academic Publishers, 2000.
- [11] A. Pikovsky, M. Rosenblum, J. Kurths, *Synchronization: A Universal Concept in Nonlinear Sciences*, Cambridge University Press, 2003.
 - [12] B. van der Pol, J. van der Mark, The heartbeat considered as a relaxation oscillation, and an electrical model of the heart, *London, Edinburgh, and Dublin Philosoph. Mag., and J. Sci. Ser. 7, Vol. 6* (1928) 763 – 775.
 - [13] A. Liénard, Etude des oscillations entretenues, *Revue générale de l'électricité* 23 (946 - 954) (1928) 901 – 912.
 - [14] A. Balanov, N. Janson, D. Postnov, O. Sosnovtseva, *Synchronization. From Simple to Complex.*, Series: Springer Series in Synergetics., 2009.
 - [15] B. van der Pol, J. van der Mark, Frequency demultiplication, *Nature* 120 (1927) 363–364.
 - [16] E. M. Izhikevich, Neural excitability, spiking and bursting, *International Journal of Bifurcation and Chaos* 10 (2000) 1171 – 1266.
 - [17] B. Lindner, J. García-Ojalvo, A. Neiman, L. Schimansky-Geier, Effects of noise in excitable systems, *Physics Reports* 392 (2004) 321–424.
 - [18] Y. Shinomoto, Y. Kuramoto, Phase transitions in active rotator systems, *Prog. Theor. Phys.* 75 (1986) 1105.
 - [19] S. H. Strogatz, *Nonlinear dynamics and chaos: With applications to physics, biology, chemistry, and engineering*, Perseus Books - Cambridge, 1994.
 - [20] R. FitzHugh, Impulses and physiological states in theoretical models of nerve membrane., *Biophysical J.* 1 (1961) 445–466.
 - [21] J. Nagumo, S. Arimoto, S. Yoshizawa, An active pulse transmission line simulating nerve axon., *Proc IRE.* 50 (1962) 2061 – 2070.
 - [22] A. Hodgkin, The local electric charges associated with repetitive action in a non-medullated axon, *J. Physiol.* 107 (1948) 165–181.
 - [23] J. Rinzel, G. B. Ermentrout, Analysis of neuronal excitability and oscillations, C. Koch and I. Segev editors *Methods in neuronal modeling*.
 - [24] P. Ball, The physical modelling of society: a historical perspective, *Physica A* 314 (2002) 1–14.
 - [25] R. Albert, A.-L. Barabási, *Statistical mechanics of complex networks*, *Reviews of Modern Physics* 74 (2002) 47.
 - [26] M. E. J. Newman, *Networks: An Introduction*, Oxford University Press, 2010.
 - [27] M. O. Jackson, *Social and Economic Networks*, Princeton University Press,

- 2008.
- [28] S. N. Dorogovtsev, J. F. F. Mendes, *Evolution of Networks*, Oxford University Press, 2003.
 - [29] S. M. Stigler, *The History of Statistics: The Measurement of Uncertainty before 1900*, Harvard University Press, 1986.
 - [30] V. Coven, *A history of statistics in the social sciences*, Gateway - An Academic Journal on the Web.
 - [31] A. Comte, *Course of Positive Philosophy*, 1830.
 - [32] C. Castellano, S. Fortunato, V. Loreto, *Statistical physics of social dynamics*, *Rev. Mod. Phys.* 81 (2009) 591.
 - [33] S. Galam, *Sociophysics: a personal testimony*, *Physica A* 336 (2004) 49 – 55.
 - [34] D. Stauffer, *Sociophysics simulations ii: opinion dynamics*, *Modeling Cooperative Behavior In The Social Sciences*. AIP Conference Proceedings 779 (2005) 56–68.
 - [35] P. Sobkowicz, *Modelling opinion formation with physics tools: Call for closer link with reality*, *Journal of Artificial Societies and Social Simulation* 12 (1) (2009) 11.
 - [36] B. Castellani, F. W. Hafferty, *Sociology and Complexity Science: A New Field of Inquiry*, Springer, 2009.
 - [37] P. Bourdieu, *La distinction: critique sociale du jugement*, Les Editions de Minuit, 1979.
 - [38] A. Giddens, *Sociology*, (5th edition) Polity, Cambridge, 2006.
 - [39] J. Habermas, *Theory of Communicative Action*, Boston: Beacon Press, 1984.
 - [40] J. Lorenz, *Continuous opinion dynamics under bounded confidence: A survey*, *Int. J. Mod. Phys. C* 18 (2007) 1819.
 - [41] G. Deffuant, D. Neau, F. Amblard, G. Weisbuch, *Mixing beliefs among interacting agents*, *Advances in Complex Systems* 3 (2000) 87.
 - [42] R. Hegselmann, U. Krause, *Opinion dynamics and bounded confidence: models, analysis and simulation*, *Journal of Artificial Societies and Social Simulation (JASSS)* 5 (3) (2002) 2.
 - [43] K. Sznajd-Weron, J. Sznajd, *Opinion evolution in closed community*, *Int. J. Mod. Phys. C* 11 (2000) 1157.
 - [44] M. Kuperman, D. Zanette, *Stochastic resonance in a model of opinion for-*

- mation on small world networks, *Eur. Phys. J. B* 26 (2002) 387.
- [45] R. Axelrod, The dissemination of culture, *J. Conflict Res.* 41 - N2 (1997) 203 – 226.
- [46] M. McPherson, L. Smith-Lovin, J. Cook, Birds of a feather: Homophily in social networks, *Annual Review of Sociology* 27 (2001) 415-44.
- [47] E. Ben-Naim, P. L. Krapivsky, S. Redner, Bifurcations and patterns in compromise processes, *Physica D* 183 (2003) 190.
- [48] M. Pineda, R. Toral, E. Hernandez-Garcia, Noisy continuous-opinion dynamics, *Journal of Statistical Mechanics: Theory and Experiment* P08001 (2009) 1.
- [49] R. Toral, C. J. Tessone, Finite size effects in the dynamics of opinion formation, *Communications in Computational Physics* 2 (2007) 177 – 195.
- [50] D. Stauffer, H. Meyer-Ortmanns, Simulation of consensus model of deffuant et al on a barabasi-albert network, *IJMPC* 15 (2) (2004) 241–246.
- [51] G. Deffuant, F. Amblard, G. Weisbuch, Modelling group opinion shift to extreme : the smooth bounded confidence model, *Proceedings of the European Social Simulation Association Conference*.
- [52] J. Lorenz, Heterogeneous bounds of confidence: Meet, discuss and find consensus!, *Complexity* 15 (2010) 4352.
- [53] W. Jager, F. Amblard, Uniformity, bipolarization and pluriformity captured as generic stylized behavior with an agent-based simulation model of attitude change, *Computational and Mathematical Organization Theory* 10 (2004) 295.
- [54] A. Radillo-Díaz, L. A. Pérez, M. D. Castillo-Mussot, Axelrod models of social influence with cultural repulsion, *Phys. Rev. E* 80 (6) (2009) 066107.
- [55] L. Salzarulo, A continuous opinion dynamics model based on the principle of meta-contrast, *Journal of Artificial Societies and Social Simulation* 9 (1) (2006) 13.
- [56] S. Huet, G. D. G., W. Jager, Rejection mechanism in 2d bounded confidence provides more conformity, *Advances in Complex Systems* 11-4 (2008) 529.
- [57] J. C. González-Avella, M. Cosenza, V. Eguíluz, M. S. Miguel, Spontaneous ordering against an external field in nonequilibrium systems, *New Journal of Physics* 12 (2010) 013010.
- [58] T. Carletti, D. Fanelli, S. Grolli, A. Guarino, How to make an efficient propaganda, *Europhys. Lett.* 74 (2) (2006) 222.

- [59] C. J. Tessone, R. Toral, Diversity-induced resonance in a model for opinion formation, *Eur. Phys. J. B* 71 (2009) 549.
- [60] P. Babinec, Stochastic resonance in the Weidlich model of public opinion formation, *Physics Letters A* 225 (1997) 179.
- [61] L. Gammaitoni, P. J. P. Hänggi, F. Marchesoni, Stochastic resonance, *Rev. Mod. Phys.* 70 (1998) 223.
- [62] P. Hänggi, F. Marchesoni, Topical issue on stochastic resonance, *Eur. Phys. J. B* 69.
- [63] T. Wellens, V. Shatokhin, A. Buchleitner, Stochastic resonance, *Rep. Prog. Phys.* 67 (2004) 45–105.
- [64] V. S. Anishchenko, A. B. Neiman, F. Moss, L. Shimansky-Geier, Stochastic resonance: noise-enhanced order, *Phys.-Usp.* 42 (1999) 7.
- [65] L. F. Lafuerza, P. Colet, R. Toral, Non-universal results induced by diversity distribution in coupled excitable systems, *Physical Review Letters* 105 (2010) 084101.
- [66] L. Bachelier, Théorie de la spéculation, *Annales scientifiques de l'École normale supérieure* 3- no 17 (1900) 21 – 86.
- [67] K. Pearson, The problem of the random walk, *Nature* 72 (1905) 294.
- [68] A. Einstein, über die von der molekularkinetischen theorie der wärme geforderte bewegung von in ruhenden flüssigkeiten suspendierten teilchen, *Annalen der Physik* 17 (1905) 549–600.
- [69] P. Hänggi, F. Marchesoni, F. Nori, Brownian motors, *Ann. Phys. (Leipzig)* 14 - No. 1 - 3 (2005) 51 – 70.
- [70] R. Benzi, A. Sutera, A. Vulpiani, The mechanism of stochastic resonance, *J. Phys. A* 14 (1981) 453.
- [71] C. Nicolis, G. Nicolis, Stochastic aspects of climatic transitions additive fluctuations, *Tellus* 33 (1981) 225.
- [72] P. Hänggi, Stochastic resonance in biology. how noise can enhance detection of weak signals and help improve biological information processing, *Chemphyschem.* 12-3(3) (2002) 285–90.
- [73] C. W. Gardiner, *Handbook of Stochastic Methods for Physics, Chemistry and the Natural Sciences*, third edition Edition, Springer-Verlag, Berlin, 2004.
- [74] H. A. Kramers, Brownian motion in a field force and the diffusion of chemical reactions, *Physica* 7 (1940) 284.

- [75] B. McNamara, K. Wiesenfeld, Theory of stochastic resonance, *Phys. Rev. A* 39 (1989) 4854.
- [76] J. Douglass, L. Wilkens, E. Pantazelou, F. Moss, Noise enhancement of information transfer in crayfish mechanoreceptors by stochastic resonance, *Nature* 365(6444) (1993) 337.
- [77] A. Longtin, Stochastic resonance in neuron models, *Journal of Statistical Physics* 70 (1993) 309.
- [78] K. Wiesenfeld, D. Pierson, E. Pantazelou, C. Dames, F. Moss, Stochastic resonance on a circle, *Phys. Rev. Lett.* 72 (14) (1994) 2125 – 2129.
- [79] H. E. Plesser, T. Geisel, Markov analysis of stochastic resonance in a periodically driven integrate-and-fire neuron, *Phys. Rev. E* 59 (6) (1999) 7008–7017.
- [80] B. McNamara, K. Wiesenfeld, R. Roy, Observation of stochastic resonance in a ring laser, *Phys. Rev. Lett.* 60 (25) (1988) 2626.
- [81] L. Gammaitoni, F. Marchesoni, E. Menichella-Saetta, S. Santucci, Stochastic resonance in bistable systems, *Phys. Rev. Lett.* 62 (1989) 349.
- [82] P. Greenwood, L. Ward, W. Wefelmeyer, Statistical analysis of stochastic resonance in a simple setting, *Phys. Rev. E* 60 (4) (1999) 4687.
- [83] T. Munakata, A. Sato, T. Hada, Stochastic resonance in a simple threshold system from a static mutual information point of view, *J. Phys. Soc. Japan* 74 (2005) 2094.
- [84] P. Jung, P. Hänggi, Stochastic nonlinear dynamics modulated by external periodic forces, *Europhys. Lett.* 8 (6) (1989) 505.
- [85] J. J. Collins, C. C. Chow, T. T. Imhoff, Aperiodic stochastic resonance in excitable systems, *Phys. Rev. E* 52 (4) (1995) R3321.
- [86] A. D. Hibbs, A. L. Singaas, E. W. Jacobs, A. R. Bulsara, J. J. Bekkedahl, Stochastic resonance in a superconducting loop with a josephson junction, *J. Appl. Phys.* 77 (1995) 2582.
- [87] A. Longtin, D. R. Chialvo, Stochastic and deterministic resonances for excitable systems, *Phys. Rev. Lett.* 81 (18) (1998) 4012.
- [88] J. F. Lindner, B. J. Breen, M. E. Wills, A. R. Bulsara, W. L. Ditto, Monostable array-enhanced stochastic resonance, *Phys. Rev. E* 63 (5) (2001) 051107.
- [89] C. Tessone, C. Mirasso, R. Toral, J. Gunton, Diversity-induced resonance, *Phys. Rev. Lett.* 97 (2006) 194101.

- [90] R. Toral, C. J. Tessone, J. V. Lopes, Collective effects induced by diversity in extended systems, *Eur. Phys. J. Special Topics* 143 (2007) 59.
- [91] Desai, Zwanzig, Statistical mechanics of a nonlinear stochastic model, *J. Stat. Phys* 19 (1978) 1– 24.
- [92] J. F. Lindner, B. K. Meadows, W. L. Ditto, M. E. Inchiosa, A. Bulsara, Array enhanced stochastic resonance and spatiotemporal synchronization, *Phys. Rev. Lett.* 75 (1) (1995) 3.
- [93] H. Wio, Stochastic resonance in a spatially extended system, *Phys. Rev. E* 54 (4) (1996) R3075.
- [94] R. Toral, E. Hernandez-Garcia, J. D. Gunton, Diversity-induced resonance in a system of globally coupled linear oscillators, *International Journal of Bifurcation and Chaos* 19- 10 (2009) 3499.
- [95] J. Acebrón, S. Lozano, A. Arenas, Amplified signal response in scale-free networks by collaborative signaling, *Phys. Rev. Lett.* 99 (2007) 128701 – 229902(E).
- [96] H. Cheng, J. Zhang, J. Liu, Structural-diversity-enhanced cellular ability to detect subthreshold extracellular signals, *Phys. Rev. E* 75 (4) (2007) 041910.
- [97] M. Gassel, E. Glatt, F. Kaiser, Doubly diversity-induced resonance, *Phys. Rev. E* 76 (1) (2007) 016203.
- [98] J. Cartwright, Emergent global oscillations in heterogeneous excitable media: The example of pancreatic β cells, *Phys. Rev. E* 62 (1) (2000) 1149.
- [99] I. Leyva, I. Sendiña-Nadal, J. A. Almendral, M. A. Sanjun, Sparse repulsive coupling enhances synchronization in complex networks, *Phys. Rev. E* 74 (2006) 056112.
- [100] C. Tessone, D. Zanette, R. Toral, Global firing induced by network disorder in ensembles of active rotators, *Eur. Phys. J. B* 62 (2008) 319.
- [101] E. Glatt, M. Gassel, F. Kaiser, Noise-induced synchronisation in heterogeneous nets of neural elements, *Europhys. Lett.* 81 (4) (2008) 40004.
- [102] C. Tessone, A. Scirè, R. Toral, P. Colet, Theory of collective firing induced by noise or diversity in excitable media, *Phys. Rev. E* 75 (1) (2007) 016203.
- [103] M. Perc, M. Gosak, S. Kralj, Stochastic resonance in soft matter systems: combined effects of static and dynamic disorder, *Soft Matter* 4 (2008) 1861.
- [104] P. N. McGraw, M. Menzinger, Laplacian spectra as a diagnostic tool for network structure and dynamics, *Phys. Rev. E* 77 (2008) 031102.

- [105] E. A. P. Young, Spin glasses and random fields, World Scientific, Singapore, 1997.
- [106] M. S. Miguel, R. Toral, Stochastic effects in physical systems, in *Instabilities and Nonequilibrium Structures VI*, eds. E. Tirapegui, J. Martínez and R. Tiemann - Kluwer Academic Publishers, 35-130, 2000.
- [107] V. N. Livina, F. Kwasniok, T. M. Lenton, Potential analysis reveals changing number of climate states during the last 60 kyr, *Clim. Past Discuss.* 5 (2009) 2223.
- [108] T. V. Martins, R. Toral, M. Santos, Divide and conquer: resonance induced by competitive interactions, *Eur. Phys. J. B* 67 (3) (2009) 329.
- [109] P. W. Anderson, Absence of diffusion in certain random lattices, *Phys. Rev.* 109 (1958) 1492 – 1505.
- [110] P. W. Anderson, Localisation theory and the cu-mn problem: Spin glasses, *Mater. Res. Bull.* 5 (1970) 549.
- [111] D. J. Watts, S. H. Strogatz, Collective dynamics of 'small-world' networks, *Nature* 393 (1998) 440.
- [112] D. Landau, K. Binder, A Guide to Monte Carlo Simulations in Statistical Physics, Cambridge University Press, 2000.
- [113] S. Maslov, K. Sneppen, Specificity and stability in topology of protein networks, *Science* 296 (2002) 910.
- [114] Y. Bar-Yam, I. R. Epstein, Response of complex networks to stimuli, *PNAS* 101 (13) (2004) 4341.
- [115] T. V. Martins, V. N. Livina, A. P. Majtey, R. Toral, Resonance induced by repulsive interactions in a model of globally coupled bistable systems, *Phys. Rev. E* 81 (2010) 041103.
- [116] J. Jalife, Mutual entrainment and electrical coupling as mechanisms for synchronous firing of rabbit sino-atrial pace-maker cells, *J Physiol* 356 (1984) 221243.
- [117] P. V. Leeuwen, D. Geue, M. Thiel, D. Cysarz, S. Lange, M. C. Romano, N. Wessel, J. Kurths, D. H. Grönemeyer, Influence of paced maternal breathing on fetal - maternal heart rate coordination, *Proc Natl Acad Sci U S A* 106 (33) (2009) 13661 – 13666.
- [118] T. Nishikawa, A. Motter, Network synchronization landscape reveals compensatory structures, quantization, and the positive effect of negative interactions, *Proc. Natl. Acad. Sci.* 107 (2010) 10342.

- [119] L. S. Tsimring, N. F. Rulkov, M. L. Larsen, M. Gabbay, Repulsive synchronization in an array of phase oscillators, *Phys. Rev. Lett.* 95 (1) (2005) 014101.
- [120] H. Daido, Population dynamics of randomly interacting self-oscillators. i, *Prog. Theor. Phys.* 77 (3) (1987) 622 – 634.
- [121] H. Daido, Quasientrainment and slow relaxation in a population of oscillators with random and frustrated interactions, *Phys. Rev. Lett.* 68 (7) (1992) 1073 – 1076.
- [122] H. Daido, Algebraic relaxation of an order parameter in randomly coupled limit-cycle oscillators, *Phys. Rev. E* 61 (2) (2000) 2145 – 2147.
- [123] L. L. Bonilla, C. Pérez-Vicente, J. Rub, Glassy synchronization in a population of coupled oscillators, *Journal of Statistical Physics* 70 (1993) 921.
- [124] N. F. Rulkov, L. Tsimring, M. L. Larsen, M. Gabbay, Synchronization and beam forming in an array of repulsively coupled oscillators, *Phys. Rev. E* 74 (5) (2006) 056205.
- [125] M. Giver, Z. Jabeen, B. Chakraborty, Phase and frequency entrainment in locally coupled phase oscillators with repulsive interactions, preprint: arXiv:1009.6004.
- [126] D. H. Zanette, Synchronization and frustration in oscillator networks with attractive and repulsive interactions, *Europhys. Lett.* 72 (2005) 190–196.
- [127] Pecora, L. M., Carroll, T. L., Master stability functions for synchronized coupled systems, *Phys. Rev. Lett.* 80 (10) (1998) 2109–2112.
- [128] Y. Kuramoto., *Chemical oscillations, waves and turbulences*, Springer - Verlag, New York (USA), 1984.
- [129] A. S. Pikovsky, J. Kurths, Coherence resonance in a noise-driven excitable system, *Phys. Rev. Lett.* 78 (5) (1997) 775–778.
- [130] A. Neiman, L. Schimansky-Geier, A. Cornell-Bell, F. Moss, Noise-enhanced phase synchronization in excitable media, *Phys. Rev. Lett.* 83 (23) (1999) 4896–4899.
- [131] C. Kurrer, K. Schulten, Noise-induced synchronous neuronal oscillations, *Phys. Rev. E* 51 (6) (1995) 6213–6218.
- [132] C. Tessone, A. Scirè, R. Toral, P. Colet, Theory of collective firing induced by noise or diversity in excitable media, *Physical Review E* 75 (2007) 016203.
- [133] J. A. Almendral, I. Leyva, I. Sendiña-Nadal, Enhancing network synchro-

nization by sparse repulsive couplings, *International Journal of Bifurcation and Chaos* 19(2) (2009) 711 – 717.

- [134] A. Arenas, A. Díaz-Guilera, J. Kurths, Y. Moreno, C. Zhou, Synchronization in complex networks, *Physics Reports* 469 (2008) 93.
- [135] Silverman, *Density estimation for statistics and data analysis*, Chapman and Hall, 1986.

Index

ϕ^4

- coupling strength, 59
- Laplacian, 62
- localisation, 60
- M, 64
- model, 52
- period, 55
- potential, 53
 - multistable, 57
- resonance, 55
- system size, 59

active rotator

- model, 14
- potential, 14

bistable

- forced, 6
- potential, 5
- Z-shaped curve, 4

Class I, 18

- real threshold, 18

Class II, 18

- soft threshold, 18

discrete bistable

- diversity-free, 80
- model, 69
- multistability, 84
- order-disorder, 72

resonance, 72

FitzHugh-Nagumo

- model, 15
- nullclines, 16

modified Deffuant

- followers, 94
- model, 93
- order-disorder, 96

modified van der Pol

- G, 110
- model, 105
- position coupling, 106
- spectral, 110
- velocity coupling, 107

sociophysics

- Comte, 19
- continuous, 21
 - master equation, 25
 - model, 23
- discrete, 21
 - model, 22
- homophily, 26
- opinion model, 20

van der Pol

- Arnold tongue, 11
- Liénard, 8
- model, 5, 7

period, 9

phase portrait, 9

synchronisation, 10

Curriculum vitae

Teresa Vaz Martins

E-mail: teresa@ifisc.uib-csic.es

Education

Graduate in Sociology, 5 years degree, University of Oporto, 1999
Thesis: *Voluntary simplicity movement*, Adviser: Carlos Gonçalves

Graduate in Physics, 4 years degree, University of Oporto, 2004
Thesis: *Tsallis statistics / Superstatistics: application to a kinetic Ising model*, Adviser: Maria Augusta Santos

M.Sc. in Physics, University of the Balearic Islands, 2010
Thesis: *Divide and Conquer*, Adviser: Raúl Toral

Awarded Fellowships

1. 2005 - Fellowship for Scientific Research, by Foundation for Science and Technology (FCT) - Centro de Física do Porto, Theoretical Physics Unit at the University of Oporto
2. 2006 - Fellowship for Doctoral Degree, by Foundation for Science and Technology (FCT), Portugal

Research Lines

- Nonlinear and Statistical Physics
- Interdisciplinary applications

Summer Schools

- 2005 - *Dynamics of Socio-Economic Systems: A Physics Perspective*, Physikzentrum Bad Honnef, SPG, Germany, 18-24 September
- 2009 - *Climate Variability and Climate Change: Estimating and Reducing Uncertainties*, Visegrad, Hungary, 8-17 June

Publications

1. T. Vaz Martins, R. Toral, M.A. Santos, Divide and Conquer: Resonance Induced by Competitive Interactions, *European Physical Journal B* **67**, 329-336 (2009)
2. T. Vaz Martins, T. Araújo, M. A. Santos, M. St Aubyn, Network effects in a human capital based economic growth model, *Physica A* **388** (11): 2207-2214 (2009).
3. T. Vaz Martins, V. N. Livina, A. P. Majtey, R. Toral, Resonance induced by repulsive interactions in a model of globally-coupled bistable systems, *Physical Review E* **81**, 041103 (2010)
4. T. Vaz Martins, M. Pineda, R. Toral, Interplay between mass media and repulsive interactions in continuous opinion dynamics, *EPL* **91**, 48003 (2010)
5. T. Vaz Martins and Raúl Toral, Resonance induced by repulsive links, in *Applications of Nonlinear Dynamics: Model and Design of Complex Systems*, edited by V. In, P. Longhini, A. Palacios, (Springer Verlag, 2009), p. 439

6. T. Vaz Martins, A. Majtey and R. Toral, Competitive induced resonance, in *Proceedings of the European Conference on Complex Systems 2009 (ECCS09)*, 2009
7. T. Vaz Martins and R. Toral, Synchronisation induced by repulsive interactions in the van der Pol oscillator (submitted to *Progress of Theoretical Physics*, arxiv: 1011.2967).

Conferences

1. 1997 - International symposium on frontiers of science, UFP, Oporto, Portugal, 25-26 October
2. 2002- Conferência da Sociedade Portuguesa de Física, Física 2002, Évora, Portugal, 6-10 September
3. 2005 - Física 2005 - Física para o Século XXI, Porto, (Alfândega), Portugal, 1-3 December, Poster - Distribuição de riqueza, uma abordagem econofísica, R. Coelho, T. Martins, R. Pinho, M.A.Santos
4. 2006- Conferência da Sociedade Portuguesa de Física, Física 2006 - Traçando o Futuro, Aveiro, 4-7 September
5. 2006 - Conference on Complex systems: from physics to biology and the social sciences, Lisbon, Portugal, 22-25 November
6. 2007 - Earth Monitoring and Climate Change (Jornadas sobre Observación de la Tierra y Cambio Global), Universitat de les Illes Balears, Spain, 8 y 9 Mayo
7. 2007 - International Workshop on Complex Systems and Networks, Sovata, Romania, 14-21 July, Talk - Network effects in an economic growth model based on human capital, T. Martins, M.A. Santos, Tanya Araújo, M. St Aubyn

8. 2007 - International Conference on Applications in Nonlinear Dynamics, Kauai, Hawaii, U.S.A., 24-27 September, Poster - Resonance induced by the presence of repulsive links, T. Vaz Martins and Raúl Toral
9. 2008 - Stochastic Resonance 2008 - Perugia, Italy, 17-21 August, Poster - Divide and Conquer, T. Vaz Martins and Raúl Toral
10. 2008 - Extreme Events: Theory, Observations, Modelling, and Prediction. Joint Workshop Program "Trends in Complex Systems" between IFISC and MPIPES, Palma de Mallorca, Spain, 10-14 November
11. 2009 - MAP - fis PhD Research Conference, Universidade do Minho, Portugal, 16-17 January, Talk - Divide and Conquer, T. Vaz Martins and Raúl Toral
12. 2009 - Climate variability and climate change: estimating and reducing uncertainties, 8-17 June 2009, Visegrad, Hungary, Poster - Divide and Conquer, T.Vaz Martins and Raúl Toral
13. 2009 - European Conference Complex Systems, 21-25th September 2009, Warwick, United Kingdom, Poster - Competitive induced resonance, Teresa Vaz Martins, Ana Majtey, and Raúl Toral
14. 2009 - International Workshop on 150 Years after Darwin: From Molecular Evolution to Language, Palma de Mallorca, Spain, November 23 - 27, 2009, Poster - Enhancement of response induced by competitive interactions, Teresa Vaz Martins
15. 2010 - First Porto Meeting on Theory and Experiment in Nonlinear Physics, Porto, Portugal, Talk - 7-9 July, Resonance induced by repulsive interactions in a model of globally coupled bistable systems.
16. 2010 ROBUST (Emergence and Design of Robustness) conference, Palma de Mallorca, 21-25 September, Poster - Divide and conquer.

Computer Skills

- Languages: C, and some use of Python and Java.
- Software: Mathematica, Octave, SPSS, AUTO
- Operating Systems: Unix/Linux, Windows